Charles University

Faculty of Science

Study programme: Biology

Branch of study: Reproduction and Developmental Biology

Bc. Andrea Burianová

Role of the Noncanonical Wnt Pathway in Craniofacial Development

Úloha nekanonické signalizační dráhy Wnt v kraniofaciálním vývoji

Diploma thesis

Supervisor: RNDr. Ondřej Machoň, Ph.D.

Prague, 2024

Declaration

I declare that I have independently prepared this diploma thesis and that I have cited all used sources of information and literature. This work or its essential part has not been submitted for obtaining any other academic degree.

Prohlášení

Prohlašuji, že jsem závěrečnou práci zpracovala samostatně a že jsem uvedla všechny použité informační zdroje a literaturu. Tato práce ani její podstatná část nebyla předložena k získání jiného nebo stejného akademického titulu.

V Praze, 20. 4. 2024

.....

Andrea Burianová

Acknowledgments

I would like to express my sincere gratitude to my supervisor, RNDr. Ondřej Machoň, Ph.D., for his invaluable guidance, encouragement, and support. His expertise and insights have been instrumental in shaping this work. Additionally, I extend my heartfelt thanks to my esteemed colleagues, Mgr. Miroslav Matějček, RNDr. Simona Vojtěchová, and Mgr. Viktorie Psutková, for their support, kindness, and insightful discussions. Special thanks to Erika Hudáčová, M.Sc., for priceless advice sessions and her time in reading and revising this thesis. I am also grateful to my friend, Tomáš Fiala, who patiently endured my countless questions and provided me with invaluable Python coding lessons. His patience and humor made learning truly enjoyable. Last but not least, I would like to thank my family and my boyfriend for their constant support and understanding during the writing process. Their love, patience, and encouragement have been a source of strength and motivation, for which I am truly thankful.

Abstract

The craniofacial region, a complex structure defining the vertebrate head, results from intricate cellular and molecular processes governed by various genetic regulations and signaling cascades, including the noncanonical Wnt pathway. Dysregulations in this pathway, particularly involving Wnt5a, have been linked to craniofacial malformations, as seen in conditions like Robinow syndrome. This study aimed to elucidate the role of Wnt5a signaling in craniofacial development using mice with targeted deletion of *Wnt5a* specifically in the neural crest cells, which give rise to craniofacial structures. Our findings highlight the critical involvement of Wnt5a in shaping craniofacial precartilage condensations and regulating cellular behaviors such as proliferation, oriented cell division, and primary cilia polarity during early craniofacial morphogenesis. Wnt5a signaling is also important for key developmental populations, such as $Msx1^+$ and $Pax3^+$ populations. These findings not only contribute to the current understanding of noncanonical Wnt signaling in craniofacial development but also offer valuable insights into the intricate regulatory networks governing this process.

Keywords: Wnt5a signaling, neural crest cells, morphogenesis

Abstrakt

Vývoj obličejové oblasti je výsledkem komplexních buněčných a molekulárních procesů, které jsou řízené činností různých signálních kaskád. Jednou z těchto signálních kaskád, které se podílejí na vývoji obličeje, je nekanonická Wnt signální dráha. Mutace v genech kódujících proteiny, které jsou součástí této signální dráhy (Wnt5a aj.), jsou spojeny s obličejovými defekty, které je možné pozorovat například u pacientů s Robinowovým syndromem. Cílem této práce bylo objasnit roli Wnt5a signalizace ve vývoji obličeje pomocí analýzy myšího kmene s kondicionální delecí genu *Wnt5a* v buňkách kraniální neurální lišty, které se významně podílejí na tvorbě obličejových struktur. V této studii jsme zjistili, že Wnt5a signalizace se ve vývoji obličeje uplatňuje tak, že reguluje tvar mezenchymálních kondenzací dávajících vzniknout chrupavkám, které ovlivňují výsledný tvar obličeje. Zároveň Wnt5a signalizace reguluje buněčnou proliferaci, orientované buněčné dělení, polaritu primárních cilií a je důležitá pro buněčné populace exprimující Msx1 nebo Pax3, které jsou pro vývoj obličeje klíčové. Tato data nejen přispívají k současnému chápání nekanonické Wnt signalizace ve vývoji obličeje, ale také nabízejí cenné poznatky o tom, jakým způsobem komplexní genové regulační sítě tento proces řídí.

Klíčová slova: Wnt5a signalizace, buňky neurální lišty, morfogeneze

Contents

List of Abbreviations

AP2	activating protein 2
APC	adenomatous polyposis coli
Arl13b	adenosine diphosphate-ribosylation factor-like protein 13B
Bmp2	bone morphogenetic protein 2
Cdc42	cell division control protein 42 homolog
CE	convergent extension
CK1	casein kinase 1
cKO	conditional knockout
E	embryonic day
ECM	extracellular matrix
Ext	exostosin
FNP	frontonasal process
Fox	forkhead box
FGF	fibroblast growth factor
Gpc	glypican
GSK3B	glycogen synthase kinase 3β
JNK	c-Jun-N-terminal kinase
KO	knockout
LEF	lymphoid enhancer factor
LRP	low-density lipoprotein receptor-related protein
Msx1	muscle segment homeobox 1
MuSK	muscle-specific kinase
NC	neural crest
NCC	neural crest cells
PA	pharyngeal arch
Papst1	adenosine 3'-phospho 5'-phosphosulfate transporter 1
PTK7	protein tyrosine kinase 7
Rac1	ras-related C3 botulinum toxin substrate 1
RhoA	ras homolog family member A
Ror	orphan receptor kinase
Rspo3	roof plate-specific spondin 3
Runx2	runt-related transcription factor 2

Ryk	related receptor tyrosine kinase
Snai2	snail family transcriptional repressor 2
Sox	sex-determining region Y box
Sdc	syndecan
TCF	T-cell factor
TGFB1	transforming growth factor β
Vangl	van Gogh-like planar cell polarity protein
Wls	wntless
Wnt	wingless/int-1

1 Introduction

The craniofacial region is a complex structure representing a distinctive feature of the vertebrate head. The impressive diversity of the vertebrate facial morphology demonstrates the power wielded by evolutionary adaptations and various genetic regulations. To resolve how such a wide spectrum of craniofacial architecture arises, it is crucial to understand the development of the craniofacial skeletal structures that dictate the final face shape. The facial bones and cartilages arise from a unique cell population, the neural crest cells (NCCs). The construction of the neural crest-derived skeletal elements forming the craniofacial region is an elaborate sequence of cellular and molecular processes, all of which require sophisticated spatiotemporal management and precise control of genetic pathways and signaling cascades.

Numerous signaling cascades, such as those mediated by members of the Wnt (wingless/int-1) family, play a pivotal role in governing the cellular behaviors involved in craniofacial morphogenesis. Among these, the noncanonical Wnt signaling emerges as a key participant due to its involvement in diverse cellular processes, including cell migration, polarity establishment, and tissue patterning. Recently, many researchers have been focusing on unraveling the contributions of Wnt5a signaling. Its significance in craniofacial development is highlighted by studies suggesting its role in various aspects of facial morphogenesis, including palate formation (F. He et al., 2008) and facial bone development (Yamaguchi et al., 1999).

Aberrations in any of the multistep processes orchestrating the development of the facial structures may result in craniofacial malformations. Dysregulations in the *Wnt5a* gene have been associated with Robinow syndrome (Person et al., 2010). Individuals with Robinow syndrome exhibit a spectrum of craniofacial anomalies, including micrognathia, short nose, wide nasal bridge, cleft palate, hypertelorism, etc. These observations underscore the critical role played by Wnt5a signaling in ensuring proper craniofacial development.

Deeper knowledge of noncanonical Wnt signaling, particularly the involvement of Wnt5a, in craniofacial development is essential. By understanding these mechanisms, we gain insights into how facial features form and have the potential to mitigate or prevent human craniofacial defects. This thesis presents recent research findings that elucidate the significance of Wnt5a signaling in craniofacial development, including experimental evidence demonstrating its pivotal role in dictating precartilage condensation shape and governing cell processes, such as proliferation, oriented division, or primary cilia polarity during craniofacial development.

2 Literature Overview

2.1 Craniofacial Development

Craniofacial development represents a phenomenal outcome of biological processes, reflecting the complex interplay of genetic programs, cellular dynamics, and environmental cues. While the posterior part of the vertebrate head is derived from mesodermal lineage, the craniofacial structures arise from a transient multipotent (Bronner-Fraser & Fraser, 1988) cell population, the neural crest cells (Noden & Trainor, 2005). Evolutionarily conserved, the neural crest (NC) serves as a remarkable source of cellular diversity, contributing to the formation of an array of craniofacial structures, including bones, cartilages, and connective tissues. According to the New Head Hypothesis (Gans & Northcutt, 1983), the NC, an exclusive vertebrate innovation, is responsible for generating diverse vertebrate craniofacial features. Additionally, Gans and Northcutt proposed that the NC facilitated a predatory lifestyle in vertebrates, contributing to their evolutionary success. Understanding the origins, migration, and fate determination of NCCs is essential for uncovering the mysteries of craniofacial morphogenesis.

2.1.1 Neural Crest

The NCCs represent a uniquely transient progenitor population with extraordinary properties. They were first described by Wilhelm His in 1868 as a "Zwischenstrang" (intermediate strand) due to their location. Within the ectoderm layer, the NCCs arise at the most dorsal aspect of the neural tube during embryo development (Le Douarin & Kalcheim, 1999). Subsequently, following their formation, the NCCs undergo extensive migration, covering long distances to populate various regions of the embryo. They remarkably contribute to the developing face, as they possess an impressive differentiation potential. Due to their exceptional migratory potential and ability to differentiate into derivatives that extend far beyond the potential of the ectodermal lineage from which they originate, the NCCs are often referred to as the "fourth germ layer".

2.1.1.1 Origins of the Neural Crest Cells Population

The NCCs emerge at the closing neural folds during the neurulation process along almost the entire anterior-posterior axis of the embryo (**see Fig. 2.1**). The first step of NC formation is an induction event that results in neural plate border specification (Meulemans & Bronner-Fraser, 2004; Stuhlmiller & García-Castro, 2012). After induction, the NC precursors start expressing distinct transcription factors, the NC specifiers, which include *AP2* (activating protein 2), *Fox* (forkhead box) *d3, Snai2* (snail family transcriptional repressor 2), *Sox* (sex-determining region

Y box) *9/10*, *Twist*, etc. (Bronner & le Douarin, 2012). The expression of both, the neural plate border specifying genes and the NC specifiers, guides a complex sequence of developmental events to specify the fate of NC. Moreover, these transcription factors initiate the epithelial-mesenchymal transition in the NCCs. During this process, the NCCs undergo a series of changes, including loss of intercellular connections, leading to their detachment from the neuroepithelium. Furthermore, as the NCCs go through various biochemical changes, they acquire crucial mesenchymal properties such as migration ability, invasiveness, and enhanced production of extracellular matrix (ECM) components (Meulemans & Bronner-Fraser, 2004).

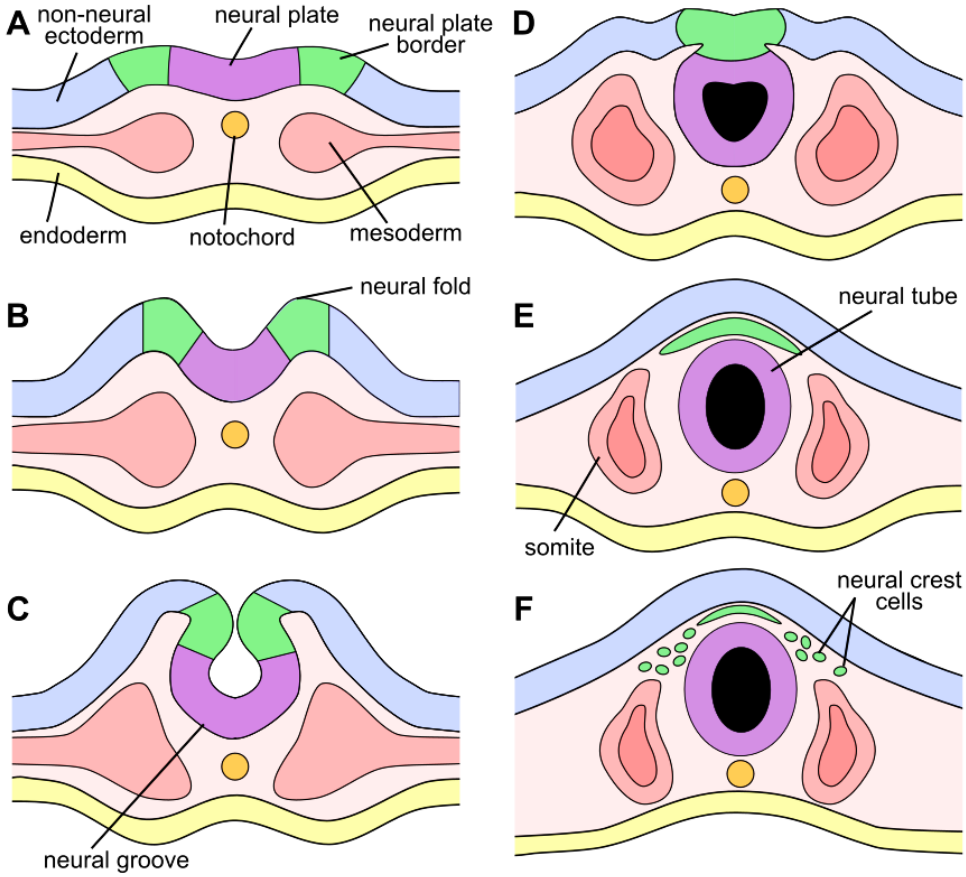

Figure 2.1 Schematic diagram illustrating a transversal view of the NCCs formation during neurulation. *(**A**) The NCC precursors occupy the neural plate border (green), a region between the neural plate (purple) and the non-neural ectoderm (blue). (**B-C**) As the neural plate invaginates once induced by the notochord, the neural folds elevate. (**D-E**) The neural folds converge at the midline and form a neural tube. (**F**) After the neural tube closure, NCCs undergo epithelial-mesenchymal transition, leading to delamination and acquisition of mesenchymal properties. Then, the NCCs migrate to various locations throughout the embryo.*

The NCCs can be classified into four subpopulations based on their initial location along the anterior-posterior axis – cranial, vagal, trunk, and sacral (Rothstein et al., 2018). These subpopulations exhibit different migratory patterns (see chapter below), gene expression profiles, and differentiation potentials, yet all of them retain a high degree of multipotency. NCCs contribute to the formation of numerous tissues and cell types, including cartilage, bone, dentin, smooth muscles, adipose tissue, melanocytes, peripheral neurons, etc. (Le Douarin & Kalcheim, 1999). Studies in mice have revealed that NCCs generate defined clonal patches (clonal envelopes) within the developing head (Kaucka et al., 2016). These clonal envelopes are areas occupied by a single NCC clone and can give rise to diverse cell fates, reflecting the remarkable NC multipotency. The regulation of NCC fate specification involves the expression of pluripotency markers within an NC stem cell niche located centrally in the dorsal neural tube (Lignell et al., 2017). As the NCCs migrate away from the neural tube, their exposure to Wnt signaling originating from the neural tube decreases. Consequently, there is a progressive decline in their multipotent properties (Bhattacharya et al., 2018).

2.1.1.2 Neural Crest Cells Migration

During craniofacial development, the cranial NCCs migrate to their target locations in a coordinated manner. This migration is a pivotal event, as any disturbance can result in significant craniofacial malformations (Tobin et al., 2008). The cranial NCCs travel along spatially distinct dorsolateral pathways, which remain consistent and stereotypical across vertebrate species (Lumsden et al., 1991; Minoux & Rijli, 2010). The NCCs arising from the prosencephalon and diencephalon migrate toward and eventually populate the anterior region of the developing head, known as the frontonasal process (FNP). The NCCs from the mesencephalon contribute to the FNP and partially to one of the pharyngeal arches (PAs), which are paired structures located in the region of the developing neck. The NCCs originating from the rhombencephalon invade the remaining PAs (Dupin et al., 2006; Noden, 1983) (**see Fig. 2.2 A**).

Directional migration of NCCs requires external guidance cues, primarily chemotaxis and cell-cell contact (Kulesa et al., 2010). During chemotaxis, cells migrate along a chemical gradient. Cell-cell contact also greatly influences NCC behavior as locomoting NCCs frequently collide with each other and subsequently display changes in motility. Cell-cell contact mediated by lamellipodia leads to repulsion (contact inhibition of cell locomotion) (Carmona-Fontaine et al., 2008). However, contact between cell bodies increases the cell's tendency to associate with each other (contact attraction) (Li et al., 2019).

Additionally, cell-ECM interactions also participate in guiding the NCCs through an embryo. NCCs feature surface integrin receptors, enabling contact with various ECM components such as collagen, fibronectin, and laminin. These ECM molecules are commonly found along the migration pathways of NCCs (Bronner-Fraser, 1993). Hyaluronan has also been linked with maintaining migratory behavior in cranial NCCs (Casini et al., 2012). Moreover, ECM-mediated mechanisms such as durotaxis and haptotaxis likely play roles in NCC migration, as suggested by the influence of ECM stiffness on NCC epithelial-mesenchymal transition (Barriga et al., 2018).

The NCCs employ diverse migratory strategies, including both collective and individual cell migration, to reach their target destinations. In collectively migrating NCCs, various hierarchical dynamics have been observed, where leader cells at the front of the migratory stream direct the movement of the cell cluster. In zebrafish trunk NCCs, ablation of a leader cell stops the migration until a new cell from the premigratory NC pool delaminates, takes over, becomes the leader, and allows the migration to proceed (Richardson et al., 2016). Similarly, cranial NCCs in *Xenopus* also establish leader/follower identities during migration. However, the role of leaders and followers is continuously exchanged, due to rear contractions pushing trailing cells forward within migratory clusters, sending leader cells toward the back (Shellard et al., 2018). In contrast, cranial NCCs in zebrafish and chick demonstrate a more flexible migratory behavior, characterized by frequent positional exchanges and a lack of this leader/follower commitment (Genuth et al., 2018; Richardson et al., 2016). In collectively migrating NCCs, such complex behaviors, which maintain tissue cohesiveness, fluidity, and polarity, require organized cell-cell interactions. N-cadherin has been found to mediate these cell-cell contacts, playing a key role in collective migration (Scarpa et al., 2015).

Individual migration has also been observed in NCCs, particularly in trunk NCCs in chick (Li et al., 2019). Studies have shown that these cells acquire front-to-back cell polarity, with a lamellipodium protruding at the leading edge and a rounded cell body retracting at the trailing edge, facilitating individual migration (Etienne-Manneville, 2008).

Despite the differences, both individually and collectively migrating NCCs share similar cellular mechanisms for migration (**see Fig. 2.2 B-C**). Such common mechanisms include chemotaxis which maintains directional movement. Chemotactic signals guide the cells toward specific targets by inducing polarization and directional migration toward or away from the source of the signal. In both individually and collectively migrating cells, this cell polarization is regulated by the distribution of small GTPases, such as Rac1 (ras-related C3 botulinum toxin

substrate 1), Cdc42 (cell division control protein 42 homolog), and RhoA (ras homolog family member A), which is essential for coordinating actin rearrangements and cell polarity (Etienne-Manneville, 2008). To illustrate, once a chemokine binds to individually migrating cell's receptors, the activity of small GTPases is polarized. While Rac1/Cdc42 activation at the leading edge of the cell promotes actin polymerization, extending lamellipodia and filopodia for new adhesions with the environment, RhoA activity at the trailing edge controls actomyosin contractions, pushing the cell forward (Etienne-Manneville, 2008) (**see Fig. 2.2 B**).

Similarly, in collectively migrating cells, chemokine binding activates Rac1/Cdc42 at the leading edge of the cell cluster, and RhoA activation in trailing cells mediates supracellular contractions to move the migratory cluster forward (Shellard et al., 2018) (**see Fig. 2.2 C**). In addition, the directionality and confinement of collectively migrating cell streams are maintained by repulsive signals from the environment, including semaphorin 3A. To illustrate, once the migrating cells receive the repulsive cue, the cells at the trailing edge of the migrating cluster inhibit Rac1 activity, leading to de-adhesion from the ECM (Bajanca et al., 2019).

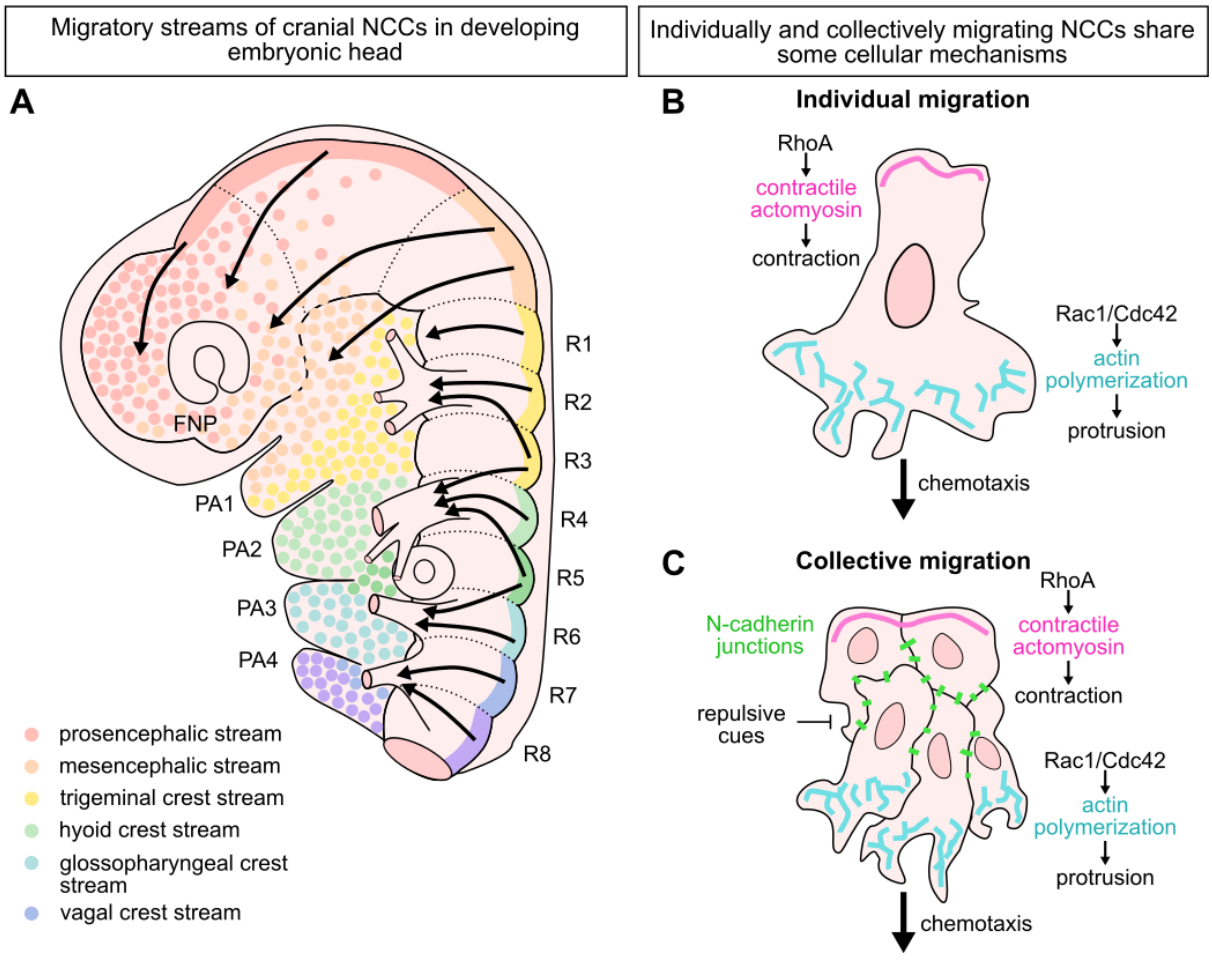

Figure 2.2 Migration of the neural crest cells. *(**A**) Schematic diagram depicting stereotypical migratory streams of cranial NCCs from rhombomeres and cephalic regions to the FNP and PAs area. The NCCs derived from the cephalic regions populate the FNP and a part of the PA1. The NCCs arising from rhombomeres 1-3 invade the PA1, while the PA2 is populated by NCCs traveling from R4-5. R5 and R6 NCCs contribute to PA3 and R8-derived NCCs form PA4. (**B-C**) Schematic diagram illustrating some of the common cellular mechanisms utilized in individual (B) and collective (C) migration of the NCCs (described above in detail). **Abbreviations**: **FNP** – frontonasal process, **PA** – pharyngeal arch, **R** – rhombomere.*

2.1.2 Craniofacial Morphogenesis

The migratory pathways of cranial NCCs lead them to crucial sites within the developing embryo, including the FNP and the pharyngeal regions. These regions play essential roles in the formation of craniofacial bones (Couly et al., 1993; Noden, 1983). Through intricate developmental processes, the FNP and the PAs converge to form a unified anatomical structure recognized as the *viscerocranium*, the facial skeleton.

The FNP gives rise to the frontonasal skeleton, while the PAs are linked with the development of other facial and neck structures. PA1, subdivided into two distinct prominences (maxillary and mandibular), contributes to the formation of the *maxilla*, zygomatic bone, hard palate, vomer bone, squamous part of the temporal bone, and Meckel's cartilage, which provides the foundation for the mandible, *malleus*, and the short limb of the *incus* (Köntges & Lumsden, 1996). PA2 is associated with the development of the stapes, long limb of the *incus*, styloid process, and lesser horns and upper part of the body of the hyoid bone (Qiu et al., 1995). The rest of the body and the greater horns of the hyoid bone arise from PA3. The remaining PAs are involved in the development of the thyroid and cricoid cartilage.

The morphogenesis of the mammalian face involves a precisely orchestrated sequence of embryonic events. The initial critical event in craniofacial tissue development involves the separation of the FNP from the PAs. Subsequently, the PA1-derived mandibular prominences merge at the midline to form the lower jaw, chin, and lower lip. The FNP extends downward, contributing to the formation of the forehead, nasal bridge, and median and lateral nasal prominences. Following that, the medial and lateral nasal prominences fuse with the PA1-derived maxillary prominence, resulting in the establishment of the central structures of the nose, upper lip, philtrum, and primary palate. This fusion occurs at the lambdoidal junction, where the three facial prominences converge (Tamarin & Boyde, 1977). These processes, guided by the proliferating activity of NCCs, establish the fundamental facial structure (Noden

& Trainor, 2005), and any disruptions, such as fusion defects, can lead to craniofacial malformations like clefts.

The initial phases of craniofacial morphogenesis show remarkable similarity between humans and mice, occurring from the 5th to the 8th week of gestation in humans (Som & Naidich, 2013) and from embryonic day (E) 9.5 to E11.5 in mice (Marcucio et al., 2015), highlighting the mouse as an excellent model for craniofacial development research. However, as embryonic development progresses, facial features gradually diverge, resulting in distinct facial appearances observed in both species.

2.1.3 Development of NC-derived Skeletal Elements

Facial bone formation marks a critical phase in craniofacial development, where NCCs transition from their migratory phase to orchestrating the formation of facial skeletal elements. This skeletogenic process involves three fundamental steps, including initiation, followed by the development, growth, and maintenance of condensation, and finally, differentiation. Depending on the ossification mechanism, the NCCs differentiate either into osteoblasts or chondroblasts within the condensation. Each of these phases involves unique cellular activities and distinct gene regulatory programs.

2.1.3.1 Initiation

The initiation process typically involves a signaling tissue that triggers the initiation and a responsive cell or tissue that alters its fate in reaction. During embryonic development, this initiation is often facilitated by reciprocal communication between epithelial and mesenchymal cells, ensuring their proper differentiation (Grobstein, 1953). Certainly, these epithelial-mesenchymal interactions play a fundamental role in the patterning and formation of craniofacial bone and cartilage (Helms et al., 2005). This complex interaction can occur before, during, or after mesenchymal cell migration. For instance, the NC-derived calvarial bones start forming once the NCCs arrive at their destination and interact with overlying epithelial dura mater in chick (Schowing, 1968, as cited in Franz-Odendaal, 2011).

Studies emphasize the critical role of FGF (fibroblast growth factor) signaling in inducing the differentiation of cranial NCCs into chondrocytes. The spatiotemporal context significantly influences the effectiveness of inductive signals, as seen in the various effects of FGF signaling from endodermal (Walshe & Mason, 2003) versus ectodermal (Richman et al., 1997) sources during craniofacial development. Experimental manipulations in chick and mouse models, including interspecies recombination, also confirm the importance of timing in epithelial-

mesenchymal interactions for bone and cartilage formation (Dunlop & Hall, 1995; Hall, 1980; Hall & Tremaine, 1979). The studies underscore the conservation of skeletogenic epithelial signaling factors, e.g. Msx1 (muscle segment homeobox 1), Msx2 (muscle segment homeobox 2), Bmp2 (bone morphogenetic protein 2), TGFB 1 (transforming growth factor β) across avian and mammalian species (Hall & Miyake, 1995).

2.1.3.2 Mesenchymal Condensation

Following the initiation of osteogenesis, mesenchymal cells, previously dispersed, undergo aggregation to form skeletogenic condensations. Grüneberg introduced the term "membranous skeleton" in 1963 to collectively describe these condensations, emphasizing their significance alongside cartilaginous and osseous skeletons. His research underscores the pivotal role of condensation formation in osteogenesis, as any disruption of the condensation stage may lead to delays or even prevention of the differentiation phase. He proposed that the "membranous skeleton" is a foundational structure for subsequent skeletal elements, dictating their size and shape (Grüneberg, 1963). Recent studies support his statements, highlighting the significance of oriented cell dynamics within the condensations, which facilitate precise shaping and development of facial skeletal structures (Kaucka et al., 2017). Indeed, condensation formation is a crucial phase of osteogenesis, however, it often receives less attention due to its transient appearance during embryonic development.

Mesenchymal condensations involve the aggregation of undifferentiated mesenchymal cells, which self-organize into compact, tightly packed structures. These condensed cell clusters, typically round or ovoid, can arise through different mechanisms (Hall & Miyake, 1992). These mechanisms include increased cell proliferation within the condensation compared to the surrounding mesenchyme, as well as inhibited cell migration away from the condensation center or guided cell migration towards the center. Additionally, factors like reduced cell death rates and shorter cell cycle times also play key roles in this process. Ultimately, condensations must reach a critical size, defined by strictly established boundaries, for differentiation to begin. The dynamic interplaying cellular processes that govern condensation formation, growth, and maintenance, including differential adhesion, proliferation, and migration are thoroughly discussed in Giffin et al., 2019 and Hall & Miyake, 2000.

2.1.3.3 Differentiation

During intramembranous ossification, mesenchymal cell aggregation gives rise to osteoblasts. The transcription factor *Runx2* (runt-related transcription factor 2) governs the differentiation of mesenchymal cells into osteoblasts upon upregulation by BMPs (bone morphogenetic proteins) (Otto et al., 1997), thereby contributing significantly to the process of osteogenesis. Studies involving *Runx2* knockout (KO) mice emphasize its function in bone formation, as the ablation of the *Runx2* gene results in the complete absence of bone structures (Otto et al., 1997). Additionally, the key involvement of the *Runx2* gene in osteogenesis was confirmed in a study utilizing *Runx2* conditional knockout (cKO) mice. In this study, the NC-specific *Runx2* absence prevented the formation of several craniofacial bones and caused defective mineralization in the mandible, *maxilla*, *premaxilla*, and nasal bones (Shirai et al., 2019). Following differentiation, the osteoblasts start the production of osteoid, a non-mineralized bone matrix. The osteoblasts then mature into osteocytes once integrated within the continuously mineralizing matrix, forming the bone tissue.

On the contrary, during endochondral ossification, condensed cells differentiate into chondroblasts. The Sox9 transcription factor, aside from its role as the NC specifier, plays a key role in the chondrogenesis process by controlling the differentiation of mesenchymal cells into chondroblasts. The function of the *Sox9* gene in cartilage development was demonstrated in a study utilizing *Sox9* KO mice, in which the chondrogenic condensations failed to form completely (Bi et al., 1999). After differentiation takes place, the chondroblasts later mature into chondrocytes when embedded in the cartilage matrix, establishing a cartilaginous scaffold (chondrocranium). Once BMP signaling induces upregulation of *Runx2* expression, this chondrocranium structure is progressively replaced by bone tissue throughout the course of development.

2.2 Wnt Signaling Pathways

Craniofacial development is a complex process that requires well-orchestrated coordination of multiple signaling pathways to properly sculpt the skeletal structures. Among these pathways, the Wnt signaling cascade emerges as a key participant, managing critical events such as facial prominence formation, palate development, and skeletal patterning. Through its various roles in regulating NC induction (García-Castro et al., 2002), cell proliferation (Hasegawa et al., 2002; Yamaguchi et al., 1999), differentiation (Hari et al., 2012), and tissue morphogenesis (Mirando et al., 2010; Yamaguchi et al., 1999), Wnt signaling contributes significantly to the precise spatial and temporal control of the construction of NC-derived facial structures.

2.2.1 Canonical vs. Noncanonical Wnt Signaling

There are two main branches of the Wnt signaling pathway, the β-catenin-dependent pathway (canonical) and the β-catenin-independent pathways (noncanonical). Canonical Wnt signaling primarily affects gene expression, thereby regulating processes including cell proliferation, differentiation, and tissue patterning (Nusse, 2005). On the other hand, noncanonical Wnt pathways involve a wide range of mechanisms that often operate via cytoskeletal rearrangements or calcium level regulation, playing critical roles in cell polarity, migration, and tissue morphogenesis.

The canonical Wnt signaling pathway, also known as the Wnt/β-catenin pathway, is characterized by the activation of β-catenin-dependent transcriptional responses (Wodarz & Nusse, 1998). In the absence of Wnt ligands, a destruction complex comprising proteins like APC (adenomatous polyposis coli), Axin, GSK3B (glycogen synthase kinase 3β), and CK1 (casein kinase 1) phosphorylates β-catenin, marking it for proteasomal degradation (Stamos & Weis, 2013) (**see Fig. 2.3 B**) However, upon Wnt ligand binding to Frizzled receptors and LRP (low-density lipoprotein receptor-related protein) 5/6 coreceptors (X. He et al., 2004), the destruction complex is inhibited, leading to the stabilization and accumulation of β-catenin in the cytoplasm (**see Fig 2.3 A**). β-catenin then enters the nucleus, where it interacts with TCF (T-cell factor)/LEF (lymphoid enhancer factor) transcription factors to activate the transcription of Wnt target genes (**see Fig 2.3 A**) involved in processes like cell proliferation, differentiation, etc.

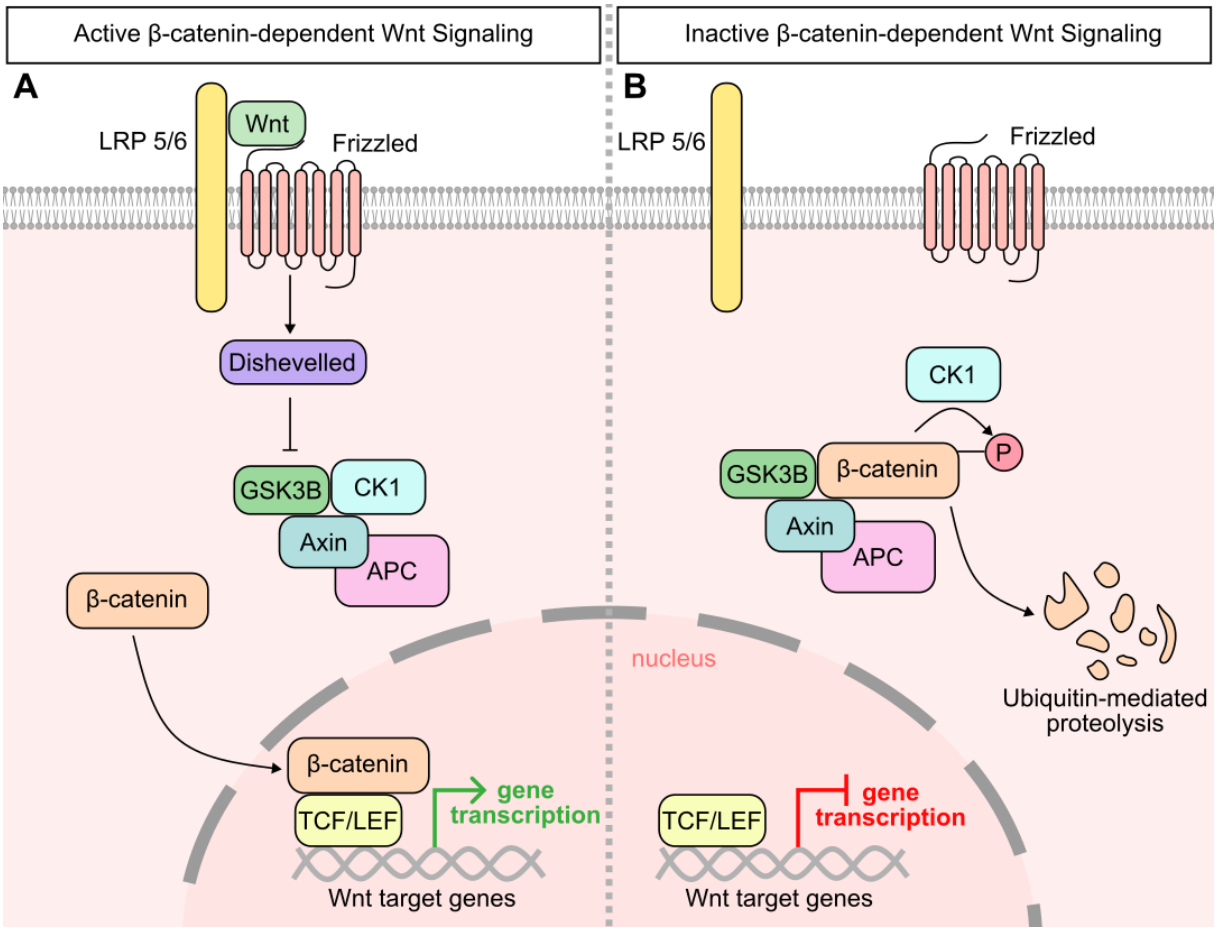

Figure 2.3 Molecular mechanisms of Wnt/β-catenin signaling cascade. *(**A**) Schematic diagram representing Wnt/β-catenin Wnt signaling. The binding of Wnt to its receptors and coreceptors results in the stabilization of β-catenin, which then activates gene expression along with TCF/LEF. (**B**) Schematic diagram demonstrating inactive Wnt/β-catenin signaling. Gene transcription is inhibited as β-catenin is phosphorylated and subsequently degraded.*

On the other hand, noncanonical Wnt signaling pathways are diverse and do not involve the stabilization of β-catenin. Instead, they regulate processes like cell polarity, migration, and differentiation. These pathways can be further classified into the Wnt/planar cell polarity (PCP) pathway and the Wnt/Ca2+ pathway. In the Wnt/PCP pathway, Wnt ligands activate c-Jun-N-terminal kinase (JNK) and small GTPases like Rho and Rac, regulating gene expression and cytoskeletal dynamics (Boutros et al., 1998; Habas et al., 2003). Ultimately, this affects cell movement, polarity, and adhesion. In the Wnt/Ca2+ pathway, Wnt ligands induce an increase in intracellular calcium levels, leading to the activation of calcium-dependent signaling molecules that influence cell behavior (Slusarski, Corces, et al., 1997; Slusarski, Yang-Snyder, et al., 1997). The Wnt/Ca2+ pathway is involved in cell adhesion, migration, and tissue morphogenesis.

2.2.2 Wnt Ligands

Wnt ligands are a large family of evolutionarily conserved secreted proteins. They are characterized by their cysteine-rich nature and hydrophobic sequence which contain a hydrophobic sequence. In early studies, Wnt ligands were subdivided into two distinct categories according to their ability to induce β-catenin buildup in the nucleus. To illustrate, so-called “canonical” Wnts, including Wnt1, Wnt3a, and Wnt8, strongly stabilize β-catenin, whereas “noncanonical” Wnts, such as Wnt4, Wnt5a, and Wnt11, do not (Du et al., 1995; Shimizu et al., 1998) and work independently of β-catenin (Heisenberg et al., 2000; Wallingford et al., 2001). These ligands were associated with the activation of "canonical" and "noncanonical" Wnt signaling pathways, respectively.

However, with emerging knowledge of molecular mechanisms of Wnt signaling, this binary subdivision of Wnt ligands has been challenged. As extracellular molecules, the Wnt proteins can bind to several different receptors and co-receptors, including Frizzled, LRP5/6, Ror (orphan receptor kinase) 1/2, Ryk (related receptor tyrosine kinase), protein tyrosine kinase 7 (PTK7), muscle-specific kinase (MuSK) and the heparan sulfate proteoglycans syndecan (Sdc) and glypican (Gpc) (Niehrs, 2012). In addition, there are 19 Wnt ligands found in human (Niehrs, 2012), offering numerous options for ligand-receptor pairings. Recently, it has been suggested that it is the particular combination of ligands and receptors, along with the availability of ligands and tissue-specific context, that determines which Wnt pathway is activated (Holmen et al., 2002; G. Liu et al., 2005; Mikels & Nusse, 2006). This contrasts with the previous belief that it was the "canonical" and "noncanonical" Wnt proteins themselves that decided which branch of Wnt signaling would get activated. Although the terms "canonical" and "noncanonical" Wnt pathways lack precise definitions, they are still widely used among researchers.

2.2.3 Wnt/PCP Pathway

One of the pivotal processes during the development of a complex multicellular organism is the establishment of cell polarity, a trait exhibited by the majority of cells within an organism. For example, epithelial cells demonstrate apical-basal polarity, while neurons maintain distinct axonal and somatodendritic compartments. Mesenchymal cells also exhibit polarity, as evidenced by the formation of leading and trailing edges necessary for directional migration (Ridley et al., 2003). A critical regulator of these diverse cellular polarities is the Wnt/PCP cascade, which represents one of the β-catenin-independent Wnt pathways.

The polarization of a field of cells within the plane of a cell sheet, referred to as PCP, has been associated with several developmental processes, including convergent extension (CE). CE is a conserved mechanism for elongating tissues, during which the tissues elongate (extension) along the anterior-posterior body axis while they narrow (converge) in the mediolateral axis. In vertebrates, disruption of CE during neurulation results in neural tube closure failure (Ciruna et al., 2006). Furthermore, PCP contributes to left-right asymmetry formation (Antic et al., 2010), the orientation of stereocilia in the cochlea (Rida & Chen, 2009), elongation of limbs and craniofacial prominences (Gao et al., 2011), axon guidance (Yoshikawa et al., 2003), and organogenesis of the heart (Takeuchi et al., 2000), lungs (Yates & Dean, 2011), etc. In addition, PCP signaling regulates cell shape, as in mice, chick, and zebrafish with disrupted Wnt5a signaling, the morphology of mesenchymal cells was changed (Gignac et al., 2019; Kilian et al., 2003; Yang et al., 2003). PCP signaling also modulates the orientation of the division plane (Kaucka et al., 2016; Ségalen et al., 2010). This is likely a consequence of the cell shape, as the mitotic spindle orients in the plane of the longest axis of the cell (Sach's and Hertwig's rule).

The cells establish the asymmetric expression of PCP components to orient themselves and their neighbors, maintaining cell directionality. Certain transmembrane proteins propagate the orientation signal to surrounding cells. An intriguing pattern in PCP proteins is the consistent opposite localization of Vangl (van Gogh-like planar cell polarity protein) and Prickle proteins to increasing Wnt gradients, while Dishevelled tends to align with these gradients. For example, during limb development, Vangl2 localizes proximally (Gao et al., 2011) to a distal-to-proximal Wnt5a gradient (Yamaguchi et al., 1999). In mouse nodes, Vangl1, Vangl2, and Prickle2 favor the anterior cell membrane, contrary to Wnt3a and Wnt5a gradients (Antic et al., 2010). Similarly, in zebrafish gastrulae, Prickle and Dishevelled enrich near anterior and posterior membranes (Yin et al., 2008). This pattern repeats in different tissues and organisms, suggesting that Wnt molecules act like a map, guiding the distribution of PCP proteins and helping cells establish their orientation.

2.3 Molecular Mechanisms of Wnt5a/PCP Signaling

Wnt5a protein has emerged as a key Wnt ligand possessing the ability to trigger the PCP pathway during development. To illustrate, in migrating cells, such as NCCs during craniofacial development, PCP signaling plays a crucial role in regulating cell polarity and directional movement (Carmona-Fontaine et al., 2008; De Calisto et al., 2005; Schambony & Wedlich, 2007). Wnt5a/PCP signaling activates RhoA, suppressing Rac activity at the cell's trailing edge, resulting in cytoskeletal rearrangements. This leads to actomyosin contractions at the trailing

edge of the cell, pushing the cell forward, and facilitating precise cell migration (discussed in Chapter 2.1.1.2). Sdc4 and PTK7 are key regulators that interact with Dishevelled, with Sdc4 directly inhibiting Rac, contributing to the regulation of neural crest migration (Matthews et al., 2008) (**see Fig. 2.4. A**).

Additionally, during craniofacial cartilage formation, the core PCP proteins (Frizzled, Vangl2) interact with receptors like Ror2 and proteoglycans such as Gpc4 (LeClair et al., 2009) to inhibit Wnt/β-catenin signaling and activate RhoA and Jun signaling pathways (Yang et al., 2003) (**see Fig. 2.4 B**). The precise coordination of these signaling pathways is essential for proper facial cartilage development. Moreover, correct processes associated with the transport of PCP proteins are required for the functionality of PCP signaling pathways. Mutations in genes involved in the processing of proteoglycans (Gpc, Sdc) and targeting them to the cell membrane can lead to congenital defects like those observed in Wnt/PCP mutants. Zebrafish mutants lacking *Gpc4* exhibit body axis compression and skeletal abnormalities due to reduced Wnt/PCP signaling (LeClair et al., 2009; Topczewski et al., 2001). In zebrafish, mutations in *exostosin* (Ext) *1* and *2* genes and *Papst1* (adenosine 3'-phospho 5'-phosphosulfate transporter 1), all of which are linked with glycosylation and transport, cause craniofacial cartilage defects (Clément et al., 2008) resembling Wnt/PCP mutants (Topczewski et al., 2001). Rspo3 (roof plate-specific spondin 3) was also found to modulate Wnt5a/PCP signaling, as it, along with Wnt5a, facilitates the clathrin-mediated endocytosis process (Ohkawara et al., 2011), which leads to the removal of specific proteins, including Gpc3 and Sdc4, from the membrane. Moreover, mutations in genes involved in protein secretion, such as *Sec23/24*, result in disorganized craniofacial phenotypes and defects in neural tube closure and organ development (Lang et al., 2006; Sarmah et al., 2010), indicating their role in PCP signaling. Overall, proteoglycans and their transport play a critical role in proper Wnt5a/PCP signaling (**see Fig. 2.4 C**).

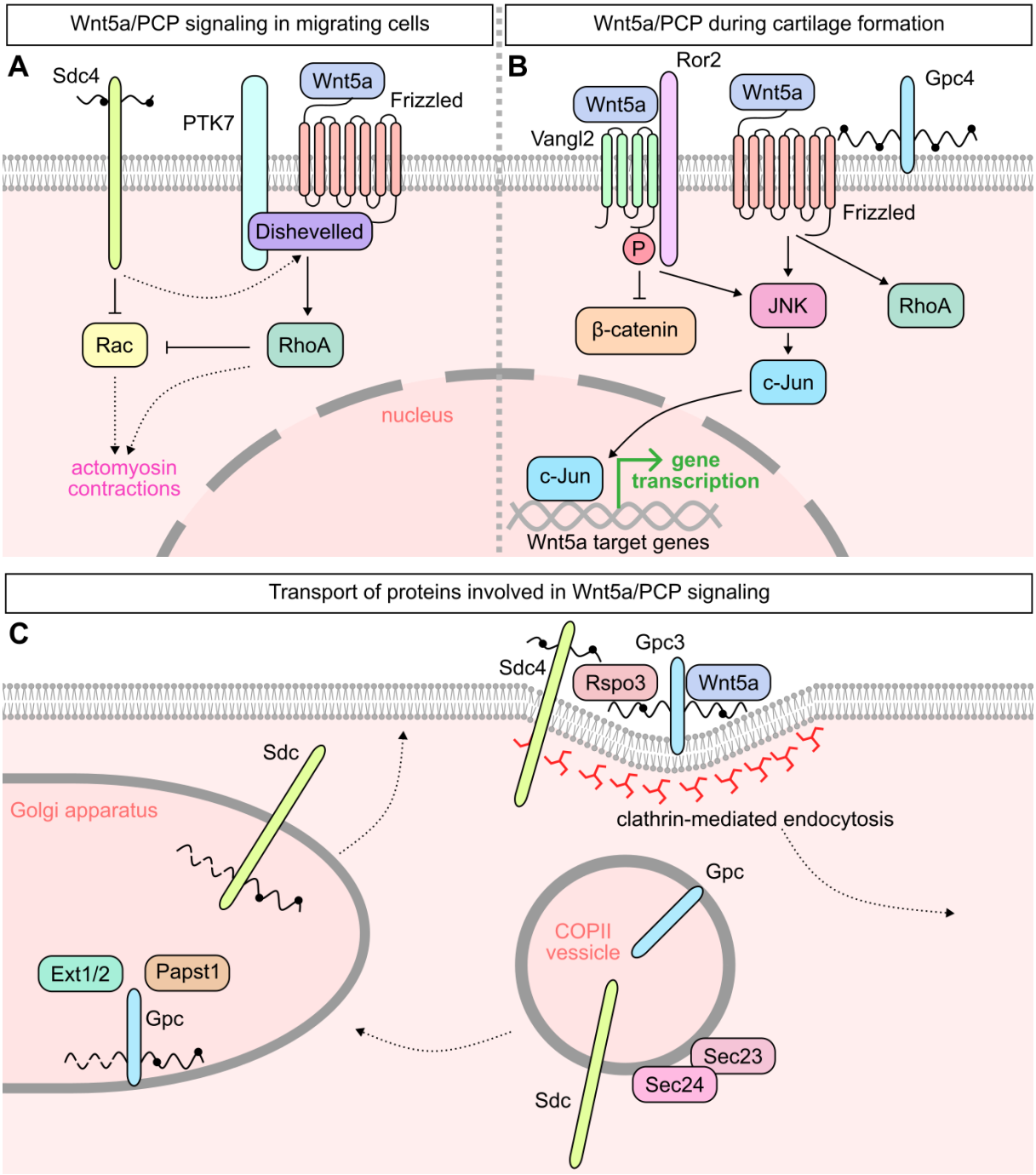

Figure 2.4 Molecular mechanisms of Wnt5a/PCP signaling. *(A) Wnt5a/PCP cascade in migrating cells. At the trailing edge of migrating cells, Wnt5a binding to the Frizzled receptor activates RhoA to inhibit Rac activity, which causes actomyosin contractions, pushing the cell forward. Rac can be inhibited directly by Sdc4 or indirectly by the interaction of PTK7 or Sdc4 proteins with Dishevelled. (**B**) Wnt5a/PCP signaling during craniofacial cartilage development. Wnt5a induces phosphorylation of Vangl2 via binding to Ror2 (Gao et al., 2011), inhibiting the Wnt/β-catenin cascade and activating Jun signaling, which regulates gene expression. Interaction of Gpc4 with Frizzled-Wnt5a complex can activate RhoA and Jun*

*signaling as well. (**C**) Transport of proteins involved in Wnt5a/PCP signaling. Proteins crucial for PCP processes are transported via a Sec23/24-dependent mechanism, ensuring their correct localization and function. Golgi-mediated protein modification, in which Ext1/2 and Papst1 play a role, is essential for their activation Additionally, a clathrin-mediated endocytosis process, facilitated by Rspo3 and Wnt5a, is responsible for the removal of Sdc4 and Gpc3 from the cell membrane.*

2.3.1 Wnt5a/PCP and Wnt/β-catenin Signaling

The Wnt5a/PCP pathway and Wnt/β-catenin signaling pathways are commonly perceived to function in opposition, where inhibition of one typically leads to the upregulation of the other. This competition occurs partly at the level of ligand-receptor binding and through competition for shared effector proteins like Dishevelled (van Amerongen & Nusse, 2009). For instance, Wnt5a ligands can suppress the β-catenin-dependent pathway by competitively inhibiting Wnt3a binding to Frizzled2 (Sato et al., 2010). PCP signaling was also shown to inhibit canonical Wnt signaling by binding Wnt5a to the Ror2 receptor (Mikels & Nusse, 2006). However, Wnt5a can also activate β-catenin signaling via Fzd4 in certain contexts (Ring et al., 2014; Van Amerongen et al., 2012). These findings suggest that Wnt5a can activate the β-catenin pathway in a tissue-dependent manner, independently of the PCP pathway. The Wnt/PCP pathway has also been shown to activate β-catenin signaling indirectly by controlling the spread of Wnt/β-catenin signaling within a tissue via cytonemes (Brunt et al., 2021).

Moreover, the PCP components Ror2 and Vangl2 play crucial roles in forming and stabilizing Wnt cytonemes (Brunt et al., 2021; Mattes et al., 2018). Ror2 induces actin polymerization via the PCP pathway upon Wnt8a binding, driving de novo formation of filopodia (Mattes et al., 2018). Whereas Vangl2 localizes Wnt8a and Ror2 on cytoneme tips, activating JNK signaling and enhancing cytoneme length and contact with receiving cells (Brunt et al., 2021). Functional Vangl2 is essential for cytoneme-mediated paracrine Wnt/β-catenin signaling. Inhibition of PCP signaling, either through mutated *Vangl2* or JNK inhibition, collapses cytonemes, reducing Wnt spread and paracrine Wnt/β-catenin signaling (Brunt et al., 2021). Therefore, Wnt proteins are believed to control their spread from producing to receiving cells, along with the strength and range of the morphogenic field, by influencing the quantity and size of filopodia, which correlates with expression levels of Ror2, Vangl2, and Wnt8a. This underscores the crosstalk between Wnt/PCP and Wnt/β-catenin signaling pathways, where PCP activation supports β-catenin signaling. However, it remains unclear whether increased filopodia length induced by Wnt5a/Ror2 signaling extends the morphogen field for other Wnt ligands, particularly whether

non-canonical Wnt5a binding to Ror2 increases canonical Wnt8a signaling in neighboring cells. Although Wnt5a treatment induces cross-correlation of Ror2 and Vangl2 complexes in zebrafish fibroblast cells (Brunt et al., 2021), the direct implications are yet to be elucidated.

2.4 Wnt5a in Craniofacial Development

The important role of Wnt5a signaling in craniofacial development has been demonstrated in several studies (Kaucka et al., 2016; Person et al., 2010; Yamaguchi et al., 1999), as *Wnt5a* mutant embryos exhibited severe abnormalities in the craniofacial region. The defects included hypertelorism, short nose, triangular mouth, *micrognathia*, etc. (Person et al., 2010; Yamaguchi et al., 1999). Moreover, analysis of daughter cell allocation in E12.5 *Wnt5a* KO mouse embryos revealed disrupted orientation of cell divisions in the facial region (Kaucka et al., 2016). This study suggests that cues responsible for aligning cell division planes in the face are, at least partially, determined by the Wnt5a gradient, influencing the distribution of daughter cells after mitosis, which ultimately shapes the clonal envelopes forming the face. The concept of a Wnt5a gradient governing the craniofacial morphology is further supported by the similarity between the phenotypes resulting from conventional *Wnt5a* KO (Yamaguchi et al., 1999) and Wnt5a overexpression (Van Amerongen et al., 2012). In both cases, the removal of the Wnt5a gradient from the tissue leads to distinct features including the shortening and widening of the face.

Furthermore, in addition to the mutations discussed in Chapter 2.3, mutations in other Wnt5a/PCP components have also been investigated, providing insight into their contribution to craniofacial development. For example, mice lacking Ror2, a Wnt5a receptor, exhibited various craniofacial abnormalities, including a shortened mandible, truncated Meckel's cartilage, thickening of the nasal capsule, presence of ectopic cartilages, hypertelorism, etc. (Schwabe et al., 2004). Disruption in cartilage elongation and craniofacial morphogenesis, along with neural tube closure defects which are often associated with dysfunctional PCP signaling, were observed in mice with a mutation in gene encoding Vangl2 (Gao et al., 2011), a core PCP component. Both studies highlight the connection of Ror2 and Vangl2 to Wnt5a/PCP signaling. Indeed, in developing limbs, research revealed that Vangl2 genetically and physically interacts with Wnt5a and Ror2 (Gao et al., 2011; Wang et al., 2011). Similarly to Vangl2, Prickle1 is another PCP protein that localizes on the membrane in an organized and oriented manner (Antic et al., 2010; Yin et al., 2008). Therefore, it is not surprising that craniofacial defects, including micrognathia, shortened nasal region, and reduced skull size, were observed in *Prickle1* mutant mice (Wan et al., 2018). These studies support the key involvement of both,

Vangl2 and Prickle1, in establishing cell polarity through oriented localization on the membrane.

Research revealed that during palatogenesis, in *Wnt5a* KO mouse embryos with cleft palate, the directional migration of mesenchymal cells in the palate was disrupted (F. He et al., 2008). The same study also showed an altered proliferation rate within the palate in the *Wnt5a* mutant. Interestingly, a notably higher level of cell proliferation was observed in the anterior palate, while a decreased rate was exhibited in the posterior palate. These findings indicate that Wnt5a signaling regulates directional migration and proliferation during palate development. Moreover, this research group suggests that the Wnt5a signaling is mediated by Ror2 during palate construction (F. He et al., 2008). In both *Ror2* and *Prickle1* mutant mice, cleft palate was also reported (Schwabe et al., 2004; Wan et al., 2018). Surprisingly, *Vangl2* mutant mice do not exhibit palatal cleft (Kibar et al., 2001), thus raising questions about the involvement of PCP signaling in palatogenesis.

2.5 Wnt5a in Human Craniofacial Disorders

The study of Wnt5a signaling holds significant clinical implications for understanding human development and disease, particularly in the context of craniofacial abnormalities. One notable rare genetic disorder linked with the dysregulation of the Wnt5a cascade is Robinow syndrome (Person et al., 2010). This condition, which exhibits both autosomal dominant and autosomal recessive inheritance patterns, is characterized by distinctive facial features, short stature, and skeletal abnormalities. In individuals with Robinow syndrome, mutations in genes associated with the Wnt/PCP pathway (*Wnt5a*, *Frizzled2*, *Ror2*, *Dishevelled1/3*) disrupt normal development, leading to craniofacial anomalies such as a broad nose, hypertelorism, mandibular dysplasia, and a prominent forehead (White et al., 2018). Beyond Robinow syndrome, dysfunctions in the Wnt/PCP pathway have been implicated in a range of other craniofacial disorders and congenital anomalies. For instance, defects in PCP signaling have been associated with orofacial clefts, a common birth defect characterized by incomplete fusion of the lip and/or palate (Chiquet et al., 2008). Additionally, abnormalities in Wnt/PCP pathway genes have been linked to craniosynostosis (Kaissi et al., 2020), a condition characterized by premature fusion of the cranial sutures, leading to abnormal skull shape and facial features. Further research could enhance clinical interventions and facilitate effective diagnosis and treatment of craniofacial abnormalities.

3 Aims of Diploma Thesis

Studying the noncanonical Wnt pathway, specifically the Wnt5a signaling, in craniofacial development is crucial due to its various roles in regulating numerous cellular processes essential for proper craniofacial morphogenesis. Understanding the mechanisms regulated by Wnt5a can provide insights into the causes of craniofacial abnormalities and congenital defects, which could lead to potential therapeutic interventions. Therefore, this project aims to clarify the role of the Wnt5a signaling cascade in the development of the craniofacial region by:

- generating *Wnt5a* cKO (*Wnt1-Cre2*; *Wnt5a*$^{fl/fl}$) embryos, lacking *Wnt5a* gene in cranial NCCs,
- describing the differences in control and *Wnt5a* cKO phenotypes,
- comparing distinct cellular processes involved in the development of craniofacial structures derived from the NC, such as proliferation, cell polarity, oriented cell division, and gene expression patterns, between control and *Wnt5a* cKO embryos in critical stages of craniofacial development.

4 Materials and Methods

4.1 Mouse Strains

To achieve tissue-specific inactivation of the *Wnt5a* gene in the NCCs, we employed the *Wnt5a*$^{fl/fl}$ mouse strain generously provided by Mgr. Jan Procházka, Ph.D. from the Institute of Molecular Genetics, CAS, CCP. This strain carries loxP sites flanking critical exons of the Wnt5a gene, facilitating conditional gene deletion. We also acquired the *Wnt1-Cre2* mouse strain from The Jackson Laboratory (Jax #022137) to drive Cre-mediated recombination specifically in NCCs. By crossing the *Wnt1-Cre2* mouse line with the *Wnt5a*$^{fl/fl}$ strain, we generated *Wnt1-Cre2*; *Wnt5a*$^{fl/fl}$ (*Wnt5a* cKO) embryos. This breeding strategy ensured tissue-specific and temporally controlled deletion of the *Wnt5a* gene exclusively within NC-derived tissues during embryonic development. Additionally, we utilized the mTmG mouse line obtained from The Jackson Laboratory (Jax #007676) as a Cre activity reporter, allowing us to define the spatiotemporal pattern of Cre-mediated recombination.

The mice were kept in a regulated environment with a 12-hour light-dark cycle and provided ad libitum access to food and water. They were housed under standard experimental conditions, maintaining a constant temperature range of 23–24 °C. During the gestation period, female mice were individually housed, and the number of offspring per litter was documented.

4.2 Mouse Breeding and Embryo Harvesting

Experimental mice were paired overnight for mating in a breeding cage. The following day, the males were removed from the breeding cage, and the females were checked for signs of mating (presence of vaginal plug). If the plug was observed, the embryos were noted as being half a day old – embryonic day 0.5 (E0.5). At the desired embryonic stage, impregnated females were anesthetized by isoflurane inhalation and euthanized by cervical dislocation. The uterine horns were dissected from the females and separated into individual embryos. The embryos were isolated using forceps.

4.3 DNA Isolation and Genotyping

Embryonic tail tips were used for DNA isolation. The tail tips were cut off and put separately to clean PCR tubes. The DNA was extracted using the DEP-25 DNA Extraction Kit (Top-Bio D227). First, DEP-25 START-Blue reagent was added to each tube. The samples were heated to 95 °C for 20 min in a thermal cycler (Biometra PCR Thermal Cycler). Then, DEP-25 STOP solution was added and the samples were mixed by vortexing. The final extract was used as a stock source of DNA template for polymerase chain reaction (PCR). Routine genotyping was performed by PCR using thermal cycler. The primers used for PCR are described in **Table 4.1**. Reaction mixture with final volume of 10 µl consisted of 5 µl of EliZyme HS Robust Mix Red (Elizabeth Pharmacon), 3 µl of water, 0.5 µl of genotype-specific forward and reverse primer mix (**Table 4.1**), and 1.5 µl of DNA template. The PCR products were evaluated by 2% agarose (SeaKem® LE Agarose, LONZA) gel electrophoresis (PowerPac™ Basic Power Supply, BIO-RAD) and detected by adding EliDNA PS Green (Elizabeth Pharmacon) to the gel.

Table 4.1 List of used primers.

Primer	Direction	Sequence	Annealing Temperature	Product Size
Wnt5a flox	forward	GGTGAGGGACTGGAAGTTGC	60 °C	TG 340 bp, WT 290 bp
	reverse	GGAGCAGATGTTTATTGCCTTC		
Wnt1-Cre2	forward	GCATTTCTGGGGATTGCTTA	60 °C	TG 250 bp
	reverse	CCCGGCAAAACAGGTAGTTA		

4.4 Immunohistochemistry

4.4.1 Paraffin Sections

On **Day 1**, the heads of isolated embryos were fixed in 4% paraformaldehyde (PFA) (Sigma-Aldrich) in PBS overnight at 4 °C. On **Day 2**, the samples were washed 3×5 min in phosphate-buffered saline (PBS) and immersed in 70% ethanol (Penta). Then, the samples were dehydrated by ascending ethanol series, cleared by xylene, and infiltrated with paraffin in an automated tissue processor (HistoCore PEGASUS Plus). On **Day 3**, embryonic heads were embedded in paraffin (Leica HistoCore Arcadia H) and sectioned at 8 µm using a microtome (Leica RM2255). The sections were then placed in an oven (Major Science, MS Incubator) at 60 °C until the wax started melting. Then, the sections were deparaffinized in xylene (Penta), rehydrated by descending ethanol series and permeabilized in 0.1% Triton X-100 (Sigma-Aldrich) in PBS (PBT). For antigen retrieval, the sections were boiled in 0.1M citrate buffer pH 6 in a pressure pot for 12 min. Afterward, the sections were cooled in running water, washed 3×5 min in PBT and then blocked, using 5% bovine serum albumin (BSA) (Serva) in PBT, for 90 min in a humidified chamber at room temperature (RT). Following that, the sections were incubated in a primary antibody solution (primary antibodies diluted in 1% BSA in PBT) overnight at 4 °C. Primary antibodies used are listed in **Table 4.2**. On **Day 4**, sections were washed 3×5 min in PBT at RT and then incubated in a secondary antibody solution (secondary antibodies diluted in 1% BSA in PBT) for 1 h at RT. Secondary antibodies used are listed in **Table 4.3**. For the secondary antibody removal, the sections were washed 3×10 min in PBT. For nuclear staining, 4′,6 diamidino 2-phenylindole (DAPI) (Roche) was added into PBT during the second wash. Finally, the sections were mounted with Mowiol 4-88 (Sigma-Aldrich). Fluorescent images were acquired using Olympus SpinSR10.

4.4.2 Frozen Sections

On **Day 1**, the heads of isolated embryos were fixed in 4% PFA in PBS overnight at 4 °C. On **Day 2**, embryonic heads were washed 3×5 min in PBS and treated with 30% sucrose (Sigma-Aldrich) overnight at 4 °C. On **Day 3**, the samples were embedded in Tissue-Tek O.C.T. Compound (SAKURA) on dry ice and sectioned at 10 µm (thin sections) or 80 µm (thick sections) at -22 °C using a cryostat (Leica CM1950).

Thin frozen sections

On **Day 3**, after sectioning, the sections were thawed at RT, then permeabilized 3×5 min in PBT at RT and blocked in 5% BSA in PBT for 90 min in a humidified chamber at RT. Afterward, the sections were stained with primary antibodies (**Table 4.2**) diluted in 1% BSA in PBT overnight at 4 °C. On **Day 4**, the sections were washed in PBT and then incubated with secondary antibodies (**Table 4.3**) diluted in the same solution as the primary antibodies for 1 h at RT. For F-actin staining, Alexa Fluor 568 phalloidin (Thermo Fisher, A12380) was added to this solution (1:2000 dilution). The sections were washed 3×5 min (second wash – DAPI in PBT) and mounted with Mowiol 4-88 on a microscopy glass. Fluorescent images were acquired using Olympus SpinSR10.

Thick frozen sections

On **Day 3**, after sectioning, the sections were placed into a well and permeabilized in 0.5% Triton X-100 in PBS for 30 min at RT. The sections were then blocked by 5% BSA in 0.5% Triton X-100 in PBS for 1 h at RT and stained with a primary antibody (**Table 4.2**) solution (primary antibodies diluted in 1% BSA in 0.5% Triton X-100 in PBS) for 2 days at 4 °C. On **Day 5**, the sections were washed and incubated with secondary antibodies (**Table 4.3**) diluted in the same solution as the primary antibodies overnight at 4 °C. On **Day 6**, after washing 3×15 min (second wash – DAPI in 0.5% Triton X-100 in PBS), the sections were mounted on a microscopy glass using Mowiol 4-88 mountant. Fluorescent images were acquired using Olympus SpinSR10.

Table 4.2 List of all primary antibodies used for fluorescent immunohistochemistry.

Primary Antibody	Host Animal	Dilution	Product Code	Source
Anti-Acetylated tubulin	mouse	1:1000	T6793	Sigma-Aldrich
Anti-Arl13b	rabbit	1:1000	17711-1-AP	Proteintech
Anti-Cas3	rabbit	1:1000	9664	Cell Signaling
Anti-Dishevelled2	rabbit	1:1000	3216	Cell Signaling
Anti-Foxf1	goat	1:2000	AF479	R&D

Anti-Msx1	goat	1:2000	AF5045	R&D
Anti-Pax3	mouse	1:2000	AB_528426	DSHB
Anti-PH3	rabbit	1:2000	06-570	Sigma-Aldrich
Anti-Prickle1	rabbit	1:1000	ab15577	Abcam
Anti-Sox9	rabbit	1:2000	AB5535	Millipore
Anti-Twist1	mouse	1:2000	sc-81417	Santa Cruz
Anti-Vangl2	rat	1:1000	MABN750	Milipore

Table 4.3 List of all secondary antibodies used for fluorescent immunohistochemistry.

Secondary Antibody	Host Animal	Dilution	Product Code	Source
Anti-goat Alexa Fluor 647	donkey	1:500	A21447	Thermo Fisher
Anti-rabbit Alexa Fluor 647	donkey	1:500	A31573	Thermo Fisher
Anti-rabbit Alexa Fluor 488	donkey	1:500	A21206	Thermo Fisher
Anti-rabbit Alexa Fluor 568	donkey	1:500	A10042	Thermo Fisher
Anti-rat Alexa Fluor 488	donkey	1:500	A21208	ThermoFisher
Anti-mouse Alexa Fluor 568	donkey	1:500	A10037	Thermo Fisher
Anti-mouse Alexa Fluor 647	donkey	1:500	A31571	Thermo Fisher

4.5 EdU Proliferation Assay

Pregnant mice were injected intraperitoneally with 5-ethynyl-2'-deoxyuridine (EdU) (1.25 mg EdU in 0.125 ml PBS per mouse) for either 2 h or 72 h before embryo harvesting.

Following fluorescent immunostaining, the sections were refixed with 4% PFA in PBS for 15 min at RT, permeabilized in 0.5% Triton X-100 in PBS for 20 min at RT, blocked in 3% BSA in PBT for 30 min at RT and washed 2×5 min in PBT (all done in a humidified chamber at RT). The sections were then stained using an EdU BaseClick kit, according to the manufacturer's instructions (incubated for 30 min at RT). After washing 3×10 min in PBT (second wash – DAPI in PBT) at RT, the sections were mounted on a microscopy glass with Mowiol 4-88. Fluorescent images were acquired using Olympus SpinSR10.

4.6 Whole-mount Skeletal Staining

On **Day 1**, embryos were isolated at E17.5, genotyped, and scalded in 65°C tap water for 30 s, facilitating tissue maceration. Then, embryos had their skin, eyes, and internal organs removed mechanically. The samples were placed into scintillation vials and fixed in 96% ethanol overnight at RT. On **Day 2**, the samples were immersed in acetone (Penta) overnight at RT. On **Day 3**, cartilaginous structures were stained by incubating the embryos in Alcian blue solution (**Table 4.4**) overnight at RT. On **Day 4**, the samples were washed 2×30 min in 70% ethanol and placed in 96% ethanol overnight at RT. On **Day 5**, the tissue was pre-cleared in 1% KOH (Penta) for 1 h at RT. The KOH solution was replaced with an Alizarin red stain (**Table 4.5**) to stain the bone for 4 h at RT. The embryos were immersed in 50% glycerol (Penta) in 1% KOH solution until cleared. Finally, the samples were placed in 100% glycerol and images were taken using a binocular microscope Olympus SYX9 and camera Olympus DP72.

Table 4.4 Alcian Blue Stain.

Reagent	Concentration [%]
Alcian Blue 8GX (Sigma-Aldrich)	0.03
Ethanol	80
Glacial acetic acid	20

Table 4.5 Alizarin Red Stain.

Reagent	Concentration [%]
Alizarin Red S (Sigma-Aldrich)	0.005
KOH	1
dH_2O	N/A

4.7 HCR FISH

The embryos were processed according to the manufacturer's protocol (Molecular Instrument) with adjustments. Probe hybridization buffer, probe wash buffer, amplification buffer, probes, and hairpins were included in the HCR™ RNA FISH bundle commercial kit.

On **Day 1**, the heads of isolated embryos were fixed with 4% PFA in PBS overnight at 4 °C. On **Day 2**, samples were washed 3×5 min in PBS, dehydrated by ascending methanol (Penta) series (up to 100%), and stored at -20 °C until use. On **Day 3** of the experiment, the samples were rehydrated by descending methanol series on dry ice and washed with 0.1% TWEEN 20 (Sigma-Aldrich) in PBS (PBST) for 10 min at RT. Then, embryonic heads were treated with proteinase K solution (Thermo Fisher) (1 µl of 20 mg/ml proteinase K in 2 ml PBST) for 15 min at RT and postfixed with 4% PFA for 20 min at RT. After fixation, the samples were washed 3×5 min in PBST and incubated in the probe hybridization buffer for 5 min at RT. Then, the samples were pre-hybridized with probe hybridization buffer for 30 min at 37 °C (ProBlot™ 6 Hybridization Oven, Labnet). After pre-hybridization, the samples were incubated in a probe solution (2 pmol of each probe set in probe hybridization buffer) overnight at 37 °C. The probes used are listed in **Table 4.6**. On **Day 4**, excess probes were removed by washing samples 4×15 min in probe wash buffer at 37 °C. Then, samples were washed 2×5 min in 5 × sodium chloride citrate (Sigma-Aldrich) in 0.1% TWEEN 20 (5×SSCT). After washing, the samples were pre-amplified with an amplification buffer for 5 min at RT. Hairpin h1 solution (5 µl of each 3µM hairpin h1 stock) and hairpin h2 solution (5 µl of each 3µM hairpin h2 stock) were prepared separately by heating at 95 °C for 90 s in a PCR cycler and then snap-cooled. The hairpin solution was prepared by adding both cooled hairpin h1 solution and hairpin h2 solution into 500 µl amplification buffer (total concentration 15 pmol) at RT. The samples were incubated in the hairpin solution overnight at RT protected from light. On **Day 5**, the samples were washed

2×5 min, 2×30 min, and 1×5 min in 5×SSCT at RT. After removing the excess hairpins by washing, the samples were treated with 30% sucrose at 4 °C overnight. On **Day 6**, the samples were embedded in O.C.T. Compound on dry ice and sectioned at 80 µm thick sections at -22 °C using a cryostat. Last, the sections were transferred on glass slides and mounted with Mowiol 4-88. Fluorescent images were acquired using Olympus SpinSR10.

Table 4.6 List of probes used for HCR FISH.

Target Gene	Probe Type	Hairpin Type	Fluorophore
Axin2	B2	B2	Alexa Fluor 568
Bmp4	B1	B1	Alexa Fluor 488
Wnt5a	B3	B3	Alexa Fluor 647

4.8 Image analysis and statistics

Quantification of proliferation in the FNP was performed on two biological replicates, which consisted of littermates obtained from separate mothers. Each biological replicate included one control embryo and one *Wnt5a* cKO embryo. Two independent experiments were carried out. Four sections from each from each specimen were analyzed. For proliferation rate analysis, the cells were counted manually using the multi-point feature in ImageJ. Percentages of EdU^+DAPI^+ cells relative to the total DAPI-stained cells in the FNP were presented as mean ± standard deviation (SD). Likewise, percentages of EdU^+Sox9^+ cells relative to $Sox9^+$ cells in the FNP were presented as mean ± SD. Statistical analysis was performed using a Student's t-test.

Apoptosis activity analysis in the FNP was performed on two biological replicates, which consisted of littermates obtained from separate mothers. Each biological replicate included one control embryo and one *Wnt5a* cKO embryo. Two independent experiments were carried out. Eight sections from each from each specimen were analyzed. To analyze apoptotic activity, both the apoptotic area and the FNP area were measured manually using the polygon selection feature in ImageJ. The apoptotic area was marked by outlining the outermost Cas^+ cells of the stereotypical apoptotic region observed within the FNP. Percentages of apoptotic area relative to the FNP area were presented as mean ± SD. Statistical analysis was performed using a Student's t-test.

Analysis of the direction of cell division in the FNP and PA1 was performed on two biological replicates, which consisted of littermates obtained from separate mothers. Each biological replicate included one control embryo and one *Wnt5a* cKO embryo. Two independent experiments were carried out. Eight sections from each from each specimen were analyzed. To assess the directionality of cell division, the orientation of the division axes was measured manually. The degree values, ranging from -90° to +90°, indicating the deviation of the division axis from the reference line, were measured using the straight line selection tool in ImageJ. The measurement was performed on $PH3^+$ cells within the FNP and the PA1 areas.

Analysis of primary cilia orientation in the FNP and PA1 was conducted on one biological replicate, which consisted of one control and one *Wnt5a* cKO embryo littermate. Nine sections from each specimen were analyzed. To analyze the primary cilia polarity, the orientation of the primary cilia was measured manually. The degree values, indicating the deviation of orientation of the primary cilium from the reference line, were measured by connecting the center of the nucleus with the cilium using the straight line selection tool in ImageJ. The measurement was performed on 250-300 cells in each of the proximal and distal regions of both the FNP and PA1 for each section.

5 Results

5.1 Generation of *Wnt5a* cKO Mouse and Its Phenotype

This study utilized a mouse model, in which the *Wnt5a* gene was selectively inactivated in NCCs, to investigate its role in craniofacial development. We employed the Cre/loxP system, which has been widely used among researchers for precise spatial and temporal control over gene expression. Through the action of Cre recombinase, recombination occurs between loxP recognition sites, enabling precise DNA rearrangements. Various NC-specific promoters have been identified, leading to the development of several Cre transgenic mouse lines for targeted genetic manipulation in the NC. Among these lines, the *Wnt1-Cre* mouse line has been frequently utilized for NC-specific KO studies. However, ectopic activation of the Wnt1 signaling pathway has been discovered in this Wnt1-Cre transgenic mouse (Lewis et al., 2013). To address this issue, the *Wnt1-Cre2* transgenic mouse line has been developed, with the absence of ectopic *Wnt1* expression while maintaining effectiveness for NC-specific KO studies (Lewis et al., 2013). For its advantages, we used the *Wnt1-Cre2* mouse line and crossed it with $Wnt5a^{fl/fl}$ strain to generate embryos with *Wnt5a* deletion in cranial NCCs (**see Fig. 5.1**).

To gain insight into the spatial distribution and activity of the Cre recombinase within the embryo, we utilized the *Wnt1-Cre2*; mTmG mouse line, which is a reporter of Cre activity. The activity was observed in mesenchymal cells forming craniofacial region (specifically, FNP and PA1) in E11.5 (**Fig. 5.1 A-A'**). To assess the spatial distribution of *Wnt5a* expression, we performed HCR FISH, which revealed that, in the E11.5 embryonic head, *Wnt5a* was expressed in a distal-proximal gradient in both, the FNP and PA1 (**Fig. 5.1 B-B'**). The *Wnt5a* cKO mutants carried a transgene expressing Cre-recombinase NC-specifically (**Fig. 5.1 C**) and two floxed Wnt5a alleles (**Fig. 5.1 D**). In contrast to *Wnt5a* KO embryos, which were reported to display significant embryonic patterning deficits such as dwarfism, shortened axis, and limb abnormalities (Yamaguchi et al., 1999), *Wnt5a* cKO (*Wnt1-Cre2*; $Wnt5a^{fl/fl}$) embryos exhibited normal anterior-posterior axis, limb, and tail structures (**Fig. 5.1 E-F**). However, they showed craniofacial abnormalities (**Fig. 5.1 E-F**) like *Wnt5a* KO embryos (Yamaguchi et al., 1999).

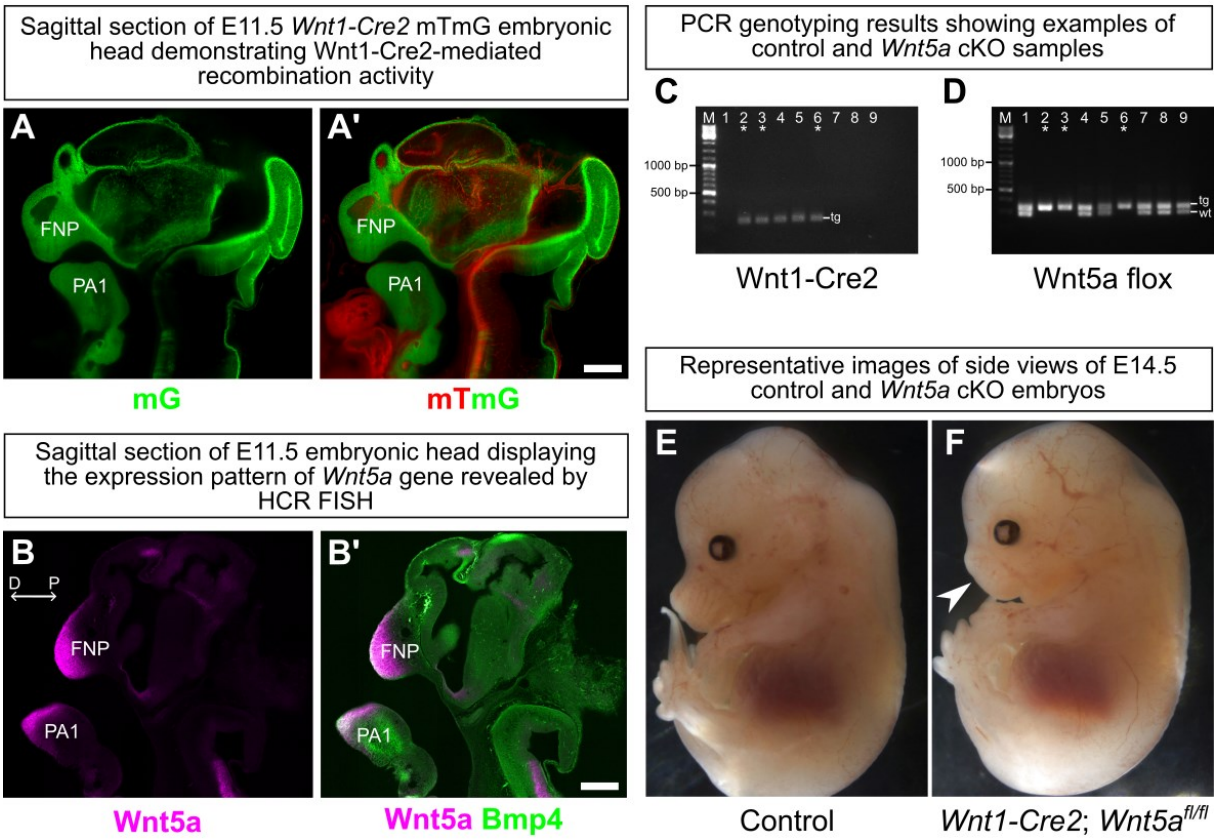

Figure 5.1 Generation of Wnt5a cKO mouse. *(**A**) Optical sagittal section of E11.5 Wnt1-Cre2 mTmG mouse embryonic head, showing recombination activity mediated by Wnt1-Cre2 (green), which also represents the NC origin of the tissue. All non-NC-derived tissues are shown in red. Magnification: 20×. (**B**) Fixed frozen thick sagittal section of E11.5 embryonic head, displaying the expression pattern of Wnt5a gene (magenta), using HCR FISH. For spatial*

context, the section is counterstained with Bmp4 (green). Magnification: 20×. Distal-proximal axis is shown (double-arrowed white line). ***(C and D)*** *Genotyping results from control and Wnt5a cKO (white asterisks) samples. PCR genotyping for Wnt1-Cre2 (C) and Wnt5a floxed allele (D) is shown.* ***(E and F)*** *Side views of representative samples of E14.5 control (E) and Wnt5a cKO (F) embryos. Mind the shortened frontonasal region (white arrowhead).* ***Abbreviations****:* ***FNP*** *– frontonasal process,* ***PA1*** *– first pharyngeal arch. Scalebars: 500 µm.*

To investigate the changes in craniofacial chondroskeletal phenotypes in *Wnt5a* cKO embryos, we performed Alcian Blue and Alizarin Red staining on E17.5 embryos to compare control (**Fig. 5.2 A-D**) and *Wnt5a* cKO (**Fig. 5.2 E-H**) embryonic skulls. We observed severely shortened facial region in the mutant in comparison to the control (**Fig. 5.2 A, E**). Moreover, a remarkable reduction in the *premaxilla* and *presphenoid,* along with abnormal patterning of *basisphenoid* and *maxilla*, was evident in the mutant (**Fig. 5.2 B, F**). Moreover, the *Wnt5a* mutant displayed mandibular hypoplasia (*micrognathia*) (**Fig. 5.2 C, G**). Major size reduction was also detected in nasal bone and nasal cartilage in the mutant compared to the control (**Fig 5.2 D, H**). Furthermore, fusion failure was observed in the mutant, i.e. cleft palate (**Fig. 5.2 F**) and bifid nasal cartilage (**Fig. 5.2 F, H**).

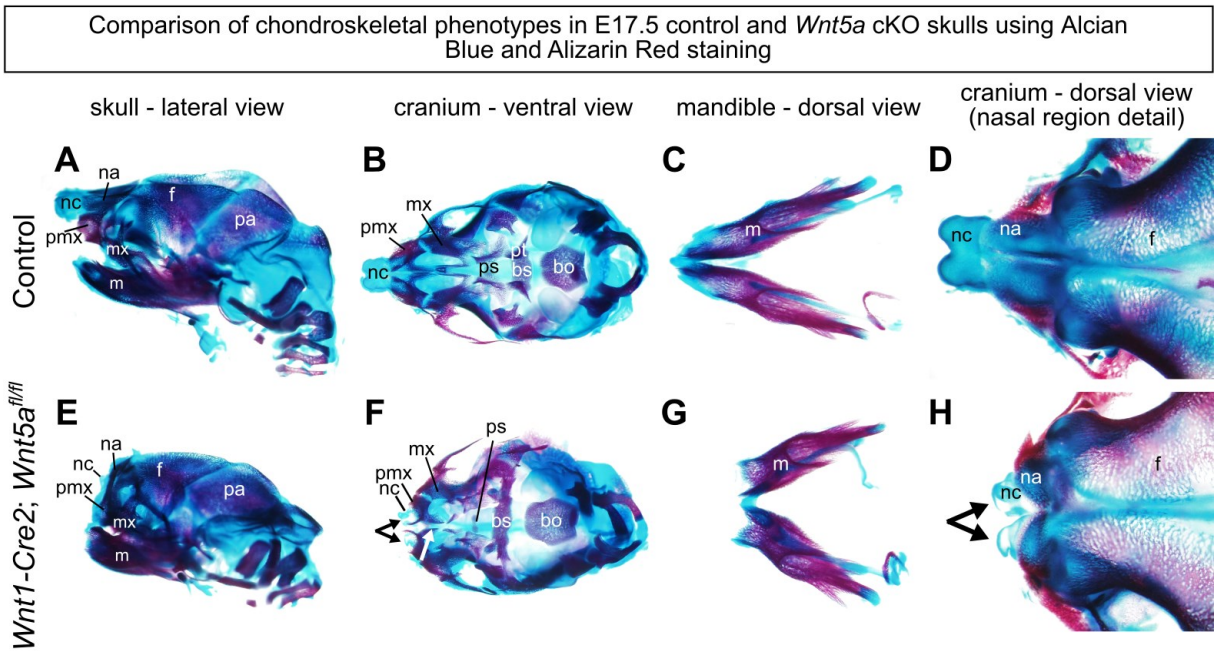

Figure 5.2 Chondroskeletal phenotypes of control and Wnt5a cKO E17.5 embryonic skulls*. (**A-H**) Alcian Blue and Alizarin Red staining results of E17.5 control (A-D) and Wnt5a cKO (E-H) embryos, comparing the cartilage (blue) and bone tissue (purple) between the samples. (**A and E**) Lateral views of control (A) and Wnt5a cKO (E) skulls. Note the abnormal facial region*

*of the mutant skull (E). (**B and F**) Ventral views of control (B) and Wnt5a cKO (F) crania. Note the reduced premaxilla, cleft palate (white arrowed line), and bifid, shortened nasal cartilage (black arrowed line) in the mutant (F). (**C and G**) Dorsal views of control (C) and Wnt5a cKO (G) mandibles. Observe the widening and size reduction of the mutant mandible (G). (**D and H**) Dorsal views of control (D) and Wnt5a cKO (H) crania, with nasal regions in detail. Examine the reduced nasal bone and the shortened, bifid nasal cartilage in the mutant sample (H). Results from four biological replicates, which consisted of littermates obtained from separate mothers, are shown. Each biological replicate included one control embryo and one mutant embryo. **Abbreviations**: **bo** – basioccipital, **bs** – basisphenoid, **f** – frontal, **m** – mandible, **mx** – maxilla, **na** – nasal, **nc** – nasal cartilage, **pa** – parietal, **pmx** – premaxilla, **ps** – presphenoid, **pt** – pterygoid.*

5.2 Analysis of Selected Cell Populations Across Development

Next, we aimed to investigate cellular dynamics at earlier developmental stages to explore the underlying mechanisms contributing to the abnormal craniofacial construction in *Wnt5a* cKO samples revealed in our studies of E17.5 control and *Wnt5a* cKO skulls. Therefore, we analyzed the expression patterns of various cell populations that are associated with craniofacial development by immunostaining in control and *Wnt5a* cKO embryos at developmental stages E11.5, E12.5, and E13.5.

During our examination, we focused on the role of Sox9 which is a marker of precartilage condensations and chondrocytes (Bi et al., 1999). These $Sox9^{+}$ mesenchymal condensations serve as the framework for the cartilaginous scaffold that shapes the facial bones, ultimately determining the morphology of the face as it develops (Grüneberg, 1963; Kaucka et al., 2017). Next, we analyzed Twist1, a transcription factor, that fundamentally contributes to craniofacial development by regulating the acquisition of mesenchymal properties in cranial NCCs and guiding their differentiation into facial structures (Bialek et al., 2004; Bildsoe et al., 2009; Soldatov et al., 2019). In addition, we studied the expression of Foxf1, a transcription factor involved in proper palate formation (J. Xu et al., 2016), NC-derived cartilage construction (P. Xu et al., 2018), and tooth development (J. Xu et al., 2016).

Our analysis revealed no significant changes in Twist1 and Foxf1 expression between *Wnt5a* cKO and control embryos across the examined developmental stages. Twist1 exhibited consistent expression patterns in both groups, primarily in distal regions of the FNP and PA1 at E11.5 (**Fig. 5.3 A, D**), extending to other facial structures, including distal nasal process, distal

mandible, palate, and tongue, in subsequent stages (**Fig. 5.3 B, C, E, F**). Similarly, Foxf1 expression remained unaffected, predominantly localized in the proximal PA1 in E11.5 (**Fig. 5.3 A, D**), extending across palate, tongue, and tooth primordia regions at the following stages of development (**Fig. 5.3 B, C, E, F**). In contrast, notable alterations were observed in Sox9 expression. In *Wnt5a* cKO embryos, Sox9-labeled precartilage condensations exhibited severe shortening and distorted morphology at E11.5 (**Fig. 5.3 D**), becoming more pronounced at E12.5 (**Fig. 5.3 E**), indicating impaired growth compared to control counterparts. By E13.5, the cartilaginous structures in the nasal region appeared deformed and disorganized in *Wnt5a* cKO (**Fig. 5.3 F**), indicative of disrupted development of cartilage primordium of the nasal bone.

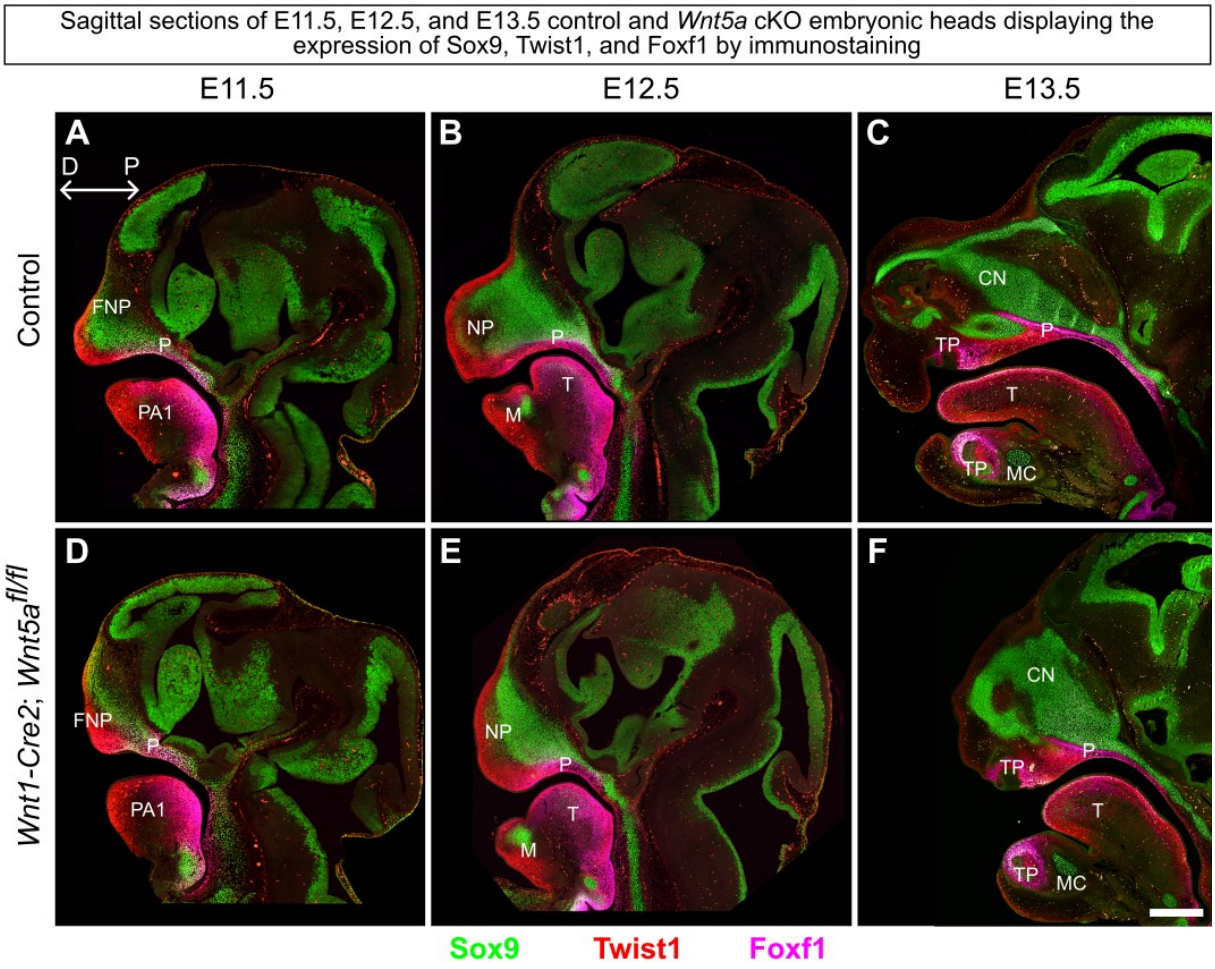

Figure 5.3 Analysis of selected cell populations in the craniofacial area in control and Wnt5a cKO embryos across developmental time points (E11.5-E13.5). *Immunostaining of fixed paraffin sections of control (**A-C**) and Wnt5a cKO (**D-F**) embryonic heads at different stages of development: E11.5 (A and D), E12.5 (B and E), E13.5 (C and F), demonstrating the expression patterns of selected cell populations. Sox9 antibody (green) was used to label prechondrogenic condensations (A, B, D, E) and chondrocytes (C-F). Twist1 (red) and FoxF1*

(magenta) antibodies were utilized to mark the localization of two distinct NC-derived mesenchymal subpopulations (Twist1$^+$ and Foxf1$^+$). Magnification: 20×. Distal-proximal axis is shown (double-arrowed white line). Results from three biological replicates, which consisted of littermates obtained from separate mothers, are shown. Each biological replicate included one control embryo and one mutant embryo. ***Abbreviations****:* ***FNP*** *– frontonasal process,* ***CN*** *– cartilage primordium of the nasal bone,* ***NP*** *– nasal process,* ***M*** *– mandible* ***MC*** *– Meckel's cartilage,* ***P*** *– palate,* ***PA1*** *– first pharyngeal arch,* ***T*** *– tongue,* ***TP*** *– tooth primordium. Scalebar: 500 μm.*

Next, we wanted to examine the expression of Msx1, as several studies confirm its key role in craniofacial morphogenesis. To be more specific, Msx1 contributes to proper palate fusion, formation of the maxillary and mandibular processes, and tooth development (Medio et al., 2012; Satokata & Maas, 1994). Given the involvement of Msx1 craniofacial development, we aimed to explore potential changes in Msx1 expression in *Wnt5a* cKO samples, as they exhibit defects including cleft palate and maxillary and mandibular dysplasia. To analyze the expression of Msx1, we performed immunostaining on control and *Wnt5a* cKO E11.5 and E12.5 samples (**Fig. 5.4**), using Msx1 antibody.

Our data revealed that, in control and *Wnt5a* cKO samples, Msx1 expression was prominent in the distal parts of both the FNP and PA1 at E11.5 (**Fig. 5.4 A, C**) and in the nasal process and mandible at E12.5 (**Fig. 5.4. B, D**). However, in *Wnt5a* cKO embryos at E12.5, a reduction in the Msx1$^+$ population was detected specifically in the distal mandibular region (**Fig. 5.4 D**). Nonetheless, the expression localization and pattern of Msx1 in other regions appeared to be unaffected in the mutant samples, suggesting localized rather than widespread alterations in the Msx1$^+$ population patterning.

Sagittal sections of E11.5 and E12.5 control and *Wnt5a* cKO embryonic heads showing the expression of Msx1 by immunostaining

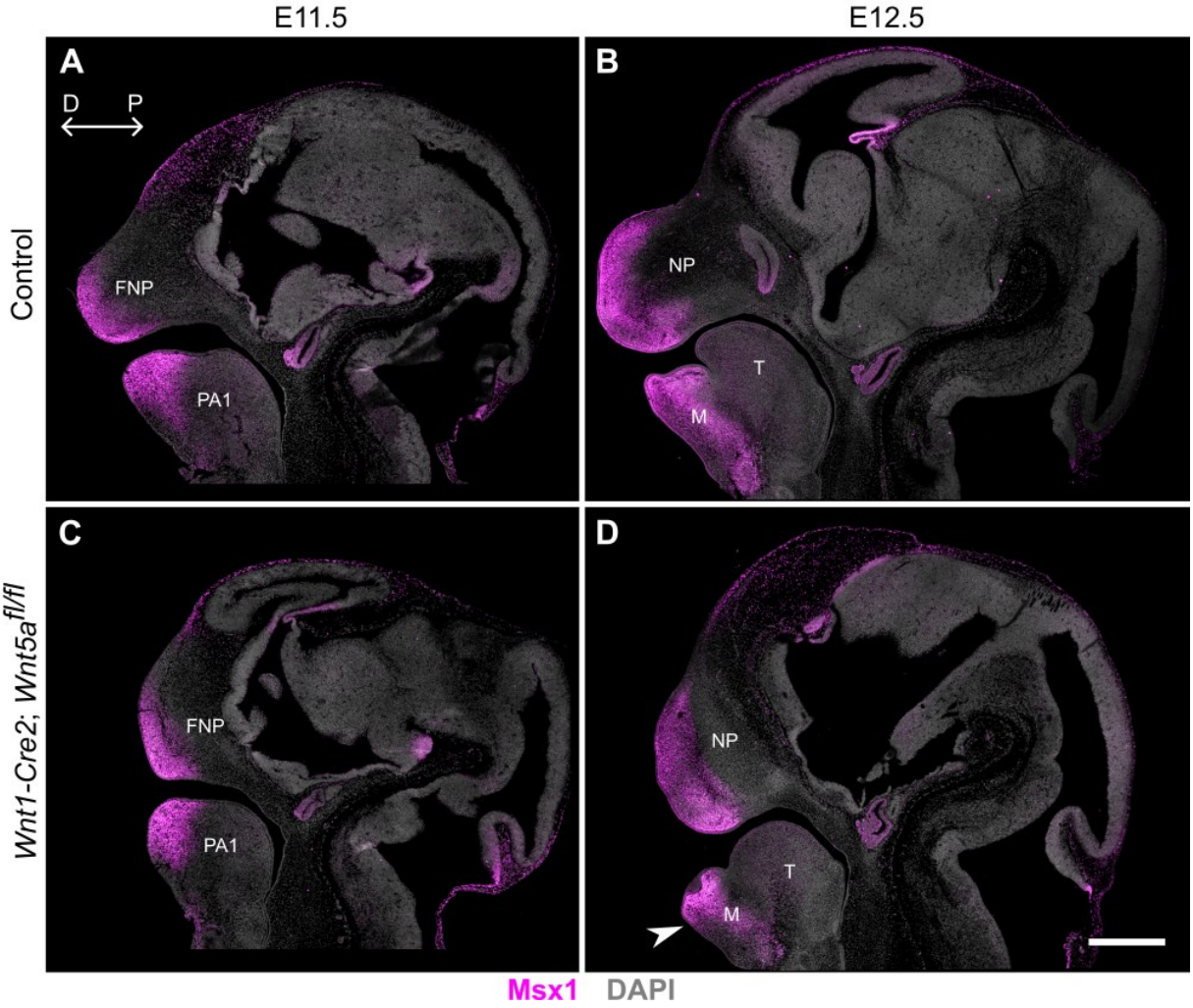

Figure 5.4 Analysis of Msx1 population in the craniofacial region in control and Wnt5a cKO embryos across developmental time points (E11.5-E12.5). *Immunostaining of fixed paraffin sections of control (**A-B**) and Wnt5a cKO (**C-D**) embryonic heads at different developmental stages: E11.5 (A and C) and E12.5 (B and D). Note the reduction of Msx1 expression in the distal mandibular region in Wnt5a cKO at stage E12.5 (D, white arrowhead). For spatial context, the sections are counterstained with DAPI (gray). Magnification: 20×. Distal-proximal axis is shown (double-arrowed white line). Results from three biological replicates, which consisted of littermates obtained from separate mothers, are shown. Each biological replicate included one control embryo and one mutant embryo.* ***Abbreviations****: **FNP** – frontonasal process, **NP** – nasal process, **M** – mandible **PA1** – first pharyngeal arch, **T** – tongue. Scalebar: 500 μm.*

Furthermore, we investigated the expression patterns of Pax3 due to its essential involvement in craniofacial region formation. Ablation of *Pax3* results in frontonasal dysplasia and clefting in mice (Zalc et al., 2015). As defects in the development of the frontonasal region along with clefting are also observed in the *Wnt5a* cKO embryos, we wanted to examine potential alterations in Pax3 expression in *Wnt5a* cKO samples. To analyze the expression of Pax3, we performed Pax3-based immunostaining on control and *Wnt5a* cKO E11.5 and E12.5 samples (**Fig. 5.5**).

Our results demonstrated prominent Pax3 expression in the distal regions of the FNP and the PA1 at E11.5 in both control (**Fig. 5.5 A**) and *Wnt5a* cKO (**Fig. 5.5 C**) embryos. Similarly, at the E12.5 stage, Pax3 expression persisted in the nasal process and mandible in both experimental groups (**Fig. 5.5 B, D**). However, a slight reduction in the Pax3 expression pattern was detected in the distal mandibular region in *Wnt5a* cKO embryos at E12.5 (**Fig. 5.5 D**). Despite this localized alteration, Pax3 expression pattern and localization in other regions remained largely unaltered in the *Wnt5a* cKO samples.

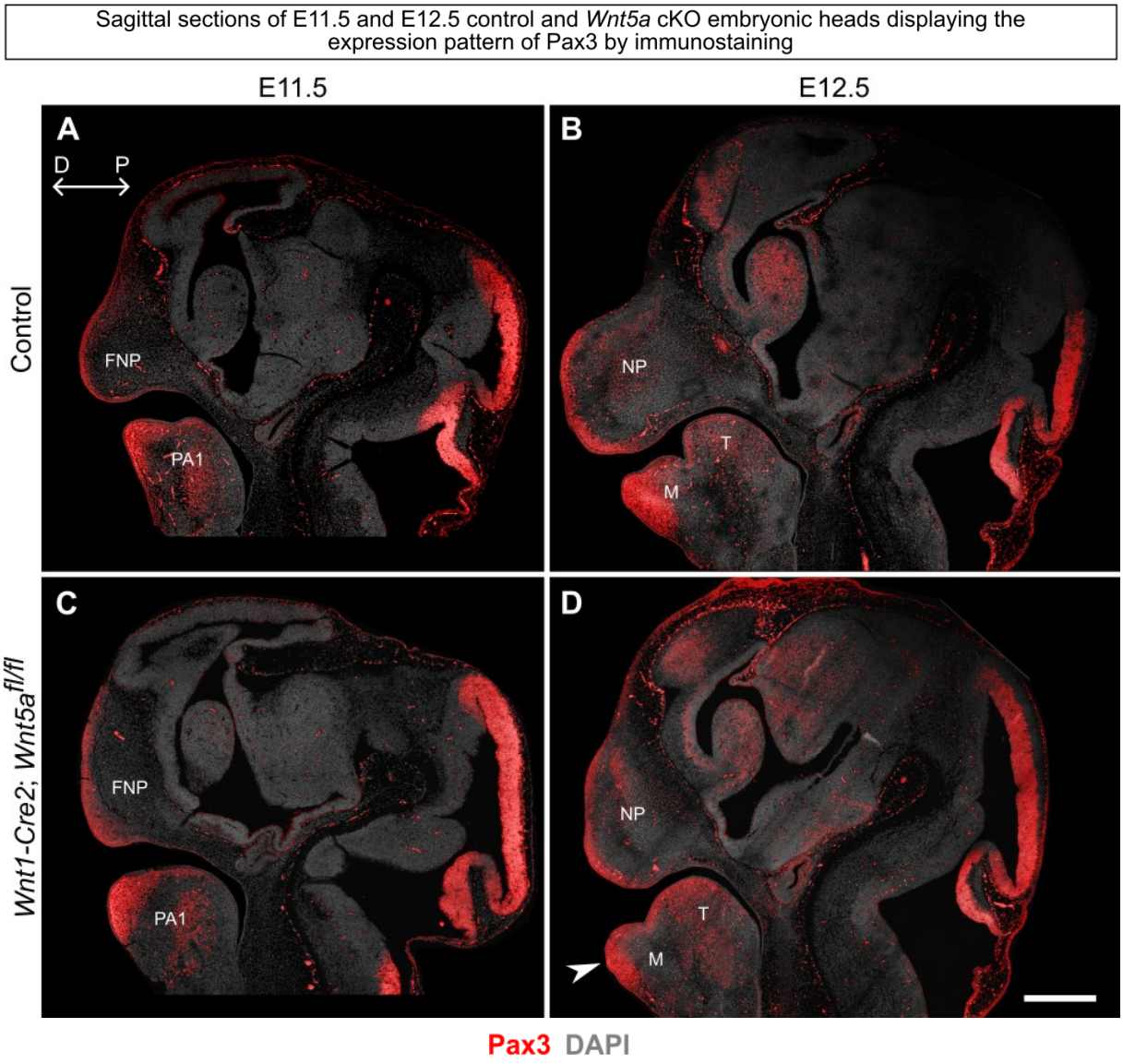

Figure 5.5 Analysis of Pax3 population in the facial area in control and Wnt5a cKO embryos across developmental time points (E11.5-E12.5). *Immunostaining of fixed paraffin sections of control (**A-B**) and Wnt5a cKO (**C-D**) embryonic heads at different developmental stages: E11.5 (A and C) and E12.5 (B and D). Note the reduction of Pax3 expression in the distal mandibular region in Wnt5a cKO at stage E12.5 (D, white arrowhead). For spatial context, the sections are counterstained with DAPI (gray). Magnification: 20×. Distal-proximal axis is shown (double-arrowed white line). Results from three biological replicates, which consisted of littermates obtained from separate mothers, are shown. Each biological replicate included one control embryo and one mutant embryo.* ***Abbreviations****: **FNP** – frontonasal process, **NP** – nasal process, **M** – mandible, **PA1** – first pharyngeal arch, **T** – tongue. Scalebar: 500 µm.*

To summarize, our analysis of expression patterns of selected proteins essential for craniofacial development (Sox9, Twist1, Foxf1, Msx1, and Pax3) revealed that *Wnt5a* cKO embryos exhibited several alterations. In *Wnt5a* cKO samples, severe changes were detected in $Sox9^{+}$ population patterning, indicating disrupted precartilage condensation formation and subsequent craniofacial defects. Moreover, at the E12.5 stage, a reduction in Msx1 and Pax3 expression in the distal mandibular region was observed in the *Wnt5a* cKO samples. However, it is important to note that by this stage, significant changes in the morphology of the mandibular area were already evident. Therefore, differences in the spatial distribution of $Msx1^{+}$ and $Pax3^{+}$ cells could be a reflection of morphological abnormalities observed in *Wnt5a* cKO embryos. Additionally, expression levels or patterns of Twist1 and Foxf1 remained largely unaffected in *Wnt5a* cKO embryos. Overall, as embryonic development progresses, the disruptions in numerous cell populations, as well as in the abnormal face shape, were more severe in the *Wnt5a* cKO embryos. Therefore, in further research, we shifted our focus to the E11.5 embryonic stage to investigate the early changes in cellular behavior that happen in *Wnt5a* cKO embryos.

5.3 Wnt/β-catenin Components Are Not Altered in E11.5 *Wnt5a* cKO Facial Region

In the following analysis, we aimed to investigate the activity of β-catenin-mediated Wnt signaling in *Wnt5a* cKO and control mouse embryos at E11.5. Canonical and noncanonical Wnt signaling pathways have been shown to interact and modulate each other's activity (discussed in **Chapters 2.2.2.** and **2.3.1.**), which led us to explore potential alterations in Wnt/β-catenin signaling in the absence of Wnt5a.

To assess the activity of Wnt/β-catenin signaling, we employed a combination of molecular techniques targeting key components of the pathway. Specifically, we performed HCR FISH to visualize the expression of *Axin2*, an established target gene of β-catenin-mediated signaling. Additionally, we utilized immunostaining techniques to detect the expression and localization of two transcription factors associated with canonical Wnt signaling: Lef1 and Tcf7l2. Axin2 serves as a robust marker for β-catenin activation, as its expression is directly induced upon activation of the canonical Wnt pathway (Jho et al., 2002). Lef1 and Tcf7l2 are transcription factors that act downstream of β-catenin and are essential for coordinating the transcriptional response to Wnt signaling, influencing various cellular processes critical for embryonic development.

Upon analysis of *Axin2*, Lef1, and Tcf7l2 expression patterns in the facial region of *Wnt5a* cKO and control embryos (**Fig 5.6**), we did not observe any distinguishable differences in either the intensity or localization of these markers between the mutant and control groups. Interestingly, *Axin2* (**Fig. 5.6. (A-B**) and Lef1 (**Fig. 5.6 C-D**) exhibited expression predominantly in the distal region of both, the FNP and PA1, in control and *Wn5a* cKO samples, suggesting potential coexpression and activation of β-catenin signaling in those areas. In contrast, Tcf7l2 expression was observed in the more proximal region of both, the FNP and PA1, in control and *Wnt5a* cKO samples (**Fig. 5.6 E-F**). Notably, it was this Tcf7l2 population in the FNP, that displayed major proximal-distal shortening, in the *Wnt5a* cKO embryo (**Fig. 5.6 F**), although its localization was comparable with the control sample (**Fig. 5.6 E**). This suggests that, in *Wnt5a* cKO, $Tcf7l2^{+}$ cell population shortening might be a reflection of disrupted FNP morphology already evident at the E11.5 stage.

Sagittal sections of E11.5 control and *Wnt5a* cKO embryonic heads visualizing the expression of Axin2 by HCR FISH

Control | *Wnt1-Cre2*; *Wnt5a*$^{fl/fl}$

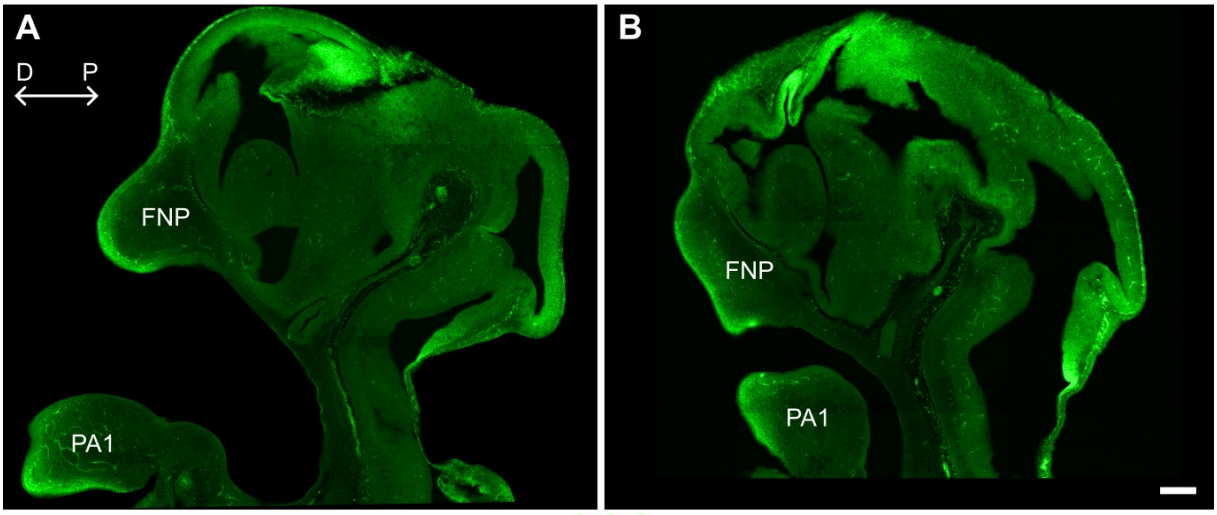

Axin2

Sagittal sections of E11.5 control and *Wnt5a* cKO embryonic heads showing the expression pattern of Lef1 by immunostaining

Control | *Wnt1-Cre2*; *Wnt5a*$^{fl/fl}$

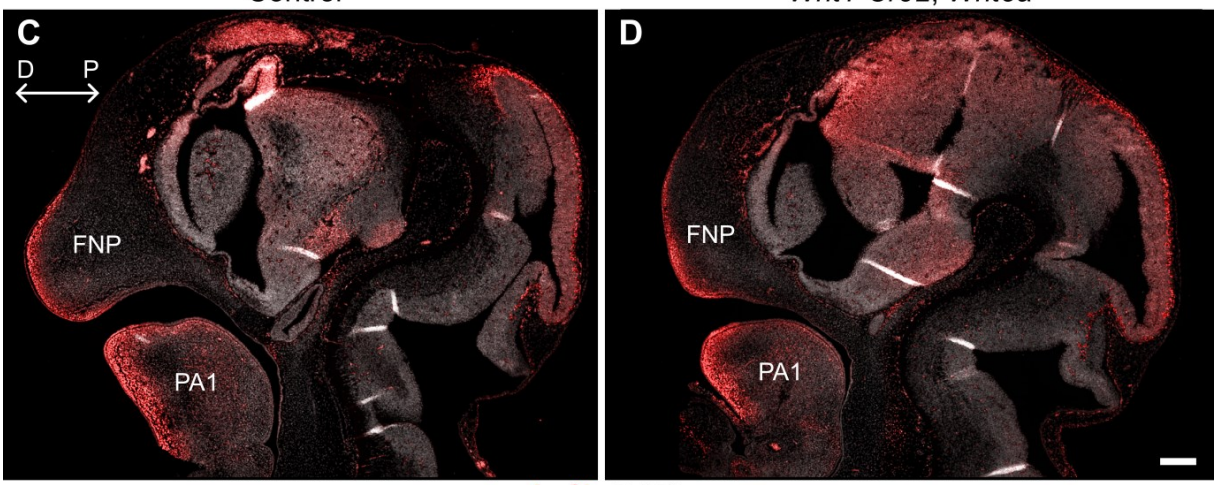

Lef1 **DAPI**

Sagittal sections of E11.5 control and *Wnt5a* cKO embryonic heads demonstrating the expression of Tcf7l2 by immunostaining

Control | *Wnt1-Cre2*; *Wnt5a*$^{fl/fl}$

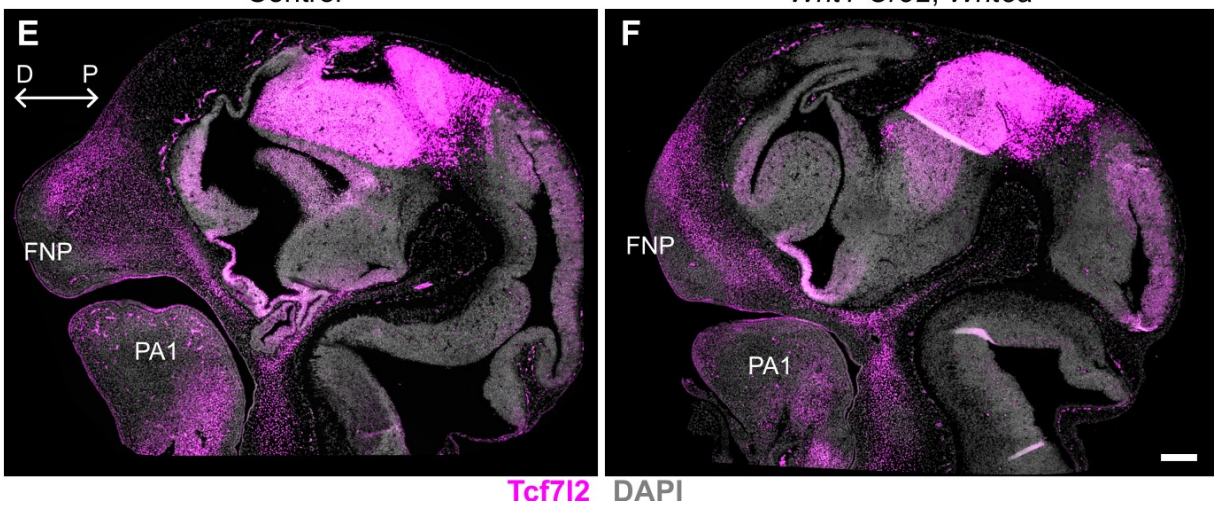

Tcf7l2 **DAPI**

Figure 5.6 Analysis of canonical Wnt signaling cascade in the facial area in control and Wnt5a cKO E11.5 embryos. *(**A-B**) Fixed frozen thick sagittal sections of E11.5 embryonic control (A) and Wnt5a cKO (B) heads, demonstrating the expression pattern of the Axin2 gene (green) using the HCR FISH method. (**C-D**) Immunostaining of fixed paraffin sagittal sections of E11.5 embryonic control (C) and Wnt5a cKO (D) head, illustrating the expression of Lef1 (red). For spatial context, the sections are counterstained with DAPI (gray). (**E-F**) Immunostaining of fixed paraffin sagittal sections of E11.5 embryonic control (E) and Wnt5a cKO (F) head, showing the expression of Tcf7l2 (magenta). For spatial context, the sections C-F are counterstained with DAPI (gray). Magnification: 20×. Distal-proximal axes are shown (double-arrowed white lines). Results from two biological replicates, which consisted of littermates obtained from separate mothers, are shown. Each biological replicate included one control embryo and one mutant embryo. **Abbreviations**: **FNP** – frontonasal process, **PA1** – first pharyngeal arch. Scalebars: 200 µm.*

5.4 Proliferation Rate Is Decreased in the FNP of E11.5 *Wnt5a* cKO

Next, we conducted an analysis of proliferation activity within the FNP in E11.5 *Wnt5a* cKO and control embryos, using the EdU proliferation assay (**Fig. 5.7 A-B**). This investigation was prompted by the observed reduction in size of the FNP in *Wnt5a* cKO mouse embryos compared to controls. Given the known role of proliferation in tissue growth and development, we hypothesized that alterations in proliferation activity could have contributed to the observed size difference.

To comprehensively assess proliferation, we analyzed two distinct cell populations within the FNP (**Fig. 5.7 C**). Firstly, we quantified proliferation in all mesenchymal cells by evaluating the proportion of EdU-labeled cells among the total DAPI-stained cells ($EdU^+/DAPI^+/DAPI^+$ cells) (**Fig. 5.7 D**). Secondly, we specifically examined proliferation in Sox9-stained cells. Sox9 is a marker for precartilage condensations, and previous research has indicated that condensation properties are crucial determinants of future cartilage and bone size and shape (Grüneberg, 1963; Kaucka et al., 2017), which ultimately dictate the final face shape. Therefore, we quantified the proportion of EdU-labeled cells among the Sox9-positive population ($Sox9^+$ $EdU^+/Sox9^+$ cells) (**Fig. 5.7 E**).

Our analysis revealed a significant decrease in proliferation activity in both cell populations within the FNP of *Wnt5a* cKO mouse embryos compared to controls. In all mesenchymal cells

within the FNP area, the proliferation rate in control samples was 37% ± 2.1%, while in Wnt5a cKO, the proliferation rate was 27% ± 1.6% (**Fig. 5.7 D**). In Sox9^{+} cells within the FNP, control samples displayed a proliferation rate of 33% ± 1.9%, whereas, in *Wnt5a* cKO, a proliferation rate of 25% ± 2% was observed (**Fig. 5.7 E**).

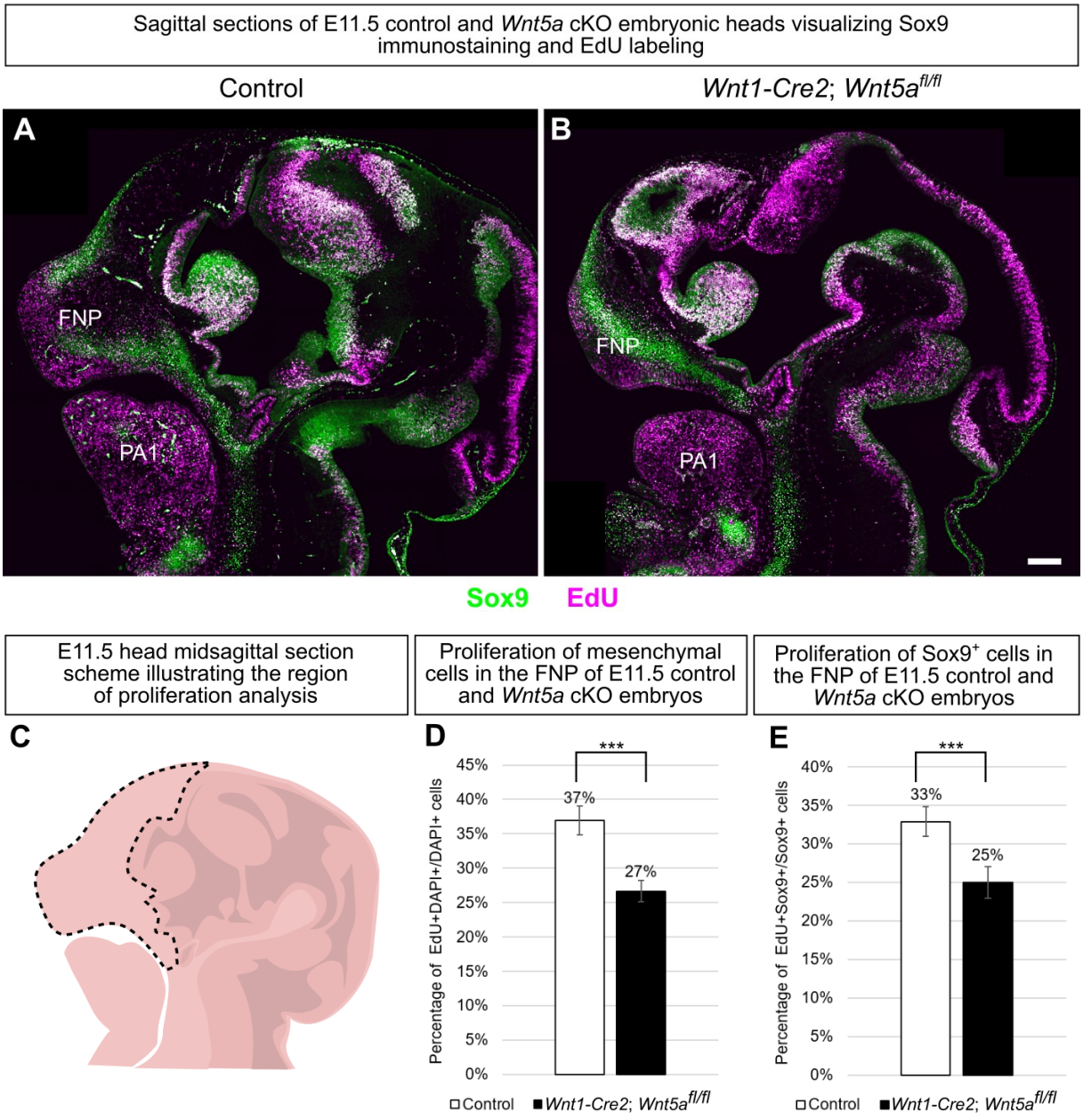

Figure 5.7 Analysis of proliferation rate in the FNP in control and Wnt5a cKO E11.5 embryos. *(**A-B**) Immunostaining of fixed paraffin sagittal sections of E11.5 embryonic control (A) and Wnt5a cKO (B) heads, demonstrating the proliferation activity in precartilage condensation. Sox9 antibody was used to label cells within the precartilage condensation (green) in the FNP and Edu labeling was used to detect the proliferation rate (magenta). Magnification: 20×. (**C**) An annotated schematic representation of the E11.5 embryonic head*

*midsagittal section, showing the FNP area where proliferation was measured (black dashed line). (**D**) Comparison of the percentage of $EdU^+DAPI^+/DAPI^+$ cells in FNP regions between control and Wnt5a cKO E11.5 embryos ($p \leq 0.001$). (**E**) Quantification of the percentage of $EdU^+Sox9^+/Sox9^+$ cells in FNP regions of control and Wnt5a cKO E11.5 embryos ($p \leq 0.001$). The error bars represent the standard deviation. Statistical analysis was performed using a paired two-tailed Student's t-test. Results from two biological replicates, which consisted of littermates obtained from separate mothers, are shown. Each biological replicate included one control embryo and one mutant embryo. **Abbreviations**: **FNP** – frontonasal process, **PA1** – first pharyngeal arch. Scalebar: 200 µm.*

5.5 Apoptotic Activity Is Not Affected in E11.5 *Wnt5a* cKO Facial Region

Although analysis indicated a decrease in proliferation activity, it was not substantial enough to account for the marked difference in size of the FNP observed between *Wnt5a* cKO and control samples. Therefore, we aimed to further investigate potential mechanisms underlying this disparity. We turned our attention to apoptosis as a potential contributing factor. We anticipated that the FNP size reduction was caused not only by decreased proliferation but also by excessive apoptosis in the FNP of *Wnt5a* cKO samples. To elucidate the level of apoptosis in craniofacial morphogenesis, we employed immunostaining with Cas3 antibody in E11.5 *Wnt5a* cKO and control embryos and quantified apoptotic activity within the tissue (**Fig. 5.8**).

The immunostaining revealed that there was almost no apoptotic activity in the PA1 in *Wnt5a* cKO nor control embryos (data not shown). However, a stereotypical apoptotic area was observed in the FNP in control (**Fig. 5.8 A, A'**) and *Wnt5a* cKO (**Fig. 5.8 B, B'**) samples. In this study, we opted to quantify this apoptotic area (**Fig. 5.8. D**) relative to the total area of the FNP (**Fig. 5.8 C**) rather than counting the number of apoptotic cells. This decision was made due to the staining characteristics of the Cas3 antibody, which labels cells in various stages of apoptosis, including unfragmented cells and apoptotic bodies, which makes accurate cell counting difficult. Measuring the area of apoptosis provided a more comprehensive assessment of apoptotic activity within the tissue, accounting for variations in cell size and morphology.

Our analysis showed that the ratio of apoptotic area to FNP area was comparable between the control and *Wnt5a* cKO samples, with values of 2.39% ± 1.15% and 2.21% ± 0.81%, respectively (**Fig. 5.8 E**). The lack of significant differences suggests that the level of apoptotic activity within the FNP was consistent between the mutant and control samples.

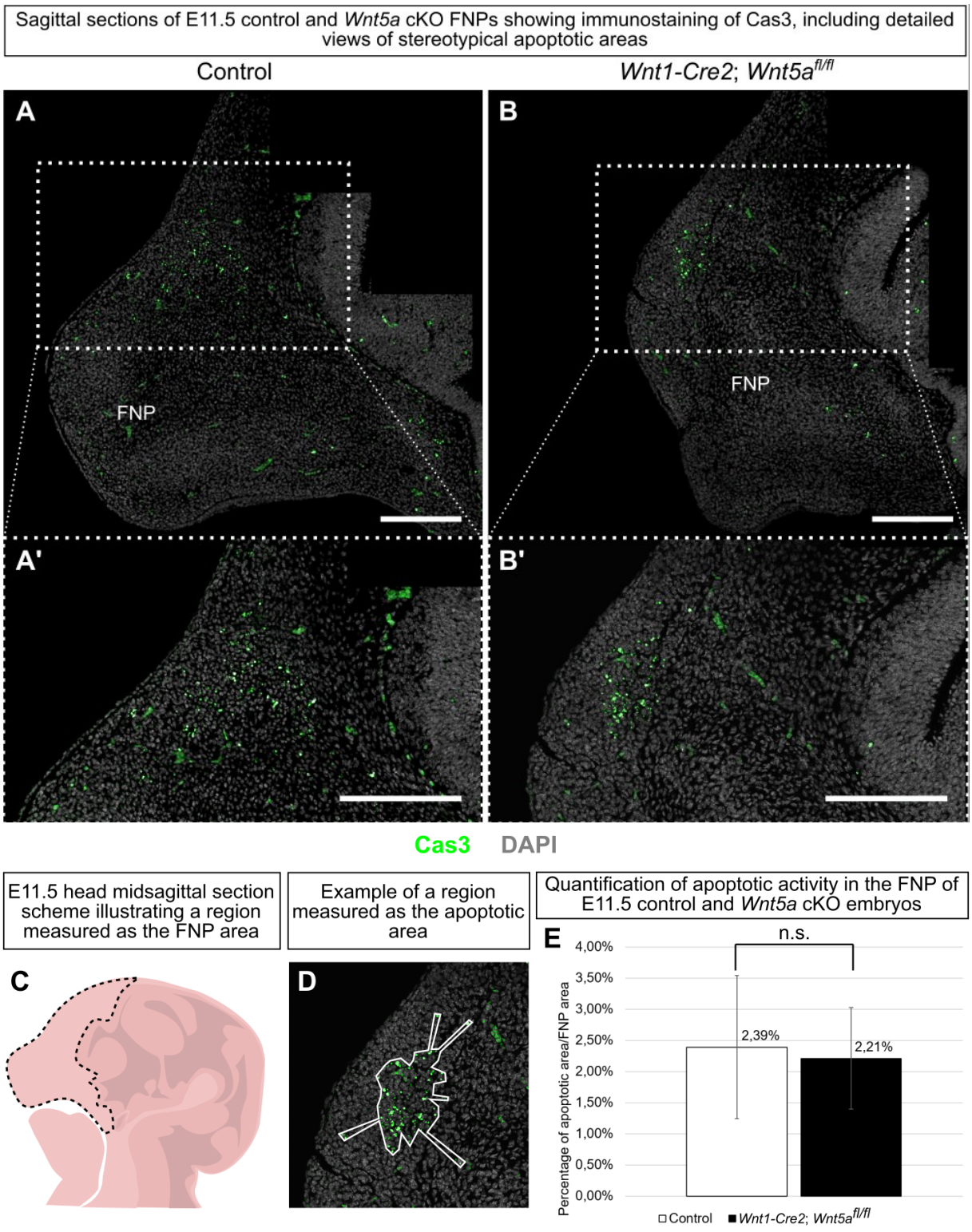

Figure 5.8 Analysis of apoptotic activity in the facial region in control and Wnt5a cKO E11.5 embryos. *(**A, B**) Immunostaining of fixed paraffin sagittal sections of E11.5 embryonic control (A) and Wnt5a cKO (B) head, showing apoptotic cells/bodies (green) labeled with Cas3 antibody. Mind that the blood cells also display a signal. For spatial context, the sections are counterstained with DAPI (gray). (**A', B'**) Detailed view of the apoptotic areas in the FNP in*

*control (A') and Wnt5a cKO (B') samples. Magnification: 20×. (**C**) An annotated schematic representation of the E11.5 embryonic head midsagittal section, showing the region measured as the FNP area (black dashed line). (**D**) Representative example of a region measured as the apoptotic area (white line). (**E**) Quantification of the percentage of apoptotic area/FNP area of control and Wnt5a cKO E11.5 embryos ($p > 0.05$). The error bars represent the standard deviation. Statistical analysis was performed using a paired two-tailed Student's t-test. Results from two biological replicates, which consisted of littermates obtained from separate mothers, are shown. Each biological replicate included one control embryo and one mutant embryo.* ***Abbreviations: FNP** – frontonasal process, **n.s**. – not significant. Scalebar: 200 µm.*

5.6 Directional Cell Division Is Disrupted in E11.5 *Wnt5a* cKO Facial Region

Previous studies have suggested a role for Wnt/PCP in governing the orientation of cell division during embryogenesis (Kaucka et al., 2016; Ségalen et al., 2010). To further investigate this phenomenon, we conducted an oriented cell division analysis in the FNP and PA1 regions of E11.5 embryos, comparing control and *Wnt5a* cKO samples (**Fig. 5.9**). Given the association of Wnt5a with directional cell division (Kaucka et al., 2016), we sought to explore whether its absence would disrupt the normal pattern of cell division in the developing embryo. We utilized immunostaining techniques, including labeling with DAPI to visualize DNA, PH3 to highlight mitotic cells, Alexafluor phalloidin to label actin filaments for cell shape visualization, and anti-acetylated tubulin antibody to detect mitotic spindles (**Fig. 5.9 A**) to assess the direction of cell division. Acetylated tubulin staining along with DAPI staining is commonly used to determine the orientation of cell division, it has been used for example in Ouspenskaia et al., 2016.

Our analysis revealed remarkable differences in cell division orientation between control and *Wnt5a* cKO embryos. In the control group, the division axis in the majority of cells aligned with or slightly (max ±40°) deviated from the reference line (direction of growth) (**Fig. 5.9 B, C**) in both FNP and PA1 regions (**Fig. 5.9 B', C'**). However, in *Wnt5a* cKO embryos, this directional pattern was markedly disrupted, with a more varied distribution of division angles observed in the FNP and PA1 (**Fig. 5.9 B", C"**). Interestingly, in the *Wnt5a* cKO, most cells demonstrated ±40-50° deviation from the reference line, while barely any cells' division axes aligned with the reference line in the FNP (**Fig. 5.9 B"**). Similarly, in the PA1, the majority of cells displayed ±70-80° deviation from the reference line, while barely any cells' division axes aligned with the reference line in *Wnt5a* cKO (**Fig. 5.9 C"**). Surprisingly, the peaks in the *Wnt5a* cKO diagrams were distributed more or less symmetrically, rather than randomly (**Fig. 5.9 B", C"**).

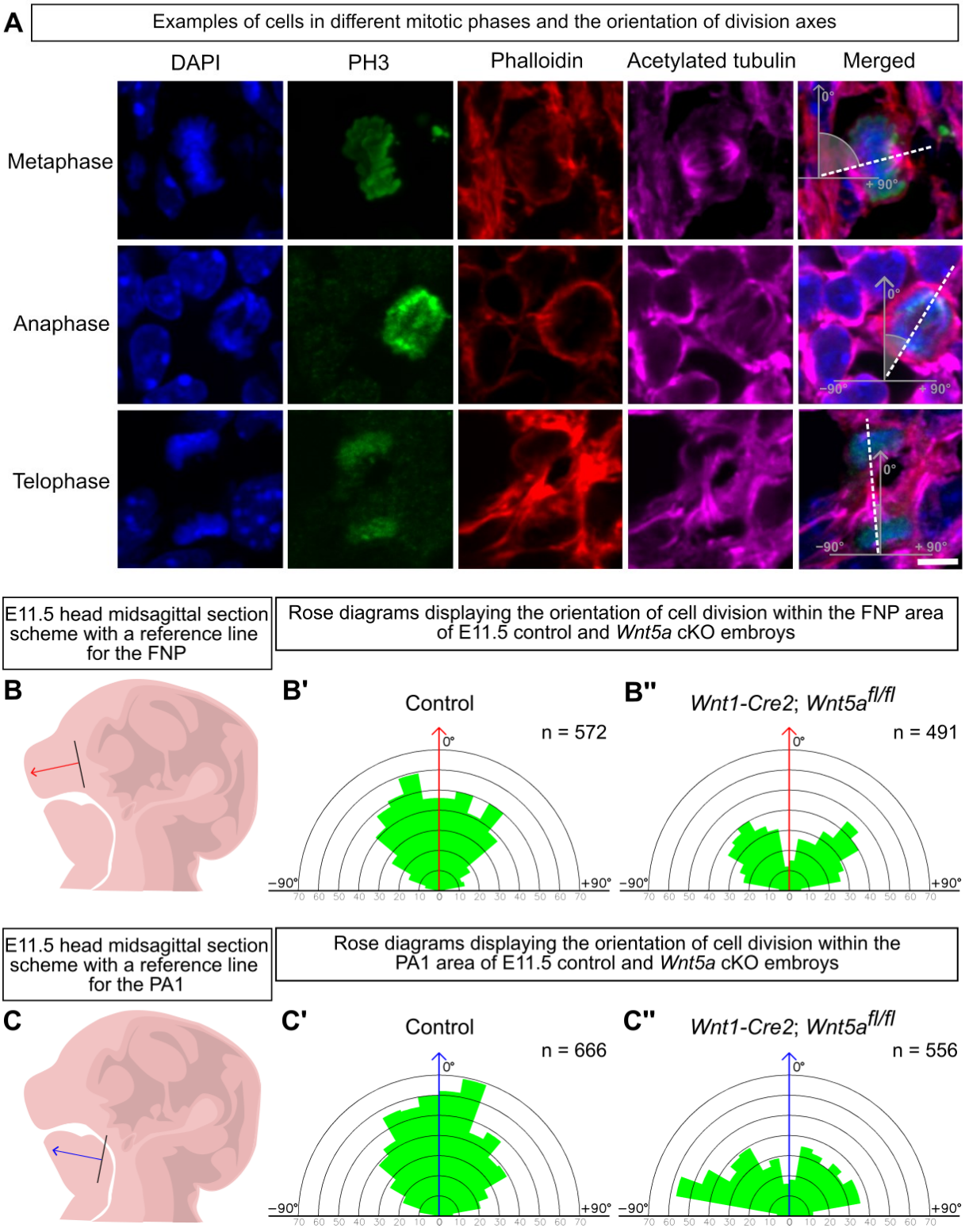

Figure 5.9 Oriented cell division analysis in the FNP and PA1 areas in control and Wnt5a cKO E11.5 embryos. *(A) Fluorescence microscopy images of immunostaining on the fixed frozen sagittal section of E11.5 embryonic head, showing representative examples of cells in different mitotic phases and orientation of the division axes (white dashed line) compared to the reference line (gray arrowed line). DAPI (blue) was used to stain the DNA, PH3 (green)*

*highlights mitotic cells, Alexafluor phalloidin (red) was used to label actin filaments to see the cell shape, and anti-acetylated tubulin (magenta) antibody was used to detect the mitotic spindles. Magnification: 60×. (**B**) An annotated schematic representation of the E11.5 embryonic head midsagittal section, featuring a reference line (red arrowed line) delineating the direction of the snout growth. This reference line serves as a guide for measuring the direction of cell division in the FNP region. (**B' and B"**) Rose diagrams visualizing the orientation of cell divisions in the FNP region of E11.5 control (B') and Wnt5a cKO (B") embryos. (**C**) An annotated schematic representation of the E11.5 embryonic head midsagittal section. A reference line (blue arrowed line) is incorporated and corresponds with the growth direction of the PA1, providing a guide for analyzing cellular division orientations within the area. (**C' and C"**) Rose diagrams outlining the directionality of cell divisions in the PA1 area of E11.5 control (C') and Wnt5a cKO (C") embryos. (B', B", C', C") The diagrams are discrete radial plots, in which the magnitude represents the number of mitotic cells and the degree value, ranging from -90° to +90°, indicates the deviation of the division axis from the reference line. Note: n value represents the total number of quantified mitotic cells. Results from two biological replicates, which consisted of littermates obtained from separate mothers, are shown. Each biological replicate included one control embryo and one mutant embryo. Scalebar: 5 µm.*

5.7 Orientation of Primary Cilia Is Disrupted in E11.5 *Wnt5a* cKO Facial Region

Given the association of Wnt5a signaling with cell polarity establishment, our study aimed to assess the polarity of mesenchymal cells within the facial region, anticipating disruptions in polarity in *Wnt5a* cKO samples due to the absence of Wnt5a signal. First, by immunostaining, we examined core PCP proteins, including the transmembrane protein Vangl2, and the cytoplasmic proteins Prickle1 and Dishevelled2. PCP proteins constitute a group of evolutionarily conserved molecules crucial for establishing and maintaining planar cell polarity. One notable characteristic of PCP proteins is their asymmetric localization across cells within a tissue layer, establishing polarized distributions within cells. However, our investigation did not reveal any detectable polarized distribution of these proteins within mesenchymal cells in the FNP and PA1 in E11.5 *Wnt5a* cKO and control embryos (data not shown). Therefore, we adopted an alternative approach to analyzing the polarity of facial mesenchymal cells (**Fig. 5.10**). We employed immunostaining of the Arl13b (adenosine diphosphate-ribosylation factor-like protein 13B) to label primary cilia in the cells (**Fig. 5.10 A)**. Primary cilia, being polarized structures of the cells (De Andrea et al., 2010; Jones et al., 2008), serve as a candidate marker of polarity even in mesenchymal cells.

Our analysis revealed a similar distribution of primary cilia polarity in both the FNP and PA1 regions in control (**Fig. 5.10 B', C'**) and *Wnt5a* cKO (**Fig. 5. 10 B", C"**) samples, with orientation degrees ranging from -180° to +180°, indicating the deviation from the reference lines (the direction of growth) (**Fig. 5.10 B, C**). Interestingly, the majority of primary cilia orientations ranged from 0° to +90° in both the FNP and PA1 regions across control and *Wnt5a* cKO embryos. However, differences were observed in the ratio of distally to proximally oriented primary cilia between the control and *Wnt5a* cKO groups. In the control group, 65% of primary cilia were distally oriented (on the distal side of cells), and 35% were proximally oriented (on the proximal side of cells), while in the mutant samples, only 59% of primary cilia were distally oriented and 41% were proximally oriented in the FNP areas (**Fig. 5.10 B'"**). Larger disparities were observed in the PA1 regions, where 67% of primary cilia were distally oriented and 33% were proximally oriented in the control group, compared to 57% and 43%, respectively, in the mutant group **(Fig. 5.10 C'"**).

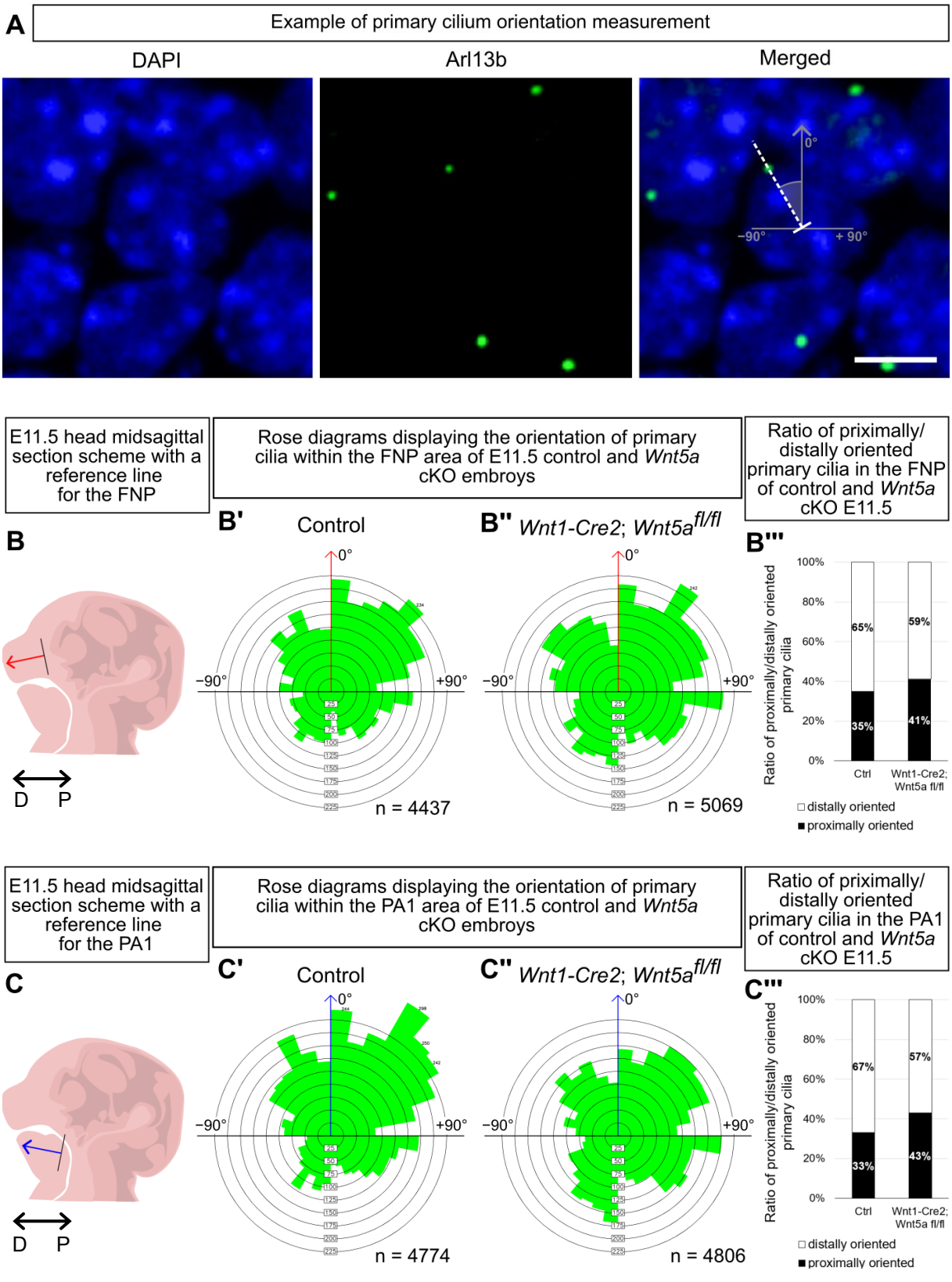

Figure 5.10 Primary cilia polarity analysis in the FNP and PA1 areas in control and Wnt5a cKO E11.5 embryos. *(A) Fluorescence microscopy images of immunostaining on the fixed thick frozen sagittal section of E11.5 embryonic head, showing a representative example of primary*

*cilium orientation (white dashed line) compared to the reference line (gray arrowed line). DAPI (blue) was used to stain the DNA and Arl13b was used to stain primary cilia. Magnification: 40×. (**B**) An annotated schematic representation of the E11.5 embryonic head midsagittal section, featuring a reference line (red arrowed line) delineating the direction of the snout growth. This reference line serves as a guide for measuring the primary cilia orientation in the FNP region. Distal-proximal axis is shown (double-arrowed black line). (**B' and B"**) Rose diagrams visualizing the orientation of primary cilia in the FNP region of E11.5 control (B') and Wnt5a cKO (B") embryos. (**C**) An annotated schematic representation of the E11.5 embryonic head midsagittal section. A reference line (blue arrowed line) is incorporated and corresponds with the growth direction of the PA1, providing a guide for analyzing primary cilia orientation within the area. Distal-proximal axis is shown (double arrowed black line). (**C' and C"**) Rose diagrams outlining the orientation of primary cilia in the PA1 area of E11.5 control (C') and Wnt5a cKO (C") embryos. (B', B", C', C") The diagrams are discrete radial plots, in which the magnitude represents the number of measured cells with primary cilia, and the degree value, ranging from -90° to +90°, indicates the deviation of the orientation of primary cilia from the reference line. (**B"' and C"'**) Ratios of proximally/distally oriented primary cilia within the FNP (B"') and the PA1 (C"') areas of control and Wnt5a cKO samples. Note: n value represents the total number of quantified cells. Results from one biological replicate, which consisted of one control and one Wnt5a cKO embryo littermate, are shown. Scalebar: 5 µm.*

6 Discussion

Wnt5a, a member of the Wnt family of secreted glycoproteins, is involved in various aspects of embryonic development and tissue homeostasis. In particular, Wnt5a has been implicated in the development of multiple structures, including the craniofacial region, where it contributes to facial morphogenesis and patterning (Yamaguchi, 1999). However, despite its significance in development, Wnt5a has received relatively less attention compared to other Wnt ligands due to its predominant association with β-catenin-independent signaling cascades. Our investigation into the role of Wnt5a in craniofacial development has revealed novel insights into the cellular mechanisms underlying tissue morphogenesis. Through a series of experiments utilizing *Wnt1-Cre2*; *Wnt5a*$^{fl/fl}$ mice, we elucidated the specific contribution of noncanonical Wnt5a signaling to the formation of craniofacial structures.

The significance of Wnt5a in the development of facial bones and tissues has been well established (Yamaguchi, 1999). However, it was unclear whether the population of NCCs,

which gives rise to the facial structures, produces this Wnt5a signal, which in turn regulates the growth and shaping of the face and skull. In other words, the tissue-specific and temporal requirements for Wnt5a signaling in craniofacial development *in vivo* were largely unexplored. To address that issue, we generated *Wnt1-Cre2*; *Wnt5a*$^{fl/fl}$ mice (*Wnt5a* cKO), with NC-specific deletion of the *Wnt5a* gene. This approach allowed us to precisely determine the role played by NC-derived Wnt5a signaling during craniofacial development. In this study, analysis of E17.5 *Wnt5a* cKO and control embryonic skull anatomy revealed that *Wnt5a* cKO samples displayed craniofacial malformations, including cleft palate, micrognathia, maxillary hypoplasia, and deformities in the nasal region, resembling those observed in conventional *Wnt5a* KO mice (Yamaguchi, 1999). These findings emphasize the importance of the Wnt5a signal produced by the NCCs as a crucial contributor to proper craniofacial development.

To understand the cellular mechanisms responsible for this phenotype, we analyzed earlier developmental stages, aiming to elucidate Wnt5a's role on a cellular level. We focused on uncovering the precise tissue-specific and temporal requirements of Wnt5a signaling during craniofacial development.

As the chondrocranium, a cartilaginous model replaced by bone tissue during development, is crucial for determining facial shape (Hall, 2015), we studied the shape of cartilage structures within the craniofacial region. To achieve this, we utilized the Sox9 antibody, a marker of developing cartilage and chondrocytes (Bi et al., 1999). Our study revealed notable alterations in the patterning of the Sox9^{+} cell population in *Wnt5a* cKO samples. Specifically, at stage E11.5, precartilage condensations were severely shortened and morphologically disrupted in the *Wnt5a* cKO samples. These distortions were further intensified by E12.5 in *Wnt5a* cKO embryos, indicating impaired growth. By E13.5, the cartilaginous structures in the nasal region appeared deformed and disorganized in *Wnt5a* cKO, suggesting disrupted development of the cartilage primordium of the nasal bone.

These results are consistent with the proposal that in Wnt/PCP mutants, the craniofacial phenotypes originate in precartilage or early chondrogenic stages, characterized by distorted mesenchymal condensations in the very early head (Kaucka et al., 2017). However, the experiments in the mentioned study were conducted using E12.5 *Wnt5*a KO mice. Here, we report that disruptions in precartilage condensations are already present at stage E11.5 in *Wnt5a* cKO embryos, suggesting that the abnormal facial shape is established even earlier in development. The results suggest that Wnt5a guides the proper formation of facial shape from

the very early stages (E11.5) of craniofacial morphogenesis by regulating the shaping of precartilage condensations.

Next, we examined Twist1 expression, as the loss of *Twist1* in NCCs and their derivatives has been associated with negative effects on skeletogenic differentiation, resulting in the absence of bones in the snout, upper face, and skull vault in mice. Moreover, studies have demonstrated a reduction in *Twist1* expression in the frontal bone of mice with ablation of *Prickle1*, a key component of the Wnt/PCP signaling pathway, indicating a connection between Wnt/PCP signaling and Twist1 (Wan et al., 2018). Twist1 has also been implicated in directing the migration of NCCs and ensuring their correct localization within the PA1 (Soo et al., 2002). However, conflicting studies suggest that Twist1 may not be essential for the migration or regionalization of NCCs, but rather its activity may be crucial for maintaining the viability of cranial NCCs after their migration is complete (Bildsoe et al., 2009). Supporting that, CRISPR–Cas9 knockdown of *Twist1* in chick cranial NCCs resulted in a reduction of mesenchymal populations (Soldatov et al., 2019). Given Twist1's association with Wnt/PCP and its role in craniofacial development, particularly in the formation of the cranial vault, frontonasal, facial, and jaw skeleton, we aimed to investigate Twist1 expression in *Wnt5a* cKO embryos displaying craniofacial defects, expecting changes in the Twist1 expression levels.

Our results showed that Twist1 expression remained unaltered at all examined developmental stages in *Wnt5a* cKO embryos compared to control littermates. These findings indicate that, despite Twist1's critical involvement in craniofacial development and its potential regulation by the Wnt/PCP pathway, its expression levels are not directly affected by Wnt5a signaling. This implies that Wnt5a may function independently of Twist1 in regulating craniofacial morphogenesis. Furthermore, the unchanged expression of Twist1 in *Wnt5a* cKO embryos suggests that the observed craniofacial phenotype cannot be attributed to alterations in Twist1 expression. In other words, the craniofacial abnormalities in *Wnt5a* cKO are not caused by disruptions in Twist1-mediated viability of cranial NCCs or skeletogenic differentiation. Instead, it suggests that Wnt5a may influence craniofacial development through alternative molecular pathways or cellular mechanisms.

Next, we examined Foxf1, a transcription factor, involved in craniofacial morphogenesis. In *Foxf1* cKO mouse embryos, palatal cleft was observed (J. Xu et al., 2016), and in zebrafish, ablation of *Foxf1* caused facial cartilage defects (P. Xu et al., 2018). Given that, we anticipated changes in Foxf1 expression in *Wnt5a* cKO embryos, as they display facial cartilage defects and cleft palate. Furthermore, research reveals an association between Wnt5a and Foxf1. For

example, in mice with *Foxf1* ablation, there was a significant *Wnt5a* expression increase in the developing gut mesenchyme (Ormestad et al., 2006). Another study proposed direct activation of *Wnt5a* transcription by Foxf1 in the developing lung mesenchyme (Ustiyan et al., 2018). Similarly, direct activation of the *Wnt5*a gene transcription by Foxf1 was also reported in lung fibroblasts (Reza et al., 2023). These findings indicate an interplay between Wnt5a and Foxf1, with evidence strongly suggesting that *Wnt5a* is a target gene of Foxf1. However, no research has implied *Foxf1* to be a downstream target of Wnt5a. Our results support these findings, showing that expression levels or patterns of Foxf1 remain unaffected in *Wnt5a* cKO embryos, indicating that the Wnt5a cascade does not regulate the Foxf1 expression during craniofacial development.

In our study, we also investigated Pax3 expression in control and *Wnt5a* cKO embryos, motivated by previous research indicating that *Pax3* ablation results in frontonasal dysplasia and clefting in mice (Zalc et al., 2015). As anomalies in the frontonasal region and clefting are also observed in *Wnt5a* cKO embryos, we aimed to examine potential alterations in Pax3 expression in these mutant samples. Our results revealed prominent expression of Pax3 in the distal regions of the FNP and PA1 at E11.5 in both control and *Wnt5a* cKO embryos, consistent with the importance of Pax3 in early craniofacial development. Similarly, Pax3 expression persisted in the nasal process and mandible at E12.5 in both experimental groups. However, a slight reduction in the $Pax3^{+}$ population was detected specifically in the distal mandibular region of *Wnt5a* cKO embryos at E12.5. Despite this localized alteration, Pax3 expression in other regions remained largely unaltered in the *Wnt5a* cKO samples.

An interesting study was conducted on mice with cKO of *Wls* (wntless), a gene encoding a protein essential for the secretion of Wnt ligands, including Wnt5a, to the extracellular space. In the *Wls* cKO mice, which demonstrated severe frontonasal hypoplasia and midfacial clefts, significantly diminished expression of both *Pax3* and *Wnt5a* was detected in the medial nasal process at stage E11.5 (Gu et al., 2022). This finding could suggest a potential regulatory relationship between Wls, Wnt5a, and Pax3, in which the disruption of Wnts secretion due to Wls deficiency might lead to altered *Pax3* expression, negatively affecting the craniofacial development in the *Wls* cKO mice. Nevertheless, *Pax3* has been predominantly known as a direct downstream target of Wnt/β-catenin signaling (Zhao et al., 2014), therefore, the researchers associated the altered *Pax3* expression with disrupted Wnt/β-catenin resulting from the *Wls* ablation. However, the Wnt5a ligand can trigger Wnt/β-catenin signaling in particular contexts (discussed in **Chapters 2.2.2** and **2.3.1**), making it a potential regulator of *Pax3*

expression in the *Wls* cKO embryos. Moreover, the relationship between Wnt5a signaling and *Pax3* expression has been indicated in another study, where siRNA-mediated knockdown of *Wnt5a* led to an increase in the expression of *Pax3* in human melanoma cells (Dissanayake et al., 2008), suggesting that Wnt5a can regulate *Pax3* expression in a specific environment.

Nevertheless, in our study in E11.5 Wnt5a cKO, Wnt/β-catenin was not affected in the facial region (see below), indicating that the *Pax3* expression is not regulated by Wnt5a-mediated β-catenin signaling in the facial area. Also, considering the insufficient amount of direct evidence of Wnt5a cascade regulating *Pax3* expression, we are not convinced that the detected reduction in $Pax3^+$ cell population in *Wnt5a* cKO marks reduced *Pax3* expression level resulting from lacking Wnt5a signaling. Rather we propose that the observed slight reduction in $Pax3^+$ mesenchymal population in the mandibular region in E12.5 *Wnt5a* cKO reflects the reduction and disruption of the mandibular region already evident at the E12.5 stage.

Next, we investigated the expression of Msx1 in the context of *Wnt5a* cKO embryos. Msx1 has been associated with the proper formation of the craniofacial region, with *Msx1* KO mice displaying defects including cleft palate and maxillary and mandibular dysplasia (Satokata & Maas, 1994). As we observed all of these defects in *Wnt5a* cKO embryos, we anticipated alterations in Msx1 expression in the mutant samples. Moreover, previous research has suggested a regulatory relationship between the Wnt5a signaling and *Msx1* expression. For instance, a study using *Wnt5a* KO mice revealed that, in the mutant, *Msx1* expression was reduced in the dental papilla at the E14.5 stage (Lin et al., 2011). Similarly, *Msx1* was found to be partially downregulated in the anterior palatal mesenchyme in *Wnt5a* KO mouse at stage E13.5 (F. He et al., 2008). In addition, a recent study revealed that exposure to Wnt5a led to upregulation of *Msx1* expression in mouse embryonic fibroblasts, showing the direct activation of *Msx1* gene transcription by Wnt5a stimulus (Medio et al., 2012).

Our findings align with these previous observations, demonstrating a reduction in the $Msx1^+$ population specifically in the distal mandibular area of E12.5 *Wnt5a* cKO embryos. This implies that dysregulation of Wnt5a signaling may contribute to craniofacial anomalies by affecting the $Msx1^+$ population. However, we did not observe alterations in Msx1 expression in the nasal process at E12.5 in the *Wnt5a* cKO sample. Likewise, no changes in Msx1 expression were detected in E11.5 in the FNP and PA1 regions, suggesting a temporally and spatially regulated effect of Wnt5a on the $Msx1^+$ population during craniofacial development. In this study, we did not conduct any experiment assessing the expression level of *Msx1*, therefore we cannot assume that *Msx1* gene expression is decreased in the absence of Wnt5a

signal, as suggested in previous studies. Rather we propose that the observed reduction in the $Msx1^+$ population in the distal mandibular region in *Wnt5a* cKO reflects the disruption and reduction of the mandibular region already apparent at the E12.5 stage.

Wnt ligands are categorized into "canonical" and "noncanonical" pathways based on their ability to induce β-catenin buildup in the nucleus. However, recent studies challenge this binary subdivision, suggesting that the specific combination of ligands and receptors, along with tissue-specific context, determines which Wnt pathway is activated (Holmen et al., 2002; G. Liu et al., 2005; Mikels & Nusse, 2006). Wnt5a, traditionally associated with the noncanonical pathway, can inhibit (Mikels & Nusse, 2006; Sato et al., 2010) or directly activate β-catenin signaling (Ring et al., 2014; Van Amerongen et al., 2012) in a context-dependent manner, suggesting a more complex interaction between the Wnt/PCP and Wnt/β-catenin pathways. In addition, alterations in the expression of Wnt/β-catenin components have been reported in Wnt/PCP mutants. For instance, In the E14.5 *Wnt5a* KO mouse, upregulation and expansion of *Axin2* expression in the enamel knot area was observed (Lin et al., 2011). As Axin2 is a direct target and reliable marker of Wnt/β-catenin signaling activity (Jho et al., 2002), their findings imply increased Wnt/β-catenin signaling activity during tooth development in the absence of Wnt5a signaling. Furthermore, in E12.5 mice with *Prickle1* ablation, expression of *Lef1*, a gene encoding Wnt/β-catenin transcription factor, was reduced in the frontal bone, suggesting that Wnt/β-catenin signaling was decreased due to incorrect Wnt/PCP function (Wan et al., 2018).

Our investigation of Wnt/β-catenin signaling activity in *Wnt5a* cKO and control E11.5 embryos was motivated by the literature suggesting changes in Wnt/β-catenin signaling in Wnt/PCP mutant mice. However, our analysis revealed no significant alterations in the expression level or localization of key Wnt/β-catenin cascade components, including Lef1, *Axin2*, and Tcf7l2, in the facial regions of *Wnt5a* cKO embryos compared to control littermates. Although the $Tcf7l2^+$ population exhibited severe proximal-distal shortening within the FNP area in the *Wnt5a* cKO, this shortening likely reflects the disrupted FNP morphology already evident at the E11.5 stage. This is also supported by our observation that the $Sox9^+$ population, an important player in determining the final shape of the face, is localized within the same area of the FNP as the $Tcf7l2^+$ population in E11.5 and is already distorted and shortened as well at the E11.5 stage embryos (compare **Fig. 5.3 A, D** with **Fig. 5.6 E, F**). This observation is supported by the localization of the $Sox9^+$ population within the same area of the FNP as the $Tcf7l2^+$ population in E11.5, and the $Sox9^+$ population's role in determining the final face shape, which is already distorted and shortened at the E11.5 stage.

Altogether, our findings suggest that the absence of Wnt5a does not significantly impact the expression or localization of key components of β-catenin-mediated Wnt signaling in the FNP and PA1 in *Wnt5a* cKO embryos as E11.5. This indicates that Wnt/β-catenin is not altered in *Wnt5a* cKO E11.5 embryos. Therefore, it appears that in craniofacial development, at least in the FNP and PA1 at stage E11.5, the regulatory influence of Wnt5a signaling on the Wnt/β-catenin cascade is minimal or absent. These results, together with the existing literature, demonstrate that, during development, the influence of the Wnt5a ligand on Wnt/β-catenin signaling is dependent on spatial and temporal context.

Upon observing a significant shortening and reduction of the FNP in E11.5 *Wnt5a* cKO embryos compared to control littermates, we hypothesized that this tissue reduction could be, at least partially, caused by a decreased proliferation rate. This hypothesis was supported by previous studies suggesting Wnt5a's regulatory role in proliferation activity during development. For example, studies on *Wnt5a* KO mice reported a decreased proliferation rate in developing limbs at E12.5 (Yamaguchi et al., 1999) and in dental epithelium and mesenchyme during tooth development at the E16.5 stage (Lin et al., 2011). Similarly, altered proliferation rates were observed in the palatal mesenchyme of E13.5 *Wnt5a* KO mouse embryos, with a higher level of cell proliferation observed in the anterior palate and a decreased rate exhibited in the posterior palate (F. He et al., 2008). Additionally, a higher level of proliferation was reported in chick diaphyses of RCAS::wtWNT5A- or RCAS::WNT5A^{C83S}-injected *ulnae* (Gignac et al., 2019).

Therefore, we aimed to analyze proliferation activity in E11.5 *Wnt5a* cKO and control embryos using the EdU Proliferation Assay. By examining the proliferation rate in the FNP of *Wnt5a* cKO embryos, we aimed to elucidate the role of Wnt5a in regulating cell proliferation during craniofacial development, particularly in the context of FNP morphogenesis. We studied the proliferation activity in all mesenchymal cells within the FNP and also in Sox9^{+} cells within the FNP. This was done considering that, during facial development, precartilage Sox9^{+} mesenchymal condensations determine the facial morphology by forming the cartilaginous scaffold which shapes the facial bones.

Our investigation revealed a significantly reduced proliferation rate within the FNP area in both DAPI^{+} and Sox9^{+} cell populations. These findings suggest that dysregulation of proliferation contributes to the observed reduction in FNP size in *Wnt5*a cKO embryos. Overall, our results, along with data from previous studies, imply that Wnt5a signaling can regulate proliferation activity, with the final effect being context-specific. However, based on our results, we conclude

that during craniofacial development, Wnt5a signaling stimulates proliferation activity in the FNP at the E11.5 stage, contributing to the proper formation of craniofacial structures.

Next, we examined apoptosis activity, assuming it might be another potential factor contributing to the reduction in the craniofacial region observed in the *Wnt5a* cKO. This is because the reduced proliferation rate alone would not be sufficient to cause such a drastic change in the craniofacial area. Our analysis of apoptosis was also prompted by the ability of Wnt5a to regulate resistance to apoptosis in fibroblast cell culture independently of β-catenin signaling (Vuga et al., 2012) and also in human stem Leydig cells through β-catenin signaling (W. Liu et al., 2024). To assess potential differences in apoptotic activity between E11.5 *Wnt5a* cKO and control samples, we utilized Cas3-based immunostaining.

Our analysis revealed minimal apoptotic activity in the PA1 and a stereotypical apoptotic area within the FNP region in both *Wnt5a* cKO and control embryos. However, we observed no significant changes in the level of apoptotic activity when comparing *Wnt5a* cKO and control E11.5 FNP regions. These results are consistent with findings from other research groups examining *Wnt5a* KO mice, which reported no alterations in apoptotic activity in the developing limb (Yamaguchi et al., 1999) and in the developing palate (F. He et al., 2008), despite disruptions in the morphology of these structures. Similarly, no alterations in apoptosis were detected in the forelimbs of chick embryos infected with RCAS::Wnt5a^{C83S} (Gignac et al., 2019). The lack of significant differences in the apoptotic area implies that apoptosis may not be a major contributing factor to the observed disparity in FNP size between the *Wnt5a* cKO and control embryos. In addition, the results support our earlier observation that the expression of Twist1, a regulator of mesenchymal cell viability, remains unaffected in *Wnt5a* cKO. This confirms that mesenchymal cells in the craniofacial region continue to survive and maintain their functionality. Collectively, the results indicate that Wnt5a does not regulate cell survival in craniofacial development.

We then turned our attention to the orientation of cell division as a possible cause of the observed craniofacial defects in *Wnt5a* cKO embryos, as the Wnt/PCP signaling has been strongly associated with guiding oriented cell division (Kaucka et al., 2016; Ségalen et al., 2010). Given the known involvement of Wnt/PCP signaling in regulating the directionality of cell division, we hypothesized that the absence of the NC-derived Wnt5a gradient in the craniofacial region of our mouse model would result in alterations in cell division orientation. Therefore, we analyzed the orientation of the mitotic spindle in dividing cells in the FNP and the PA1 area in E11.5 *Wnt5a* cKO and control embryos.

Our findings indicate a remarkable disruption in the direction of cell division in both analyzed facial areas of *Wnt5a* cKO samples, as compared to control samples. The results suggest a loss of proper proximal-distal cell division orientation in the absence of Wnt5a signaling, which might contribute to the disrupted craniofacial morphology observed in *Wnt5a* cKO. These observations are consistent with data from a study on E12.5 *Wnt5a* KO mice, where the allocation of post-mitotic daughter cells in the nasal region was analyzed to assess cell division directionality (Kaucka et al., 2016). In that study, E12.5 *Wnt5a* KO samples also exhibited disrupted cell division orientation. However, while the distribution of cell division direction appeared random in the previous study, our findings in E11.5 *Wnt5a* cKO suggest a noticeable pattern, implying the presence of some regulatory mechanism in the absence of the Wnt5a gradient. The difference in randomness could be attributed to variations in embryonic stage (E12.5 vs. E11.5), methodological approaches (quantification of daughter cell allocation vs. quantification of mitotic spindle axis), or the representativeness of the data reflected by the number of quantified cells (75-107 vs. 491-666).

Based on our data, we conclude that Wnt5a signaling provides an essential polarizing cue during the early critical stages of craniofacial development (E11.5) and governs the proper construction of craniofacial structures by regulating oriented cell division. We also suggest the involvement of other signals dictating the orientation of cell division planes in *Wnt5a* cKO, as evidenced by the observed pattern in the distribution of cell division direction.

Given the established association between Wnt5a and PCP (**discussed in Chapter 2.2.3**), we examined the localization of core PCP proteins (Vangl2, Dishevelled2, Prickle1) in facial mesenchymal cells of E11.5 control and *Wnt5a* cKO embryos to assess potential alterations in cell polarity. Our observations revealed a lack of protein polarization, with proteins exhibiting a random distribution along the membrane and cytoplasm. This finding is consistent with a previous study demonstrating the absence of PCP protein polarization (Vangl2, Ror2) in mouse precartilage limb bud mesenchyme at E11.5, whereas asymmetrical protein localization was observed in differentiated chondrocytes at E12.5 (Gao et al., 2011). Our results, along with previous data, suggest that PCP stabilization does not occur in loose facial mesenchyme at E11.5 and may require close cell-cell contact established within densely packed differentiated chondrocytes in later developmental stages.

Continuing our investigation into cell polarity, we shifted our focus to an alternative approach for assessing polarity in facial mesenchymal cells of control and *Wnt5a* cKO E11.5 embryos. We chose to analyze the polarization of primary cilia, as they have been linked with PCP and

have been shown to reflect cell polarity in various tissues (De Andrea et al., 2010; Jones et al., 2008; Patel et al., 2008). Our analysis revealed some disparities in primary cilia orientation between E11.5 *Wnt5a* cKO samples and control samples in both FNP and PA1 regions. These findings suggest that Wnt5a signaling may play a role in regulating primary cilia orientation in facial mesenchymal cells during craniofacial development. The observed differences in primary cilia orientation imply potential disruptions in cell polarity in the absence of Wnt5a.

7 Conclusion

This study aimed to assess the role of noncanonical Wnt signaling during craniofacial development. Despite the significant implication of noncanonical Wnt signaling in craniofacial morphogenesis, its precise role and the cellular mechanisms involved have remained largely unexplored. To address this gap, we generated *Wnt1-Cre2*; *Wnt5a*$^{fl/fl}$ (*Wnt5a* cKO) mice with deletion of *Wnt5a*, a gene encoding Wnt5a ligand associated with activating noncanonical Wnt pathways, specifically in the NCCs responsible for craniofacial structure formation.

The generated *Wnt5a* cKO embryos exhibited craniofacial malformations, including cleft palate, *micrognathia*, maxillary hypoplasia, and nasal deformities, underscoring the critical role of NC-derived Wnt5a signaling in facial morphogenesis. These observations of severely deformed craniofacial morphology in *Wnt5a* cKO mice led us to explore potential cellular mechanisms underlying these phenotypic changes. Through our investigation, we confirmed the involvement of Wnt5a signaling in shaping craniofacial precartilage condensations, which influence early craniofacial morphogenesis, and ultimately determine the final face shape. Furthermore, our results suggest that Wnt5a signaling may contribute to craniofacial morphogenesis through its temporally and spatially regulated effect on Msx1^{+} and Pax3^{+} mesenchymal populations, both of which are key regulators of craniofacial development. Additionally, we provide evidence that Wnt5a signaling does contribute to proper craniofacial morphogenesis through regulating cellular processes, including proliferation activity, oriented cell division, and primary cilia polarity in the facial region during critical early stages of craniofacial development. Our investigation also showed that Wnt5a signaling does not regulate craniofacial region construction through modulating Wnt/β-catenin signaling, apoptosis resistance, or the expression patterns of transcription factors critical for craniofacial development, such as Twist1 and Foxf1.

Our study provided new insights into the role of the noncanonical Wnt pathway, specifically Wnt5a signaling, in craniofacial development by analyzing cellular mechanisms at earlier developmental stages. This extends previous research on Wnt/PCP mutants, which focused on later developmental stages. However, further exploration is needed to unravel the intricate regulatory networks governed by Wnt5a signaling in craniofacial development. With a deeper understanding of the molecular processes regulating craniofacial morphogenesis, we can gain insights into how facial features arise and potentially prevent human craniofacial defects.

8 References

Antic, D., Stubbs, J. L., Suyama, K., Kintner, C., Scott, M. P., & Axelrod, J. D. (2010). Planar Cell Polarity Enables Posterior Localization of Nodal Cilia and Left-Right Axis Determination during Mouse and Xenopus Embryogenesis. *PLOS ONE*, *5*(2), e8999.

Bajanca, F., Gouignard, N., Colle, C., Parsons, M., Mayor, R., & Theveneau, E. (2019). In vivo topology converts competition for cell-matrix adhesion into directional migration. *Nature Communications*, *10*(1), 1518.

Barriga, E. H., Franze, K., Charras, G., & Mayor, R. (2018). *Tissue stiffening coordinates morphogenesis by triggering collective cell migration in vivo*.

Bhattacharya, D., Rothstein, M., Azambuja, A. P., & Simoes-Costa, M. (2018). Control of neural crest multipotency by Wnt signaling and the Lin28/ let-7 axis. *ELife*, *7*.

Bi, W., Deng, J. M., Zhang, Z., Behringer, R. R., & De Crombrugghe, B. (1999). Sox9 is required for cartilage formation. *Nature Genetics*, *22*(1), 85–89.

Bialek, P., Kern, B., Yang, X., Schrock, M., Sosic, D., Hong, N., Wu, H., Yu, K., Ornitz, D. M., Olson, E. N., Justice, M. J., & Karsenty, G. (2004). A Twist Code Determines the Onset of Osteoblast Differentiation. *Developmental Cell*, *6*(3), 423–435.

Bildsoe, H., Loebel, D. A. F., Jones, V. J., Chen, Y. T., Behringer, R. R., & Tam, P. P. L. (2009). Requirement for Twist1 in frontonasal and skull vault development in the mouse embryo. *Developmental Biology*, *331*(2), 176–188.

Boutros, M., Paricio, N., Strutt, D. I., & Mlodzik, M. (1998). Dishevelled Activates JNK and Discriminates between JNK Pathways in Planar Polarity and wingless Signaling. *Cell*, *94*(1), 109–118.

Bronner, M. E., & le Douarin, N. M. (2012). Development and evolution of the neural crest: an overview. *Developmental Biology*, *366*(1), 2–9.

Bronner-Fraser, M. (1993). Cell Interactions in Neural Crest Cell Migration. *Advances in Developmental Biology (1992)*, *2*(C), 119–152.

Bronner-Fraser, M., & Fraser, S. E. (1988). Cell lineage analysis reveals multipotency of some avian neural crest cells. *Nature*, *335*(6186), 161–164.

Brunt, L., Greicius, G., Rogers, S., Evans, B. D., Virshup, D. M., Wedgwood, K. C. A., & Scholpp, S. (2021). Vangl2 promotes the formation of long cytonemes to enable distant Wnt/β-catenin signaling. *Nature Communications*, *12*(1), 2058.

Carmona-Fontaine, C., Matthews, H. K., Kuriyama, S., Moreno, M., Dunn, G. A., Parsons, M., Stern, C. D., & Mayor, R. (2008). Contact inhibition of locomotion in vivo controls neural crest directional migration. *Nature 2008 456:7224*, *456*(7224), 957–961.

Casini, P., Nardi, I., & Ori, M. (2012). Hyaluronan is required for cranial neural crest cells migration and craniofacial development. *Developmental Dynamics*, *241*(2), 294–302.

Chiquet, B. T., Blanton, S. H., Burt, A., Ma, D., Stal, S., Mulliken, J. B., & Hecht, J. T. (2008). Variation in WNT genes is associated with non-syndromic cleft lip with or without cleft palate. *Human Molecular Genetics*, *17*(14), 2212–2218.

Ciruna, B., Jenny, A., Lee, D., Mlodzik, M., & Schier, A. F. (2006). Planar cell polarity signalling couples cell division and morphogenesis during neurulation. *Nature*, *439*(7073), 220–224.

Clément, A., Wiweger, M., Von Der Hardt, S., Rusch, M. A., Selleck, S. B., Chien, C. Bin, & Roehl, H. H. (2008). Regulation of Zebrafish Skeletogenesis by ext2/dackel and papst1/pinscher. *PLOS Genetics*, *4*(7), e1000136.

Couly, G. F., Coltey, P. M., & le Douarin, N. M. (1993). The triple origin of skull in higher vertebrates: a study in quail-chick chimeras. *Development (Cambridge, England)*, *117*(2), 409–429.

De Andrea, C. E., Wiweger, M., Prins, F., Bovée, J. V. M. G., Romeo, S., & Hogendoorn, P. C. W. (2010). Primary cilia organization reflects polarity in the growth plate and implies loss of polarity and mosaicism in osteochondroma. *Laboratory Investigation*, *90*(7), 1091–1101.

De Calisto, J., Araya, C., Marchant, L., Riaz, C. F., & Mayor, R. (2005). Essential role of non-canonical Wnt signalling in neural crest migration. *Development*, *132*(11), 2587–2597.

Dissanayake, S. K., Olkhanud, P. B., O'Connell, M. P., Carter, A., French, A. D., Camilli, T. C., Emeche, C. D., Hewitt, K. J., Rosenthal, D. T., Leotlela, P. D., Wade, M. S., Yang, S. W., Brant, L., Nickoloff, B. J., Messina, J. L., Biragyn, A., Hoek, K. S., Taub, D. D., Longo, D. L., … Weeraratna, A. T. (2008). Wnt5A regulates expression of tumor-

associated antigens in melanoma via changes in signal transducers and activators of transcription 3 phosphorylation. *Cancer Research*, *68*(24), 10205–10214.

Du, S. J., Purcell, S. M., Christian, J. L., McGrew, L. L., & Moon, R. T. (1995). Identification of Distinct Classes and Functional Domains of Wnts through Expression of Wild-Type and Chimeric Proteins in Xenopus Embryos. *Molecular and Cellular Biology*, *15*(5), 2625–2634.

Dunlop, L. L., & Hall, B. K. (1995). Relationships between cellular condensation, preosteoblast formation and epithelial-mesenchymal interactions in initiation of osteogenesis. *Int. J. Dev. Biol.*, *39*(2), 357–371.

Dupin, E., Creuzet, S., & le Douarin, N. (2006). The contribution of the neural crest to the vertebrate body. *Advances in Experimental Medicine and Biology*, 99–116.

Etienne-Manneville, S. (2008). Polarity proteins in migration and invasion. *Oncogene 2008 27:55*, *27*(55), 6970–6980.

Franz-Odendaal, T. A. (2011). Induction and patterning of intramembranous bone. In *Frontiers in Bioscience* (Vol. 16).

Gans, C., & Northcutt, R. G. (1983). Neural Crest and the Origin of Vertebrates: A New Head. *Science*, *220*(4594), 268–274.

Gao, B., Song, H., Bishop, K., Elliot, G., Garrett, L., English, M. A., Andre, P., Robinson, J., Sood, R., Minami, Y., Economides, A. N., & Yang, Y. (2011). Wnt Signaling Gradients Establish Planar Cell Polarity by Inducing Vangl2 Phosphorylation through Ror2. *Developmental Cell*, *20*(2), 163–176.

García-Castro, M. I., Marcelle, C., & Bronner-Fraser, M. (2002). Ectodermal Wnt function as a neural crest inducer. *Science (New York, N.Y.)*, *297*(5582), 848–851.

Genuth, M. A., Allen, C. D. C., Mikawa, T., & Weiner, O. D. (2018). Chick cranial neural crest cells use progressive polarity refinement, not contact inhibition of locomotion, to guide their migration. *Developmental Biology*, *444*, S252–S261.

Giffin, J. L., Gaitor, D., & Franz-Odendaal, T. A. (2019). The forgotten skeletogenic condensations: A comparison of early skeletal development amongst vertebrates. *Journal of Developmental Biology*, *7*(1).

Gignac, S. J., Hosseini-Farahabadi, S., Akazawa, T., Schuck, N. J., Fu, K., & Richman, J. M. (2019). Robinow syndrome skeletal phenotypes caused by the WNT5AC83S variant are due to dominant interference with chondrogenesis. *Human Molecular Genetics*, *28*(14), 2395–2414.

Grobstein, C. (1953). Epithelio-mesenchymal specificity in the morphogenesis of mouse sub-mandibular rudiments in vitro. *Journal of Experimental Zoology*, *124*, 383–413.

Grüneberg, H. (1963). *The pathology of development: a study of inherited skeletal disorders in animals*.

Gu, R., Zhang, S., Saha, S. K., Ji, Y., Reynolds, K., McMahon, M., Sun, B., Islam, M., Trainor, P. A., Chen, Y., Xu, Y., Chai, Y., Burkart-Wac, D., & Zhou, C. J. (2022). Single-cell transcriptomic signatures and gene regulatory networks modulated by Wls in mammalian midline facial formation and clefts. *Development (Cambridge, England)*, *149*(14).

Habas, R., Dawid, I. B., & He, X. (2003). Coactivation of Rac and Rho by Wnt/Frizzled signaling is required for vertebrate gastrulation. *Genes & Development*, *17*(2), 295–309.

Hall, B. K. (1980). Tissue interactions and the initiation of osteogenesis and chondrogenesis in the neural crest-derived mandibular skeleton of the embryonic mouse as seen in isolated murine tissues and in recombinations of murine and avian tissues. *J. Embryol. Exp. Morphol.*, *58*, 251–264.

Hall, B. K. (2015). *Bones and Cartilage : Developmental and Evolutionary Skeletal Biology*. Elsevier Science & Technology.

Hall, B. K., & Miyake, T. (1992). The membranous skeleton: the role of cell condensations in vertebrate skeletogenesis. *Anatomy and Embryology*, *186*(2), 107–124.

Hall, B. K., & Miyake, T. (1995). Divide, accumulate, differentiate: cell condensation in skeletal development revisited. *Int. J. Dev. Biol.*, *39*(6), 881–893.

Hall, B. K., & Miyake, T. (2000). *All for one and one for all: condensations and the initiation of skeletal development*.

Hall, B. K., & Tremaine, R. (1979). Ability of neural crest cells from the embryonic chick to differentiate into cartilage before their migration away from the neural tube. *Anatomical Record*, *194*(3), 469–475.

Hari, L., Miescher, I., Shakhova, O., Suter, U., Chin, L., Taketo, M., Richardson, W. D., Kessaris, N., & Sommer, L. (2012). Temporal control of neural crest lineage generation by Wnt/β-catenin signaling. *Development*, *139*(12), 2107–2117.

Hasegawa, S., Sato, T., Akazawa, H., Okada, H., Maeno, A., Ito, M., Sugitani, Y., Shibata, H., Miyazaki, J. I., Katsuki, M., Yamauchi, Y., Yamamura, K. I., Katamine, S., & Noda, T. (2002). Apoptosis in neural crest cells by functional loss of APC tumor suppressor gene. *Proceedings of the National Academy of Sciences of the United States of America*, *99*(1), 297–302.

He, F., Xiong, W., Yu, X., Espinoza-Lewis, R., Liu, C., Gu, S., Nishita, M., Suzuki, K., Yamada, G., Minami, Y., & Chen, Y. P. (2008). Wnt5a regulates directional cell migration and cell proliferation via Ror2-mediated noncanonical pathway in mammalian palate development. *Development (Cambridge, England)*, *135*(23), 3871–3879.

He, X., Semenov, M., Tamai, K., & Zeng, X. (2004). LDL receptor-related proteins 5 and 6 in Wnt/β-catenin signaling:Arrows point the way. *Development*, *131*(8), 1663–1677.

Heisenberg, C.-P., Tada, M., Rauch, G.-J., Saúde, L., Concha, M. L., Geisler, R., Stemple, D. L., Smith, J. C., & Wilson, S. W. (2000). Silberblick/Wnt11 mediates convergent extension movements during zebrafish gastrulation. *Nature*, *405*(6782), 76–81.

Helms, J. A., Cordero, D., & Tapadia, M. D. (2005). New insights into craniofacial morphogenesis. *Development*, *132*(5), 851–861.

His W. (1868). *Untersuchungen über die erste Anlage des Wirbelthierleibes: die erste Entwickelung des Hühnchens im Ei*. Leipzig: F.C.W. Vogel.

Holmen, S. L., Salic, A., Zylstra, C. R., Kirschner, M. W., & Williams, B. O. (2002). A Novel Set of Wnt-Frizzled Fusion Proteins Identifies Receptor Components That Activate β-Catenin-dependent Signaling. *Journal of Biological Chemistry*, *277*(38), 34727–34735.

Jho, E., Zhang, T., Domon, C., Joo, C.-K., Freund, J.-N., & Costantini, F. (2002). Wnt/β-Catenin/Tcf Signaling Induces the Transcription of Axin2, a Negative Regulator of the Signaling Pathway. *Molecular and Cellular Biology*, *22*(4), 1172–1183.

Jones, C., Roper, V. C., Foucher, I., Qian, D., Banizs, B., Petit, C., Yoder, B. K., & Chen, P. (2008). Ciliary proteins link basal body polarization to planar cell polarity regulation. *Nature Genetics*, *40*(1), 69–77.

Kaissi, A. Al, Kenis, V., Shboul, M., Grill, F., Ganger, R., & Kircher, S. G. (2020). Tomographic Study of the Malformation Complex in Correlation With the Genotype in Patients With Robinow Syndrome: Review Article. *Journal of Investigative Medicine High Impact Case Reports*, *8*.

Kaucka, M., Ivashkin, E., Gyllborg, D., Zikmund, T., Tesarova, M., Kaiser, J., Xie, M., Petersen, J., Pachnis, V., Nicolis, S. K., Yu, T., Sharpe, P., Arenas, E., Brismar, H., Blom, H., Clevers, H., Suter, U., Chagin, A. S., Fried, K., … Adameyko, I. (2016). Analysis of neural crest–derived clones reveals novel aspects of facial development. *Science Advances*, *2*(8).

Kaucka, M., Zikmund, T., Tesarova, M., Gyllborg, D., Hellander, A., Jaros, J., Kaiser, J., Petersen, J., Szarowska, B., Newton, P. T., Dyachuk, V., Li, L., Qian, H., Johansson, A.-S., Mishina, Y., Currie, J. D., Tanaka, E. M., Erickson, A., Dudley, A., … Adameyko, I. (2017). Oriented clonal cell dynamics enables accurate growth and shaping of vertebrate cartilage. *ELife*, *6*, e25902.

Kibar, Z., Vogan, K. J., Groulx, N., Justice, M. J., Underhill, D. A., & Gros, P. (2001). Ltap, a mammalian homolog of Drosophila Strabismus/Van Gogh, is altered in the mouse neural tube mutant Loop-tail. *Nature Genetics*, *28*(3), 251–255.

Kilian, B., Mansukoski, H., Barbosa, F. C., Ulrich, F., Tada, M., & Heisenberg, C. P. (2003). The role of Ppt/Wnt5 in regulating cell shape and movement during zebrafish gastrulation. *Mechanisms of Development*, *120*(4), 467–476.

Köntges, G., & Lumsden, A. (1996). Rhombencephalic neural crest segmentation is preserved throughout craniofacial ontogeny. *Development (Cambridge, England)*, *122*(10), 3229–3242.

Kulesa, P. M., Bailey, C. M., Kasemeier-Kulesa, J. C., & McLennan, R. (2010). Cranial neural crest migration: new rules for an old road. *Developmental Biology*, *344*(2), 543–554.

Lang, M. R., Lapierre, L. A., Frotscher, M., Goldenring, J. R., & Knapik, E. W. (2006). Secretory COPII coat component Sec23a is essential for craniofacial chondrocyte maturation. *Nature Genetics 2006 38:10*, *38*(10), 1198–1203.

Le Douarin, N., & Kalcheim, C. (1999). *The Neural Crest*. Cambridge University Press.

LeClair, E. E., Mui, S. R., Huang, A., Topczewska, J. M., & Topczewski, J. (2009). Craniofacial skeletal defects of adult zebrafish Glypican 4 (knypek) mutants. *Developmental Dynamics*, *238*(10), 2550–2563.

Lewis, A. E., Vasudevan, H. N., O'Neill, A. K., Soriano, P., & Bush, J. O. (2013). The widely used Wnt1-Cre transgene causes developmental phenotypes by ectopic activation of Wnt signaling. *Developmental Biology*, *379*(2), 229.

Li, Y., Vieceli, F. M., Gonzalez, W. G., Li, A., Tang, W., Lois, C., & Bronner, M. E. (2019). In Vivo Quantitative Imaging Provides Insights into Trunk Neural Crest Migration. *Cell Reports*, *26*(6), 1489-1500.e3.

Lignell, A., Kerosuo, L., Streichan, S. J., Cai, L., & Bronner, M. E. (2017). Identification of a neural crest stem cell niche by Spatial Genomic Analysis. *Nature Communications*, *8*(1).

Lin, M., Li, L., Liu, C., Liu, H., He, F., Yan, F., Zhang, Y., & Chen, Y. P. (2011). Wnt5a regulates growth, patterning, and odontoblast differentiation of developing mouse tooth. *Developmental Dynamics*, *240*(2), 432–440.

Liu, G., Bafico, A., & Aaronson, S. (2005). The Mechanism of Endogenous Receptor Activation Functionally Distinguishes Prototype Canonical and Noncanonical Wnts. *Molecular and Cellular Biology*, *25*, 3475–3482.

Liu, W., Du, L., Cui, Y., He, C., & He, Z. (2024). WNT5A regulates the proliferation, apoptosis and stemness of human stem Leydig cells via the β-catenin signaling pathway. *Cellular and Molecular Life Sciences : CMLS*, *81*(1).

Lumsden, A., Sprawson, N., & Graham, A. (1991). Segmental origin and migration of neural crest cells in the hindbrain region of the chick embryo. *Development*, *113*, 1281–1291.

Marcucio, R., Hallgrimsson, B., & Young, N. M. (2015). Facial Morphogenesis: Physical and Molecular Interactions Between the Brain and the Face. *Current Topics in Developmental Biology*, *115*, 299–320.

Mattes, B., Dang, Y., Greicius, G., Kaufmann, L. T., Prunsche, B., Rosenbauer, J., Stegmaier, J., Mikut, R., Özbek, S., Nienhaus, G. U., Schug, A., Virshup, D. M., & Scholpp, S. (2018). Wnt/PCP controls spreading of Wnt/β-catenin signals by cytonemes in vertebrates. *ELife*, *7*.

Matthews, H. K., Marchant, L., Carmona-Fontaine, C., Kuriyama, S., Larraín, J., Holt, M. R., Parsons, M., & Mayor, R. (2008). Directional migration of neural crest cells in vivo is regulated by Syndecan-4/Rac1 and non-canonical Wnt signaling/RhoA. *Development*, *135*(10), 1771–1780.

Medio, M., Yeh, E., Popelut, A., Babajko, S., Berdal, A., & Helms, J. (2012). Wnt/β-catenin signaling and Ms×1 promote outgrowth of the maxillary prominences. *Frontiers in Physiology*, *3*, 375.

Meulemans, D., & Bronner-Fraser, M. (2004). Gene-Regulatory Interactions in Neural Crest Evolution and Development. *Developmental Cell*, *7*(3), 291–299.

Mikels, A. J., & Nusse, R. (2006). Purified Wnt5a Protein Activates or Inhibits β-Catenin–TCF Signaling Depending on Receptor Context. *PLOS Biology*, *4*(4), e115.

Minoux, M., & Rijli, F. M. (2010). Molecular mechanisms of cranial neural crest cell migration and patterning in craniofacial development. In *Development* (Vol. 137, Issue 16, pp. 2605–2621).

Mirando, A. J., Maruyama, T., Fu, J., Yu, H.-M. I., & Hsu, W. (2010). β-catenin/cyclin D1 mediated development of suture mesenchyme in calvarial morphogenesis. *BMC Dev. Biol.*, *10*(1), 116.

Niehrs, C. (2012). The complex world of WNT receptor signalling. *Nature Reviews Molecular Cell Biology*, *13*(12), 767–779.

Noden, D. M. (1983). The role of the neural crest in patterning of avian cranial skeletal, connective, and muscle tissues. *Developmental Biology*, *96*(1), 144–165.

Noden, D. M., & Trainor, P. A. (2005). Relations and interactions between cranial mesoderm and neural crest populations. *Journal of Anatomy*, *207*(5), 575–601.

Nusse, R. (2005). Wnt signaling in disease and in development. *Cell Research 2005 15:1*, *15*(1), 28–32.

Ohkawara, B., Glinka, A., & Niehrs, C. (2011). Rspo3 Binds Syndecan 4 and Induces Wnt/PCP Signaling via Clathrin-Mediated Endocytosis to Promote Morphogenesis. *Developmental Cell*, *20*(3), 303–314.

Ormestad, M., Astorga, J., Landgren, H., Wang, T., Johansson, B. R., Miura, N., & Carlsson, P. (2006). Foxf1 and Foxf2 control murine gut development by limiting mesenchymal Wnt signaling and promoting extracellular matrix production. *Development*, *133*(5), 833–843.

Otto, F., Thornell, A. P., Crompton, T., Denzel, A., Gilmour, K. C., Rosewell, I. R., Stamp, G. W., Beddington, R. S., Mundlos, S., Olsen, B. R., Selby, P. B., & Owen, M. J. (1997). Cbfa1, a candidate gene for cleidocranial dysplasia syndrome, is essential for osteoblast differentiation and bone development. *Cell*, *89*(5), 765–771.

Ouspenskaia, T., Matos, I., Mertz, A. F., Fiore, V. F., & Fuchs, E. (2016). WNT-SHH Antagonism Specifies and Expands Stem Cells prior to Niche Formation. *Cell*, *164*(1–2), 156–169.

Patel, V., Li, L., Cobo-stark, P., Shao, X., Somlo, S., Lin, F., & Igarashi, P. (2008). Acute kidney injury and aberrant planar cell polarity induce cyst formation in mice lacking renal cilia. *Human Molecular Genetics*, *17*(11), 1578–1590.

Person, A. D., Beiraghi, S., Sieben, C. M., Hermanson, S., Neumann, A. N., Robu, M. E., Schleiffarth, J. R., Billington, C. J., Van Bokhoven, H., Hoogeboom, J. M., Mazzeu, J. F., Petryk, A., Schimmenti, L. A., Brunner, H. G., Ekker, S. C., & Lohr, J. L. (2010). WNT5A mutations in patients with autosomal dominant Robinow syndrome. *Developmental Dynamics*, *239*(1), 327–337.

Qiu, M., Bulfone, A., Martinez, S., Meneses, J. J., Shimamura, K., Pedersen, R. A., & Rubenstein, J. L. R. (1995). Null mutation of Dlx-2 results in abnormal morphogenesis of proximal first and second branchial arch derivatives and abnormal differentiation in the forebrain. *Genes & Development*, *9*(20), 2523–2538.

Reza, A. A., Kohram, F., Reza, H. A., Kalin, T. R., Kannan, P. S., Zacharias, W. J., & Kalinichenko, V. V. (2023). FOXF1 Regulates Alveolar Epithelial Morphogenesis through Transcriptional Activation of Mesenchymal WNT5A. *American Journal of Respiratory Cell and Molecular Biology*, *68*(4), 430–443.

Richardson, J., Gauert, A., Briones Montecinos, L., Fanlo, L., Alhashem, Z. M., Assar, R., Marti, E., Kabla, A., Härtel, S., & Linker, C. (2016). Leader Cells Define Directionality of Trunk, but Not Cranial, Neural Crest Cell Migration. *Cell Reports*, *15*(9), 2076–2088.

Richman, J. M., Herbert, M., Matovinovic, E., & Walin, J. (1997). Effect of fibroblast growth factors on outgrowth of facial mesenchyme. *Developmental Biology*, *189*(1), 135–147.

Rida, P. C. G., & Chen, P. (2009). Line up and listen: Planar cell polarity regulation in the mammalian inner ear. *Seminars in Cell & Developmental Biology*, *20*(8), 978–985.

Ridley, A. J., Schwartz, M. A., Burridge, K., Firtel, R. A., Ginsberg, M. H., Borisy, G., Parsons, J. T., & Horwitz, A. R. (2003). Cell Migration: Integrating Signals from Front to Back. *Science*, *302*(5651), 1704–1709.

Ring, L., Neth, P., Weber, C., Steffens, S., & Faussner, A. (2014). β-Catenin-dependent pathway activation by both promiscuous "canonical" WNT3a–, and specific "noncanonical" WNT4– and WNT5a–FZD receptor combinations with strong differences in LRP5 and LRP6 dependency. *Cellular Signalling*, *26*(2), 260–267.

Rothstein, M., Bhattacharya, D., & Simoes-Costa, M. (2018). The molecular basis of neural crest axial identity. *Developmental Biology*, *444 Suppl 1*(Suppl 1), S170–S180.

Sarmah, S., Barrallo-Gimeno, A., Melville, D. B., Topczewski, J., Solnica-Krezel, L., & Knapik, E. W. (2010). Sec24D-Dependent Transport of Extracellular Matrix Proteins Is Required for Zebrafish Skeletal Morphogenesis. *PLOS ONE*, *5*(4), e10367.

Sato, A., Yamamoto, H., Sakane, H., Koyama, H., & Kikuchi, A. (2010). Wnt5a regulates distinct signalling pathways by binding to Frizzled2. *EMBO Journal*, *29*(1), 41–54.

Satokata, I., & Maas, R. (1994). Msx1 deficient mice exhibit cleft palate and abnormalities of craniofacial and tooth development. *Nature Genetics*, *6*(4), 348–356.

Scarpa, E., Szabó, A., Bibonne, A., Theveneau, E., Parsons, M., & Mayor, R. (2015). Cadherin Switch during EMT in Neural Crest Cells Leads to Contact Inhibition of Locomotion via Repolarization of Forces. *Developmental Cell*, *34*(4), 421–434.

Schambony, A., & Wedlich, D. (2007). Wnt-5A/Ror2 Regulate Expression of XPAPC through an Alternative Noncanonical Signaling Pathway. *Developmental Cell*, *12*(5), 779–792.

Schwabe, G. C., Trepczik, B., Süring, K., Brieske, N., Tucker, A. S., Sharpe, P. T., Minami, Y., & Mundlos, S. (2004). Ror2 knockout mouse as a model for the developmental pathology of autosomal recessive Robinow syndrome. *Developmental Dynamics*, *229*(2), 400–410.

Ségalen, M., Johnston, C. A., Martin, C. A., Dumortier, J. G., Prehoda, K. E., David, N. B., Doe, C. Q., & Bellaïche, Y. (2010). The Fz-Dsh Planar Cell Polarity Pathway Induces Oriented Cell Division via Mud/NuMA in Drosophila and Zebrafish. *Developmental Cell*, *19*(5), 740–752.

Shellard, A., Szabó, A., Trepat, X., & Mayor, R. (2018). Supracellular contraction at the rear of neural crest cell groups drives collective chemotaxis. *Science*, *362*(6412), 339–343.

Shimizu, H., Julius, M. A., Giarré, M., Zheng, Z., Brown, A., & Kitajewski, J. (1998). Transformation by Wnt family proteins correlates with regulation of ??-catenin. *Cell Growth & Differentiation : The Molecular Biology Journal of the American Association for Cancer Research*, *8*, 1349–1358.

Shirai, Y., Kawabe, K., Tosa, I., Tsukamoto, S., Yamada, D., & Takarada, T. (2019). Runx2 function in cells of neural crest origin during intramembranous ossification. *Biochemical and Biophysical Research Communications*, *509*(4), 1028–1033.

Slusarski, D. C., Corces, V. G., & Moon, R. T. (1997). Interaction of Wnt and a Frizzled homologue triggers G-protein-linked phosphatidylinositol signalling. *Nature*, *390*(6658), 410–413.

Slusarski, D. C., Yang-Snyder, J., Busa, W. B., & Moon, R. T. (1997). Modulation of Embryonic Intracellular Ca2+ Signaling by Wnt-5A. *Developmental Biology*, *182*(1), 114–120.

Soldatov, R., Kaucka, M., Kastriti, M. E., Petersen, J., Chontorotzea, T., Englmaier, L., Akkuratova, N., Yang, Y., Häring, M., Dyachuk, V., Bock, C., Farlik, M., Piacentino, M. L., Boismoreau, F., Hilscher, M. M., Yokota, C., Qian, X., Nilsson, M., Bronner, M. E., … Adameyko, I. (2019). Spatiotemporal structure of cell fate decisions in murine neural crest. *Science*, *364*(6444).

Som, P. M., & Naidich, T. P. (2013). Illustrated review of the embryology and development of the facial region, part 1: Early face and lateral nasal cavities. *AJNR. American Journal of Neuroradiology*, *34*(12), 2233–2240.

Soo, K., O'Rourke, M. P., Khoo, P. L., Steiner, K. A., Wong, N., Behringer, R. R., & Tam, P. P. L. (2002). Twist Function Is Required for the Morphogenesis of the Cephalic Neural Tube and the Differentiation of the Cranial Neural Crest Cells in the Mouse Embryo. *Developmental Biology*, *247*(2), 251–270.

Stamos, J. L., & Weis, W. I. (2013). The β-Catenin Destruction Complex. *Cold Spring Harbor Perspectives in Biology*, *5*(1), a007898.

Stuhlmiller, T. J., & García-Castro, M. I. (2012). Current perspectives of the signaling pathways directing neural crest induction. *Cellular and Molecular Life Sciences*, *69*(22), 3715–3737.

Takeuchi, S., Takeda, K., Oishi, I., Nomi, M., Ikeya, M., Itoh, K., Tamura, S., Ueda, T., Hatta, T., Otani, H., Terashima, T., Takada, S., Yamamura, H., Akira, S., & Minami, Y. (2000). Mouse Ror2 receptor tyrosine kinase is required for the heart development and limb formation. *Genes to Cells*, *5*(1), 71–78.

Tamarin, A., & Boyde, A. (1977). Facial and visceral arch development in the mouse embryo: a study by scanning electron microscopy. *Journal of Anatomy*, *124*(Pt 3), 563.

Tobin, J. L., Di Franco, M., Eichers, E., May-Simera, H., Garcia, M., Yan, J., Quinlan, R., Justice, M. J., Hennekam, R. C., Briscoe, J., Tada, M., Mayor, R., Burns, A. J., Lupski, J. R., Hammond, P., & Beales, P. L. (2008). Inhibition of neural crest migration underlies craniofacial dysmorphology and Hirschsprung's disease in Bardet-Biedl syndrome. *Proceedings of the National Academy of Sciences of the United States of America*, *105*(18), 6714–6719.

Topczewski, J., Sepich, D. S., Myers, D. C., Walker, C., Amores, A., Lele, Z., Hammerschmidt, M., Postlethwait, J., & Solnica-Krezel, L. (2001). The Zebrafish Glypican Knypek Controls Cell Polarity during Gastrulation Movements of Convergent Extension. *Developmental Cell*, *1*(2), 251–264.

Ustiyan, V., Bolte, C., Zhang, Y., Han, L., Xu, Y., Yutzey, K. E., Zorn, A. M., Kalin, T. V., Shannon, J. M., & Kalinichenko, V. V. (2018). FOXF1 Transcription Factor Promotes Lung Morphogenesis by Inducing Cellular Proliferation in Fetal Lung Mesenchyme. *Developmental Biology*, *443*(1), 50.

Van Amerongen, R., Fuerer, C., Mizutani, M., & Nusse, R. (2012). Wnt5a can both activate and repress Wnt/β-catenin signaling during mouse embryonic development. *Developmental Biology*, *369*(1), 101–114.

van Amerongen, R., & Nusse, R. (2009). Towards an integrated view of Wnt signaling in development. *Development*, *136*(19), 3205–3214.

Vuga, L. J., Ben-Yehudah, A., Kovkarova-Naumovski, E., Oriss, T., Gibson, K. F., Feghali-Bostwick, C., & Kaminski, N. (2012). WNT5A Is a Regulator of Fibroblast Proliferation and Resistance to Apoptosis.

Wallingford, J., Vogeli, K., & Harland, R. (2001). Regulation of convergent extension in Xenopus by Wnt5a and Frizzled-8 is independent of the canonical Wnt pathway. *The International Journal of Developmental Biology*, *45*, 225–227.

Walshe, J., & Mason, I. (2003). Fgf signalling is required for formation of cartilage in the head. *Developmental Biology*, *264*(2), 522–536.

Wan, Y., Lantz, B., Cusack, B. J., & Szabo-Rogers, H. L. (2018). Prickle1 regulates differentiation of frontal bone osteoblasts. *Scientific Reports*, *8*(1).

Wang, B., Sinha, T., Jiao, K., Serra, R., & Wang, J. (2011). Disruption of PCP signaling causes limb morphogenesis and skeletal defects and may underlie Robinow syndrome and brachydactyly type B. *Human Molecular Genetics*, *20*(2), 271–285.

White, J. J., Mazzeu, J. F., Coban-Akdemir, Z., Bayram, Y., Bahrambeigi, V., Hoischen, A., van Bon, B. W. M., Gezdirici, A., Gulec, E. Y., Ramond, F., Touraine, R., Thevenon, J., Shinawi, M., Beaver, E., Heeley, J., Hoover-Fong, J., Durmaz, C. D., Karabulut, H. G., Marzioglu-Ozdemir, E., … Carvalho, C. M. B. (2018). WNT Signaling Perturbations Underlie the Genetic Heterogeneity of Robinow Syndrome. *The American Journal of Human Genetics*, *102*(1), 27–43.

Wodarz, A., & Nusse, R. (1998). Mechanisms of Wnt signaling in development. *Annual Review of Cell and Developmental Biology*, *14*(Volume 14, 1998), 59–88.

Xu, J., Liu, H., Lan, Y., Aronow, B. J., Kalinichenko, V. V., & Jiang, R. (2016). A Shh-Foxf-Fgf18-Shh Molecular Circuit Regulating Palate Development. *PLOS Genetics*, *12*(1), e1005769.

Xu, P., Balczerski, B., Ciozda, A., Louie, K., Oralová, V., Huysseune, A., & Crump, J. (2018). Fox proteins are modular competency factors for facial cartilage and tooth specification. *Development*, *145*, dev.165498.

Yamaguchi, T. P., Bradley, A., McMahon, A. P., & Jones, S. (1999). A Wnt5a pathway underlies outgrowth of multiple structures in the vertebrate embryo. *Development*, *126*(6), 1211–1223.

Yang, Y., Topol, L., Lee, H., & Wu, J. (2003). Wnt5a and Wnt5b exhibit distinct activities in coordinating chondrocyte proliferation and differentiation. *Development*, *130*(5), 1003–1015.

Yates, L. L., & Dean, C. H. (2011). Planar polarity: A new player in both lung development and disease. *Organogenesis*, *7*(3), 209–216.

Yin, C., Kiskowski, M., Pouille, P. A., Farge, E., & Solnica-Krezel, L. (2008). Cooperation of polarized cell intercalations drives convergence and extension of presomitic mesoderm during zebrafish gastrulation. *Journal of Cell Biology*, *180*(1), 221–232.

Yoshikawa, S., McKinnon, R. D., Kokel, M., & Thomas, J. B. (2003). Wnt-mediated axon guidance via the Drosophila Derailed receptor. *Nature 2003 422:6932*, *422*(6932), 583–588.

Zalc, A., Rattenbach, R., Auradé, F., Cadot, B., & Relaix, F. (2015). Pax3 and Pax7 Play Essential Safeguard Functions against Environmental Stress-Induced Birth Defects. *Developmental Cell*, *33*(1), 56–66.

Zhao, T., Gan, Q., Stokes, A., Lassiter, R. N. T., Wang, Y., Chan, J., Han, J. X., Pleasure, D. E., Epstein, J. A., & Zhou, C. J. (2014). β-catenin regulates Pax3 and Cdx2 for caudal neural tube closure and elongation. *Development (Cambridge, England)*, *141*(1), 148–157.